universität wien

MASTERARBEIT / MASTER'S THESIS

Titel der Masterarbeit / Title of the Master's Thesis

„Studying aichivirus A1 infection: from 2D to 3D cell culture systems“

verfasst von / submitted by

Martin Groznica BSc

angestrebter akademischer Grad / in partial fulfilment of the requirements for the degree of

Master of Science (MSc)

Wien, 2021 / Vienna, 2021

Studienkennzahl lt. Studienblatt / degree programme code as it appears on the student record sheet:	UA 066 830
Studienrichtung lt. Studienblatt / degree programme as it appears on the student record sheet:	Masterstudium Molecular Microbiology, Microbial Ecology and Immunobiology
Betreut von / Supervisor:	Mag. Dr. Heinrich Kowalski

ACKNOWLEDGMENTS

I would like to thank my supervisors Prof. Heinrich Kowalski and Prof. Dieter Blaas for giving me the opportunity to work on multiple projects and especially the aichivirus A1 project. Thank you so much for all the great ideas, your guidance and the relaxed lab meetings.

My next big fat thanks go to my colleague Dr. Antonio Real-Hohn. I am so thankful for all your mentoring and your great support. I truly enjoyed our endless discussions while having a cup of coffee. And it did not matter what went wrong, but you always stayed cool and I knew I could count on you.

Special thanks go to Konstantin Wiese. The way you handled the work with such passion and effortlessness was always inspiring. I am very happy that we had you in the team before closure of the lab since you were a main driving force in wrapping up the projects. I am very thankful for all the help and insights from Irene Gösler und Irmgard Fischer. Without you, this work would certainly not have been possible. I would like to thank Bernhard Alber for all the fun moments in the lab while we struggled our way through the membrane extraction protocol.

Finally, and most importantly, I am so grateful to have had you at my side Linda. Thank you so much for always being there for me, for being my anchor when times were not so pretty and your endless love. Thank you so much for your phenomenal meals that carried me through the day and I always eagerly looked forward to. Thank you so much for all the funny and encouraging slogans on my coffee mug every morning.

ABSTRACT

According to the Global Burden of Diseases, Injuries, and Risk Factors Study from 2016 acute gastroenteritis was the eighth-leading cause of fatalities for all age groups worldwide. While bacteria are the main cause in the elderly, viruses preferentially affect children. Set aside the most prominent noro-, rota-, adeno-, and astrovirus, in many instances the pathogen causing diarrhoeal diseases remains unknown.

Due to advances in sequencing technology, already known viruses are discovered as putative pathogens involved in gastroenteritis, as is the case of aichivirus A1 (AiV-A1). As single-stranded positive sense RNA virus, AiV-A1 belongs to the genus *Kobuvirus* in the family *Picornaviridae*, which includes other significant human pathogens including poliovirus, EV-D68, and EV-71. Since its discovery in 1989, AiV-A1 has been detected worldwide, but conclusive *in vitro* data supporting the epidemiological observations linking it to infections of the intestinal tract have been missing.

In this work, we evaluated various continuous human cell lines for their susceptibility to AiV-A1, examined its growth in an organotypic model and in short-term cultivated human small intestine-derived explants, as well as shed light on the early events during cell entry. We demonstrate for the first time AiV-A1 replication in human stem cell-derived intestinal epithelium, substantiating AiV-A1 as a possible causative agent for acute gastroenteritis. AiV-A1 preferentially infected absorptive and proliferative enterocytes causing only a weak antiviral response in combination with insignificant tissue damage. By employing various pharmacological inhibitors that block different stages of the intracellular routing pathways, we found in monkey-derived Vero cells, that AiV-A1 strongly depends on dynamin for its

uptake and to a lesser extent on factors involved in macropinocytosis. AiV-A1 infection furthermore requires endosomal acidification and most likely exploits the late endosome/lysosome pathway.

ZUSAMMENFASSUNG

Die akute Gastroenteritis, eine Erkrankung die mit Diarrhö und Erbrechen einhergeht, wurde laut dem GBD-Bericht von 2016 als achthäufigsten Todesursache für alle Altersgruppen weltweit eingestuft. Während bakterielle Infektionen die häufigste Ursache für ältere Personen darstellt, konstituieren Viren die andere Gruppe von ätiologischen Erregern, im Besonderen für Kinder. Neben prominenten viralen Vertretern wie Noro-, Adeno-, Rota-, und Astroviren, bleibt jedoch in vielen Fällen von Durchfallerkrankungen das ursächliche Pathogen unbekannt.

Aufgrund des Fortschritts in der molekularbiologischen Diagnostik werden bereits bekannte Viren in Fällen von Gastroenteritis neu entdeckt und als potenzielle Erreger verantwortlich gemacht. So auch im Fall von Aichivirus A1 (AiV-A1). Beschrieben als ein positives einzelsträngiges RNA-Virus, wird AiV-A1 der Gattung *Kobuvirus* in der Familie *Picornaviridae* zugeordnet, welche weitere bekannte Humanpathogene beinhaltet, wie Poliovirus, EV-D68 und EV-71. Seit der Entdeckung von AiV-A1 in 1989 wird es weltweit detektiert, jedoch fehlen konklusive *in vitro* Daten zur Untermauerung der epidemiologischen Beobachtungen.

In dieser Arbeit evaluierten wir die Anfälligkeit unterschiedlicher humaner Zelltypen für eine Aichivirus A1 Infektion, wir untersuchten sein Wachstum in einem organotypischen Model und kurzzeitig kultivierten Dünndarm abstammenden Explantat, so wie die frühen Ereignisse des Zelleintritts. Erstens demonstrieren wir die Replikation von AiV-A1 in Stammzell-basiertem humanem Dünndarmepithel, welche die Vermutung substanziiert, dass AiV-A1 ein weiterer Erreger für akute Gastroenteritis ist. Des Weiteren infizierte AiV-A1 vorzugsweise absorptive und proliferative Enterozyten, wobei nur ein schwacher Anstieg der

antiviralen Antwort gemessen und kein merklicher Gewebsschaden festgestellt wurde. Mittels pharmakologischer Inhibitoren, welche unterschiedliche Schritte der intrazellulären Transportwege blockieren, konnten wir in von Affennieren stammenden Vero-Zellen zeigen, dass die Endozytose von AiV-A1 stark von Dynamin abhängt und im geringeren Maß von Komponenten der Makropinozytose. Weiters benötigt die Infektion einen sauren endosomalen pH und nützt sehr wahrscheinlich den späten endosomalen-lysosmalen Transportweg aus.

TABLE OF CONTENTS

LIST OF TABLES

LIST OF FIGURES

ABBREVIATIONS

%w/w	Percentage weight to weight
AiV-A1 A846/88	Aichivirus A1 strain A846/88 (Japanese strain) (accession no. JQ281544), used in this study
AiV-A1 kvgh2010	Aichivirus A1 strain kvgh99012632/2010 (Taiwanese strain) (accession no. JX564249)
BSL	Biosafety level
CPE	Cytopathic effect
CVB	Group B coxsackieviruses
CVB3	Coxsackievirus B3
DAB	3,3'-Diaminobenzidin
DMEM	Dulbecco's modified eagle medium
DMSO	Dimethylsulfoxid
DNA	Deoxyribonucleic acid
dsRNA	Double-stranded RNA
E11	Echovirus 11
ECV	Endosomal carrier vesicle
EDTA	Ethylenediaminetetraacetic acid
EGA	4-bromobenzaldehyde N-(2,6 dimethylphenyl) semicarbazone
ERC	Endocytic recycling compartment
EV-A71	Enterovirus A71
FBS	Foetal calf serum
GAGs	Glycosaminoglycan
GALT	Gut-associated lymphoid tissue
HAE	Human airway epithelium
HIE	Human intestinal epithelium
HPeV	Human parechovirus
IF	Immunofluorescence
IHC	Immunohistochemistry

IM	Infection medium
LDH	Lactate dehydrogenase
LOD	Limit of detection
MOI	Multiplicity of infection
Ns	Not significant
o/n	Over night
PBS	Phosphate-buffered saline
Pen-Strep	Penicillin and streptomycin
PFU	Plaque forming units
pi	post infection
PRR	Pattern recognition receptor
RLRs	RIG-like receptors
RNA	Ribonucleic acid
Rpm	Rotation per minute
rRNA	Ribosomal ribonucleic acid
RT	Room temperature
RV	Rhinovirus
RV-A54	Rhinovirus A54
scRNAseq	Single-cell RNA sequencing
SD	Standard deviation
SN	Supernatant
TAE buffer	Tris-acetate-EDTA buffer
vRNA	Viral ribonucleic acid

1. INTRODUCTION

Kobuviruses, belonging to the family of *Picornaviridae*, have been identified worldwide and in various host species. Based on epidemiological observations, some members have been associated with acute gastroenteritis in humans and animals. However, little to nothing on the transmission or pathogenic mechanisms of these viruses is known. To date, the putative human pathogen AiV-A1 strain A846/88 is the best-studied kobuvirus. These investigations have been largely confined to usage of the African green monkey kidney-derived Vero cell line, which is permissive for all human kobuvirus strains. While a few human cell lines were identified to support modest replication of a different AiV-A1 strain (AiV-A1 kvgh99012632/2010), they are all cancer-derived and lack the highly differentiated phenotype of the intestinal tract tissue. The current dearth of suitable cell culture systems and of susceptible animal models contributes to the overall considerable lack of information on the AiV-A1 pathobiology. In recent years, stem cell-based technologies have been developed to promote their controlled differentiation into organotypic models resembling the structural complexity and cellular diversity of the human small intestine. These models have been utilized in the past to study replication of various enteric pathogens but have not yet been explored for their suitability to recapitulate AiV-A1 infection of the human intestinal tract.

1.1. Kobuviruses

Kobuviruses belong to one of the largest viral families, *Picornaviridae*, which comprises 63 genera including 147 different species (https://talk.ictvonline.org/ictv-reports/ictv_online_report/positive-sense-rna-viruses/w/picornaviridae). The most prominent picornaviral genera are *Aphthovirus* (e.g. FMDV), *Avihepatovirus* (e.g. DHAV) *Cardiovirus* (e.g. EMCV), *Enterovirus* (e.g. EV-A71, EV-D68, CVB3, RV, PV), *Erbovirus* (e.g. ERBV), *Hepatovirus* (e.g. HAV), *Kobuvirus* (e.g. AiV) and *Parechovirus* (e.g. HPeV), *Sapelovirus*, *Senecavirus*, *Teschovirus* and *Tremovirus*.

The genus *Kobuvirus* was established in 1999 and initially contained three different prototype strains: (i) aichivirus A1 strain A846/88 (human), (ii) bovine kobuvirus strain U-1 (cattle) and (iii) porcine kobuvirus strain S-1-HUN (swine) [1-3]. Due to advances in sequencing technology, more kobuviruses have been identified in recent years in multiple different host taxa such as humans, chiroptera (bats), rodentia, lagomorpha (rabbits), artiodactyla, aves and carnivora expanding the genus to six species: *Aichivirus A–F* [4-10]. The word "kobu" is derived from Japanese and means bump or knob due to the characteristic bumpy morphology of the virion under electron microscopy [11]. So far, *aichivirus A–D* have been detected in cases of human and animal gastroenteritis [12-15]. It is assumed that kobuviral transmission occurs primarily via the faecal-oral route. However, detailed studies on the pathogenesis including the cellular tropism, internalisation and dissemination pathways are still missing. Additionally, the cell surface receptor remains unknown.

1.1.1. Genome organisation

Basically, all kobuviruses share the same genome organisation (Figure 1) [16]. The full length single-stranded, positive-sense RNA of kobuviruses is approximately 8,200 nt long and has an unusually high guanine and cytosine content (approximately 59%), reportedly the highest among picornaviruses [17]. Furthermore, bioinformatics analyses revealed kobuviruses to possess the highest degree of structured RNA among all picornaviruses [18]. The genome is flanked by untranslated regions (UTRs) at the 5′ and 3′ end [19]. The 5′ terminus contains the covalently attached VPg (viral protein genome-linked) followed by the highly structured region termed the internal ribosomal entry site (IRES). The IRES is located within the 5′ UTR and is important for the cap-independent initiation of translation by recruiting ribosomal subunits and other host co-factors [20]. While most kobuviruses have a type V IRES, *aichivirus C* has a type IV IRES instead [3, 21]. The VPg is attached via a conserved tyrosine residue and is essential for viral RNA synthesis. Additionally, three stem-loop structures (SL-A, SL- B and SL-C) were identified in the 5′ UTR to be important for RNA replication and encapsidation [19, 22], thus, being the first encapsidation motif to be found in picornaviruses. The 3′ end harbours a poly A-tail which conveys genome stability [23]. The genome consists of one ORF (approximately 7,300 nt) that encodes a single polyprotein precursor of 2433 aa. This precursor is co-, and post-translationally cleaved only by the viral proteases 3C and 3CD into the leader (L) protein, the structural proteins P1 (VP0, VP3, VP1) and the non-structural proteins P2 (2A, 2B, 2C) and P3 (3A, 3B, 3C, 3D) [19, 24] .

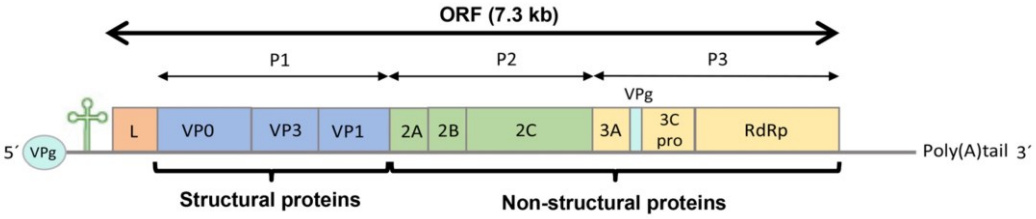

Figure 1. Schematic representation of kobuvirus genome organisation. The positive-sense, single-stranded RNA harbours one ORF which is flanked 5′ and 3′ by UTRs. The 5′ UTR is covalently linked to the VPg and comprises the highly structured IRES, the 3′ UTR ends in a poly A-tail. The ORF encodes one giant polyprotein that is proteolytically cleaved into structural and non-structural proteins. VPg, L, and RdRp stand for virus protein genome-linked, leader and RNA-dependent RNA polymerase, respectively. This figure was adapted from Springer Nature Customer Service Centre GmbH: Springer Virologica Sinica Rivadulla and Romalde (2020) [25] Copyright.

1.2. Aichivirus A1

The AiV-A1 strain A846/88 was the first kobuvirus to be discovered in 1989 in Japan in faecal samples from patients suffering from acute gastroenteritis [14] in a large-scale outbreak in the Japanese Prefecture Aichi. It involved the consumption of raw oysters in nine different schools with more than 3000 schoolchildren and teachers showing symptoms [26]. The outbreak could not be assigned to any known viral or bacterial pathogen at that time. Electron microscopy revealed a viral particle, which appeared like an astrovirus and was therefore dubbed "cytopathic small round viruses". In 1998, a complete genome sequencing determined that this until then orphan virus belonged to the family *Picornaviridae* [17] and was subsequently classified in the new genus *Kobuvirus* [1]. Currently, the species *Aichivirus A* is divided in six types: A1–A10, of which the type aichivirus A1 (AiV-A1) is considered a putative pathogen for humans. Moreover, the type AiV-A1 is further divided in three genotypes A, B and C [27] (Figure 2). Types A2–A10 have been described in different animals [25], thus raising the possibility of a potential cross-species transmission. This is a major concern as many

pathogens of relevance for the public health are zoonotic as recently seen with the COVID-19 pandemic [28, 29].

So far, AiV-A1 has been detected worldwide such as Europa, Africa, Asia, South and North America and Australia and not just in human diarrheal specimens but also in different environmental samples (e.g. water, biosolid and shellfish) [25, 30]. Only AiV-A1 genotype C has not been found in environmental samples.

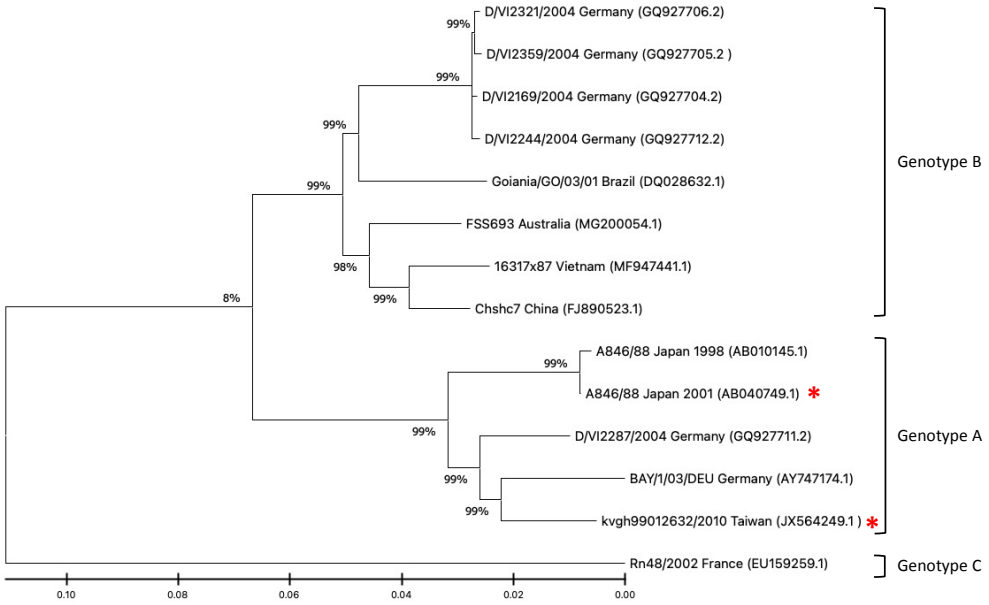

Figure 2. Phylogenetic tree of AiV-A1 genotypes. AiV-A1 is subdivided in three genotypes: A, B and C. The phylogenetic tree was constructed using the neighbour-joining method in MEGA 11 based on full length genome sequences of 14 selected AiV-A1 strains exemplifying the different genotypes [31]. The tree describes the strain name, location of identification and GenBank accession number. Red asterisks indicate the presently better studied AiV-A1 strains and country of isolation (Japan: A846/88 and Taiwan: kvgh99012632/210). Scale bar represents nucleotide substitutions per site. More information in Table S1.

1.2.1. Epidemiological and clinical observations

Since its first link with acute gastroenteritis, it has remained unclear if AiV-A1 is to be considered an aetiological agent, mainly due to the ambiguity in the epidemiological observations. Some surveys frequently co-detected AiV-A1 with other prominent enteric pathogens (e.g. norovirus and rotavirus) while others found mono-infections with AiV-A1 materialising in overall low incidence rates of 0.9% – 4.1% [32-35]. On top of that, many AiV-A1 infections continued subclinical while others resulted in diarrhoea, abdominal pain, nausea, vomiting and fever [14, 36]. Additionally, a chronic AiV-A1 infection, which systemically spread to different tissues, was found in a X-linked agammaglobulinemia patient suffering from chronic multi-organ disease and chronic kidney failure [37]. Two cases have been reported in which, beside intestinal disease, respiratory symptoms were also observed [38, 39].

Seroprevalence studies around the world determined that 80–95% of adults older than 40 years have antibodies against AiV-A1 and to a lesser extent at younger age [25]. This suggests a frequent circulation of AiV-A1 in different human populations and that exposure likely occurs during childhood. Additionally, many seroconverted individuals had neutralising antibodies [40]. Cases of AiV-A1 often involved the consumption of shellfish including oysters [25]. Studies found a higher prevalence of AiV-A1 when shellfish was harvested from sewage-polluted seawater [41].

1.2.2. Capsid structure

Kobuviruses are non-enveloped viruses with a diameter of approximately 300 Å [42]. The capsid has a pseudo T=3 icosahedral symmetry exhibiting 2-, 3- and 5-fold symmetry axes. Compared to other picornaviruses (e.g. enteroviruses), which are comprised of four capsid proteins VP4 (1A), VP2 (1B), VP3 (1C), VP1 (1D), kobuviruses only possess three capsid proteins VP0 (1AB), VP3 (1C) and VP1 (1D), each present in 60 copies. The kobuviruses VP0 is not auto-catalytically cleaved into VP4 and VP2 which falls in line with 11 other picornaviruses including human parechovirus [17, 43]. The size of VP0, VP3 and VP1 are 39.1, 29.9 and 24.2 kDa, respectively.

So far, the human AiV-A1 A846/88 is the only kobuvirus for which a high-resolution capsid structure is available [42, 44]. The capsid harbours an unusually high proline content and has three poly-L-proline type II (PPII) helices, one in VP0 and two in VP1 [42]. The longest PPII helix is at the C-terminus of VP1 pointing outwards from the capsid. These PPII helices are unprecedented in picornaviruses; for example, some enteroviruses have an arginine-glycine-aspartic acid (RGD) motif at this approximate position which is important for cell adhesion via recognition of integrin [45]. PPII helices are often involved in protein-protein interactions such as antigen recognition and signal transduction [46]. Therefore, the long external PPII helix could be utilised for cellular receptor recognition or may serve as virulence factor. HIV-1 and influenza A virus also possess PPII motifs that are important for their pathogenicity [47, 48]. Pre-treatment of AiV-A1 A846/88 or Vero cells with a peptide of the long PPII helix reduced CPE by about 40% at 48 h pi suggesting a potential competition for binding to the elusive host cell receptor [42].

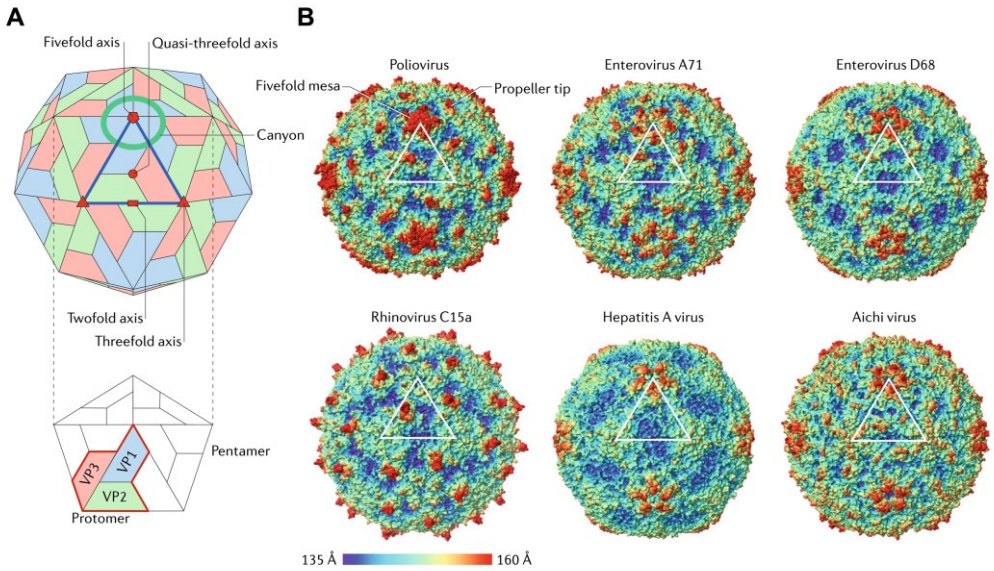

Figure 3. Schematic representation of a picornavirus capsid. (A) Schematic representation of a picornavirus capsid displaying the icosahedral asymmetric subunit (blue outline), the 2-, 3-, and 5-fold symmetry axes (red symbols) and the position of the "canyon" (green circle). The capsid shell is formed of sixty protomers comprised of VP1, VP3 and either VP2 and VP4 (e.g. enterovirus) or VP0 (e.g. kobuvirus). **(B)** Comparison of capsid surfaces between the genus Enterovirus (poliovirus, enterovirus A71, enterovirus D68 and rhinovirus C15a), the genus Hepatovirus (hepatitis A virus) and the genus Kobuvirus (aichivirus A1). White triangle outlines icosahedral asymmetric subunit. Capsids are rainbow-coloured based on the distance from the capsid centre ranging between 135 and 160 Å. This figure was adapted from Springer Nature Customer Service Centre GmbH: Springer Nature Reviews Microbiology Baggen et al. (2018) [49] Copyright.

1.2.3. Infection cycle

The cycle of infection can be divided in four steps: (i) attachment and internalisation, (ii) viral RNA translation and polyprotein processing, (iii) viral RNA replication and (iv) virion assembly and release. Figure 4 depicts a schematic overview on the life cycle of enteroviruses as they are the best-studied enteric picornaviruses.

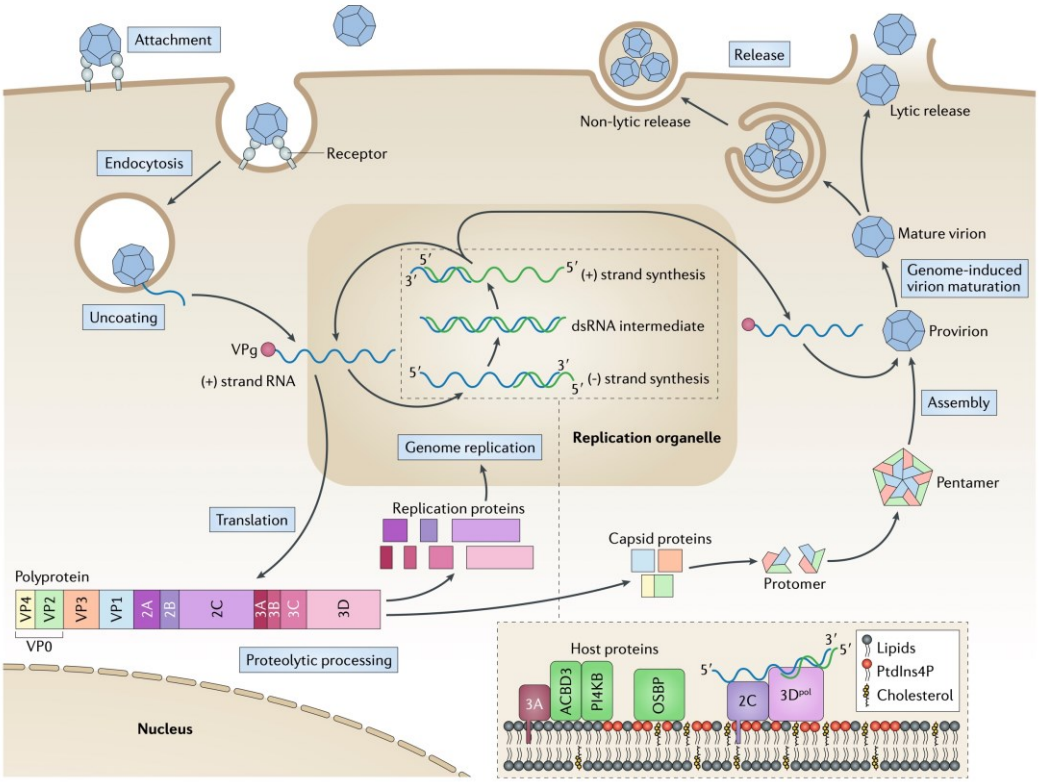

Figure 4. Schematic overview of the enterovirus life cycle. After attachment to the cell surface receptor, the virus is endocytosed and routed to a compartment suitable for uncoating and transfer of the genomic RNA into the cytoplasm. The genomic RNA is translated into a single polyprotein which is cleaved by viral proteases into capsid (VP0, VP1 and VP3) and viral proteins (2A–2C and 3A–3D). Viral replication is conducted by the RNA-dependent RNA polymerase which synthesises negative (-) strand RNA that serves as template for the synthesis of new positive (+) strand genomic RNA. While early in infection, they are further used for minus strand synthesis, they are utilised for translation or encapsidation into progeny viruses in later stages. Replication occurs in membranous organelles known as replication organelles. Capsid proteins self-arrange into protomers and pentamers and, with the help of the replication machinery, encapsidate the genomic RNA, forming provirions. In most picornaviruses (e.g. enterovirus), the provirions further convert by cleavage of VP0 into VP4 and VP2 into mature virions, presumably catalysed by the encapsidated RNA. The progeny particles are released either non-lyticly and/or lyticly. This figure was adapted from Springer Nature Customer Service Centre GmbH: Springer Nature Reviews Microbiology Baggen et al. (2018) [49] Copyright.

Attachment and internalisation

The cell surface receptor(s), which at least in part determine(s) the tissue tropism is/are still unknown for AiV-A1. Additionally, the entry mechanism and subsequent endosomal routing remain to be characterized. In enteric picornavirus infections, the host usually sheds infectious viral particles in the intestinal lumen, which are transmitted by stool and finally taken up orally by the next host via contaminated foods or surfaces. In the next host, the virus passes through the gastrointestinal tract until it reaches the small intestinal epithelium expressing the cognate attachment receptor(s). The receptor(s) interaction triggers internalisation which is mediated via endocytosis. Once the particle has been directed to an endosomal pathway, cellular factors contribute to the overall uncoating process. During this process the capsid proteins undergo a conformational change which results in the ejection of the viral genome from the endosome into the cytoplasm [49].

Viral RNA translation and polyprotein processing

After the arrival of the viral genome in the cytoplasm, the viral translation commences. In AiV-A1, the IRES initiates the translation of the one ORF into a single polyprotein that is co- and post-translationally cleaved by the viral protease 3C and 3CD resulting in viral proteins as described above. AiV-A1 A846/88 3C protein is a cysteine protease that contains a catalytic triad formed by histidine, aspartate/glutamate, and cysteine which is highly conserved among picornaviruses [17]. However, studies showed that the cleavage site between VP1-2A, which is normally facilitated by the 2A protein, is insufficiently cleaved by the 3C protein and rather a complex of 3CD and 2A proteins is required [24]. Unlike many other picornaviruses, the kobuviral L and 2A protein lack protease activity [17]. In poliovirus and other enteroviruses,

the 2A protein is involved in genome replication and polyprotein cleavage [24, 50]. Interestingly, 2A of AiV-A1 shares a conserved H-NC box motif, occasionally encompassing a transmembrane domain, with 11 other picornavirus genera, including human parechovirus [51]. This motif is related to the phospholipase PLA2G16 (also known as Hrev107) which has been identified as an enterovirus host factor [52-54]. The kobuvirus L protein contributes to viral replication and genome encapsidation [55]. Moreover, the L protein of AiV-A1 A846/88 was classified as a novel class 4 integrated stress response (ISR) antagonist that abrogates cellular induced shut-down of translation similar to the beluga whale coronavirus protein AcP10 [56].

Replication

The replication of the genomic RNA is conducted by the 3D protein, an RNA-dependent RNA polymerase. Similar to other positive-strand RNA viruses, the replication itself takes place in virus generated membranous structures often referred to replication organelles (ROs) [57]. For poliovirus, ROs formation requires the viral membrane-associated proteins 2BC and 3A that hijack cellular components involved in lipid metabolism resulting in a massive rearrangement of cellular membranes [58]. It is thought that the main source are the endoplasmic reticulum and the Golgi apparatus, but details on the ROs formation are still fragmentary [49]. Recently, AiV-A1 kvgh2010 has been shown to induce autophagic flux in A549 cells (human lung carcinoma-derived cell line) resulting in the formation of autophagosomes [59]. Importantly, ROs are thought to mask and shield the viral replication machinery from the innate immunity and thus from degradation [60].

Virion assembly and release

The encapsidation of the genomic viral RNA is believed to happen in the vicinity of membranous compartments such as the ROs and/or autophagosomes [61]. The capsid proteins VP0, VP3 and VP1 self-assemble into the 5S protomers and further into the 14S pentamers. These pentamers assemble into either empty 75S procapsids or genomic viral RNA-containing 150S provirions [62]. The exact mechanism of genomic RNA encapsidation for kobuviruses has not been elucidated yet. Nevertheless, the 5′ stem-loop SL-A — the first nucleic acid packaging signal to be found in picornaviruses — and the L protein were determined to be essential for AiV-A1 A846/88 packaging [22, 63]. Moreover, AiV-A1 VP0 is not auto-catalytically cleaved into VP4 and VP2, thus the assembled 150S provirion already represents the infectious viral particle.

Finally, progeny viruses are released via lytic or non-lytic egress mechanisms [64]. While lytic egress results in cell death, non-lytic egress occurs through membranous enclosures (e.g. exosome, microvesicles and secretory autophagosomes). Which egress mechanism ensues depends on the infected cell line and the picornavirus type.

1.3. Endocytic and endosomal pathways

Endocytosis describes the uptake of fluid, solutes, ligands, components of the plasma membrane as well as particles by invagination of the plasma membrane [65]. This allows the cell to interact with its environment through nutrient uptake, extracellular milieu sensing, maintaining and homeostasis of plasma membrane (PM) composition (chemical aspect) and surface area and tension [66]. In general, endocytosis can be separated in two steps: (i) uptake mechanism and (ii) endocytic trafficking. After a cargo has been internalised, it is ferried through an elaborate network of vesicular-tubular compartments referred to as endosomes. The following chapters illustrate endocytic pathways particularly exploited in the context of viral infections.

1.3.1. Uptake mechanisms

Currently, six major types of uptake mechanisms have been described: (i) clathrin-(coated-mediated endocytosis (CME), (ii) fast endophilin-mediated endocytosis (FEME), (iii) clathrin-independent carrier/glycosylphosphatidylinositol-anchored protein enriched early endocytic compartment (CLIC/GEEC) endocytosis, (iv) macropinocytosis, (v) phagocytosis and (vi) caveolin-mediated endocytosis [67] (Figure 5). Several authors also distinguish a lipid raft-mediated endocytosis, in part by participation of the fotillin-1/2 integral membrane proteins [66]. It is of note that not every cell line engages all uptake mechanisms and new pathways selectively used in specialized cells are still being described. Additionally, while several uptake pathways have unique features, some share components resulting sometimes in a blur between the boundaries.

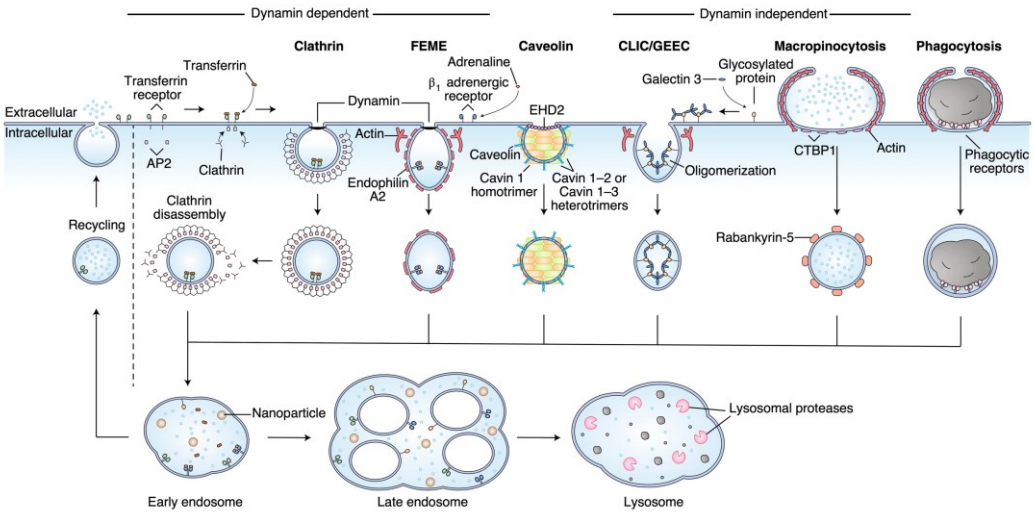

Figure 5. Schematic overview of different endocytic uptake mechanisms. In general, the different pathways can be divided by the usage of clathrin and dynamin. **(i)** The adaptor complex, AP2, commences CME (clathrin-coated pit-mediated endocytosis) by guiding clathrin to the cytosolic receptor domains, orchestrating the formation of a clathrin-coated pits. **(ii)** FEME (fast endophilin-mediated endocytosis) is initiated by receptor–ligand interactions and controlled by actin polymerization and endophilin A2 recruitment. CME and FEME depend on dynamin for fission of vesicles from the plasma membrane. **(iii)** Caveolae formation requires caveolin and cavin proteins. The caveolae neck is stabilised by EHD2. **(iv)** clathrin-independent carrier (CLIC)/ glycosylphosphatidylinositol-anchored protein enriched early endocytic compartment (GEEC) is dynamin and clathrin independent and requires galectin for clustering of glycolipids and glycoproteins for invagination. **(v)** Macropinocytosis necessitates receptor stimulation and results in the formation of large vesicles. Actin and BAR domains orchestrate CLIC/GEEC endocytosis and macropinocytosis. Macropinocytosis also critically depends on the small GTPases ARF6 and Rac1. **(vi)** Phagocytosis involves actin polymerisation and massive membrane protrusions for cargo uptake, which is almost exclusively performed by professional phagocytes (neutrophiles, macrophages and dendritic cells). After internalisation, the many vesicles fuse with early endosomes before being sorted and directed to distinct pathways. This figure was adapted from Springer Nature Customer Service Centre GmbH: Springer Nature Nanotechnology Rennick et al. (2021) [67] Copyright.

Clathrin-mediated endocytosis (CME)

CME is the by far best-studied endocytic uptake mechanism which involves the uptake of macromolecules such as growth factors, transferrin (iron), low-density lipoproteins (cholesterol) [68]. Cargo binding to cognate receptors at the surface leads to receptor clustering and/or phosphorylation of their cytosolic domain [69]. This in turn initiates the recruitment of soluble clathrin, a scaffold protein, via the adapter complex AP-2 that connects clathrin to the plasma membrane, which results in the formation of clathrin-coated pits (CCP) and their subsequent maturation into clathrin-coated vesicles (CCV). Beside AP-2, the small GTPase dynamin is necessary for the CCV scission in combination with the AP-2 binding protein eps15 and the membrane-bending protein amphiphysin [70]. After the formation of CCV, clathrin becomes removed by the heatshock protein hsc70 accompanied by ATP hydrolysis, making the membrane accessible for fusion with early endosomes. Several rhinoviruses including major (e.g. RV-89) and minor (e.g. RV-A2) group representatives have been shown to exploit CME for infection via intercellular adhesion molecule 1 (ICAM-1) and low-density lipoprotein receptor (LDLR) interaction, respectively [71, 72].

Fast endophilin-mediated endocytosis (FEME)

FEME is clathrin-independent but dynamin-dependent and is a recently described important pathway for rapid endocytosis [73]. Endocytic carrier formation is tiggered by specific ligand-receptor interaction involving G-protein-coupled receptors such as the IL-2 receptor and growth factor receptors (e.g. EGFR). The SH3 domain of endophilin interacts directly or indirectly through intermediary proteins with the cognate receptor and is further stabilised by the membrane-binding protein lamellipodin. EV-A71 exploits the FEME for infection of polarised Caco-2 cells [74].

Clathrin-independent carrier / glycosylphosphatidylinositol-anchored protein enriched early endocytic compartment (CLIC/GEEC)

CLIC/GEEC is dynamin and clathrin independent and occurs constitutively in cells featuring this pathway. It is a high-capacity pinocytic pathway and does not need a specific ligand-receptor interaction [75]. Various surface proteins are being internalised via this mechanism such as glycosylphosphatidylinositol-anchored proteins (GPI). Intracellularly it is regulated by small GTPases Cdc42 and ARF1 and involves the BAR domain protein GRAF1 [76]. At the cell surface, it is proposed that clustering of glycosylated proteins or glycosphingolipids is facilitated by galectins (carbohydrate binding protein) which coordinate the invagination and formation of pleomorphic tubular structures [77]. SV40, an oncogenic DNA virus, is known to hijack the CLIC/GEEC mechanism [67].

Macropinocytosis

Macropinosomes are formed by plasma membrane protrusions driven by actin assembly which results in the enclosure of large extracellular volumes as the macropinosome collapses back [78]. Depending on the cell type, macropinocytosis can be a constitutive or an induced mechanism [79]. Induction is stimulated by various stimuli such as proteoglycans or G-protein-coupled receptors and receptor tyrosine kinase family receptors (e.g. EGFR). Furthermore, actin ruffling at the plasma membrane is essential as well as the small GTPases ARF6 and Rac1. Only a small number of viruses have been reported to utilise this entry mechanism for infection. [80]. Recently, it has been suggested that E30 follows a macropinocytic uptake mechanism [81].

Caveolin-mediated endocytosis

Caveolae are the second best-studied entry mechanism substantiated by an extensive literature associating it with endocytosis. However, the field remains controversial since knockout of caveolar components in any system have not revealed an absolute requirement of caveolae for endocytic uptake [82, 83]. It has been proposed that the FEME and the CLIC/GEEC pathways may have been mistaken for caveolin-mediated endocytosis, due to poor specificity of endocytic inhibitors [67]. Additionally, only a few cargos are proposed to depend on caveolae. Caveolae are formed by caveolin and cavin and require accessory factors such as the dynamin-related ATPase EHD2. Caveolins are integral membrane proteins and found in various different compartments. It is believed that this homogeneous distribution contributed to the confusion over the importance of caveolae in endocytic pathways. So far, only a few viruses have been reported to preferentially hijack this pathway such as H1N1 influenza virus and human coronavirus 229E [84-86].

1.3.2. Endosomal trafficking

After cargo internalisation by one or more endocytic uptake mechanisms mentioned above, the vesicles become part of an endosomal network which allows for vectorial transport between distinct membranous compartments [70]. The main function of the endosomal network is to gather, sort and direct the cargo to their final destination. Upon uptake, the initial vesicles undergo homotypic fusion forming early endosomes which conduct the sorting process [87]. Ultimately, sorted cargo can be sent back to the cell surface via (i) the recycling pathway or is degraded via (ii) the lysosomal pathway (Figure 6). The regulation of endosomal trafficking is accomplished by a strict spatial and temporal control of endosomal identity [70]. This identity is shaped by a combination of elevating acidification, composition

and exchange of phosphatidylinositol phospholipids, Rab family GTPases and various effector proteins. Rab proteins are essential regulators for endosomal trafficking [88]. They switch between a GTP-bound active state and a GDP-bound inactive state. Furthermore, they need to interact with specialised effector proteins to form higher-order molecular assemblies to carry out various functions such as vesicle tethering, fusion, budding and motility.

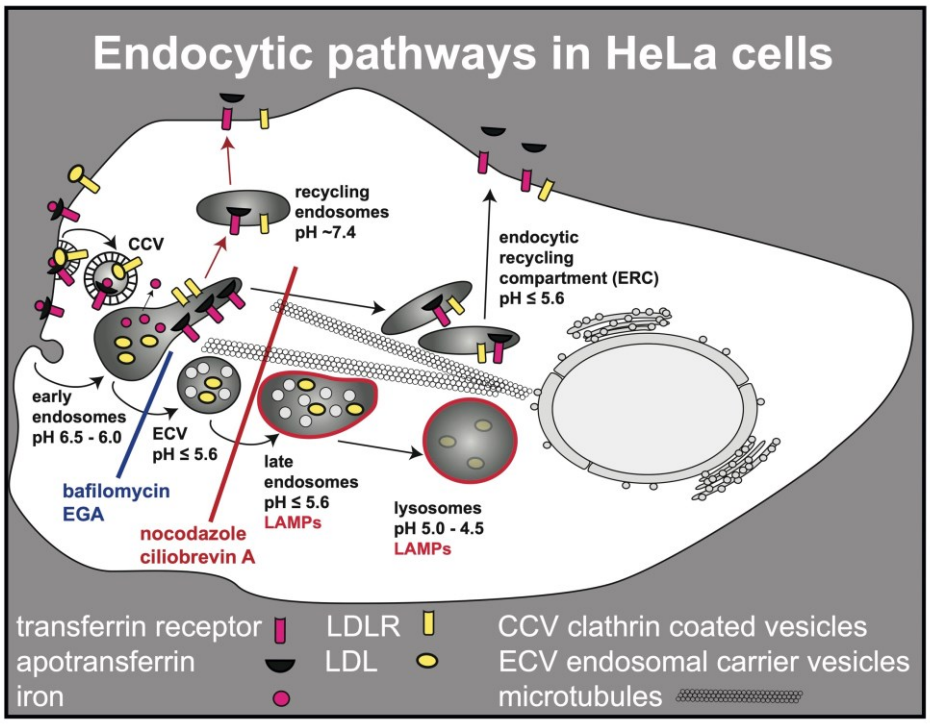

Figure 6. Schematic overview of endosomal trafficking exemplified by LDLR and TfR. Upon clathrin-mediated internalization of LDLR and TfR, the initial vesicles fuse into early endosomes which sort cargo for vectorial transport via endosomal networks. LDLR and TfR lose their cargo, LDL and iron, respectively, in the early endosome due to the mild acidic milieu. While LDL is further routed towards the lysosome for degradation, the LDLR and TfR are recycled back to the cell surface via recycling endosomes (fast route) or via the endocytic recycling compartment (ERC) (slow route). Early endosomes mature into late endosomes which can be accompanied by endosomal carrier vesicles (ECV). Bafilomycin A1 and EGA arrest the cargo transport from early to late endosomes. Nocodazole and ciliobrevin A target the late endosome/lysosome and ERC transport by acting on the microtubule and dynein network. Figure was adapted from Conzemius et al. (2016) [89].

Well-studied examples of endosomal sorting and trafficking are the LDLR and transferrin receptor (TfR) [88]. Both arrive in the early endosome via clathrin-mediate endocytosis [90, 91]. Early endosomes are characterized by a mildly low pH from approximately 6.8 to 6.3 which is attributed to the V-type vacuolar H^+ ATPase pump, which actively pumps hydrogen into the endosomal lumen [92]. Additionally, Rab4, Rab5 and the Rab5 effector protein early endosome antigen 1 (EEA1) are well-described markers for early endosomes [88]. Due to the mildly acidic environment the LDLR and TfR lose their cargo LDL and iron, respectively.

While the LDL remains in the early endosome, the LDLR and TfR, as for most membrane proteins and receptors, are routed by Rab4 to one of the two recycling pathways which requires extensive tubulation of the early endosome [88]. The recycling endosome has the fastest kinetic ($t_{1/2}$ = 5 min) and a relatively physiological pH. The endocytic recycling compartment (ERC) additionally harbours Rab11 and proceeds much slower ($t_{1/2}$ = 15–30 min) and the pH drops below 5.6 [93].

The early endosome continues to mature, accompanied by Rab7 and increasing acidification, into a late endosome and cargo is further sorted by inward budding to form intraluminal vesicles (ILVs). Late endosomes are often referred to as multivesicular bodies [94]. Proteins destined for degradation are sorted into ILVs by the endosomal sorting complexes required for transport (ESCRT) which recognises a monoubiquitylation. During the maturation phase small vesicles containing nascent Rab7 can fission off from early endosome termed endosomal carrier vesicles (ECV) and later fuse again with more stable late endosomes [95]. Finally, the late endosome fuses with a lysosome resulting an endolysosome in which the cargo is being degraded at approximately pH 4.5 to 4.0. [93]. Late endosomes

and lysosomes are marked by heavily glycosylated transmembrane proteins called lysosome-associated membrane proteins (LAMPs), a key biomarker for their identification [89].

The ERC and the late endosome/lysosomal pathway depend on a microtubule network for directional transport of their vesicles [96-98]. This is facilitated by motor proteins such as dynein that walk from the cell periphery towards the microtubule-organizing centre (MTOC) at the microtubules minus ends [99].

In the past, the endosomal trafficking of various rhinoviruses have been studied on numerous occasions [100]. While LDLR-binding RV-A2 is ferried towards the lysosomal pathway where it uncoats in the late endosome, ICAM-1-binding RV-A89 is routed to the much longer ERC pathway for genomic RNA release [89, 101, 102]. Interestingly, RV-B14, also a major group rhinovirus that requires ICAM-1 for internalisation, uncoats en route to the lysosome by rupturing endosomes [103]. It is believed that the stronger affinity of RV-A89 for ICAM-1 is responsible for its routing to the ERC, while RV-B14 already dissociates from ICAM-1 in the early endosomes and thus, is ferried along the lysosomal pathway [72, 89]. Additionally, this exemplifies the complexity of viral endosomal trafficking, since a common entry receptor is not a prerequisite for routing to the same endosomal compartment.

1.4. The Antiviral State

During or after internalisation, viruses are confronted by the innate immunity, which consistently keeps a lookout for pathogens, and in case of their detection, raise a cellular alarm. While the adaptive immunity requires several days for build-up due to cellular activation and proliferation (e.g. T cells and B cells) which results in a highly specified targeting of certain molecules, the innate immunity acts rapidly due to their fast activation and its continuous state of full functionality [104].

In general, pattern recognition receptors (PRRs) sense pathogen associated molecular patterns (PAMPs) which triggers downstream signalling cascades leading to the production of interferons (IFNs). IFNs are key players of the innate immunity as they inform on the antiviral state by secretion and sensing in a autocrine and paracrine manner which in turn induces the expression of interferon-stimulated genes (antiviral effector proteins), in many instances ultimately clearing the viral infection (ISGs) [105].

IFNs are a diverse group of cytokines and currently three main types are being differentiated: type I, type II and type III IFN [106]. Type I IFN has been discovered more than 60 years ago and constitute the largest IFN family in humans with 17 different types: IFN-α (13 in humans), IFN-β, IFN-ϵ, IFN-κ, IFN-ω. Additionally, they have the broadest functionality such as anti-pathogen activities (antiviral, antibacterial and antifungal), anti-proliferative functions and modulation of innate and adaptive immunity [107]. IFN type I is universally expressed and sensed by the heterodimeric IFN-α receptor 1 and 2 (IFNAR) which is expressed on all nucleated cells [108, 109].

Type II IFN only harbours one member, IFN-γ, which is mainly produced by natural killer cells, natural killer T cells (NKT) and innate lymphoid cells (ILCs). Although being a key modulator of the cellular innate and adaptive immunity, it is not directly involved in the intracellular defence mechanisms [110].

Type III IFN have been discovered more recently and were thought to be redundant to type I IFN as they share very similar signalling pathways and ISG expression [106]. However, research showed that type III IFN elicit distinct mode of actions and functions compared to type I IFN. Type III IFN is comprised of four members: IFN-λ1 (IL-29), IFN-λ2 (IL-28A), IFN-λ3 (IL-28B) and IFN-λ4 [111]. While the function of IFN-λ1, IFN-λ2, IFN-λ3 are well established, the role of IFN-λ4 during infection remains controversial [112]. They are

expressed by most cell types and they interact with the heterodimeric interferon lambda receptor 1(IFNLR1 or IL-28R) and the interleukin 10 receptor 2 (IL-10R2) [113]. However, not all cell types can sense type III IFNs as IFNLR1 is mainly found on epithelial cells (e.g. lung, intestine, vaginal and hepatocytes) [114].

PRRs are differentiated based on their sensed PAMP and their location within the cell. The most important PRRs for the detection of RNA viruses are: Toll-like receptors (TLRs) 3, 7, 8 and RIG-like receptors (RLRs) [104]. TLR 3, 7 and 8 are located in endosomes as transmembrane proteins detecting single-stranded (ss) and double-stranded (ds) RNA, respectively. RLRs are comprised of the retinoic acid-inducible gene I (RIG-I) and melanoma differentiation- associated protein 5 (MDA5) and laboratory of genetics and physiology 2 (LGP2) and located within the cytosol where they detect ssRNA. However, LGP2 lacks the caspase activation and recruitment domain (CARD) and thus rather has a regulatory function in RLR sensing than signal transduction [115].

Due to their different localisation, each PRR interacts with different key adaptor proteins to convey the signalling cascade. For TLR3, TLR7/8 and RLRs it is TIR-domain-containing adapter-inducing interferon-β (TRIF), myeloid differentiation primary response 88 (MyD88) and mitochondrial antiviral-signalling protein (MAVS), respectively [116]. Ultimately, each pathway results in the induction of the protein complexes TBK1/IKK-ϵ and IKK-$\alpha/\beta/\gamma$ [115, 117]. Tank binding protein (TBK1) and IκB kinase I (IKK-ϵ) phosphorylate the transcription factors interferon regulatory factor (IRF) 3 and 7 which leads in homo-dimerization and their translocation to the nucleus. Concurrently, IKK-$\alpha/\beta/\gamma$ induce proteasomal degradation of the NFκB inhibitor IκB-α by phosphorylation which confers NFκB modification which allows its shuttling to the nucleus. In the nucleus, IRF3, 7, NFκB

and other co-factors form the enhanceosome that binds to promotors resulting in type I and III IFN transcription

Translated and secreted type I and type III IFNs act in an autocrine and paracrine manner on their cognate receptors triggering the Jak-STAT signalling pathway. The Janus family tyrosine kinases Jak1 and Tyk2 phosphorylate the signal transducers and activators of transcription (STATs) 1 and 2 allowing for homo- and heterodimerisation and transport to the nucleus. While STAT1 dimers bind to the gamma interferon stimulation site (GAS), STAT1 and STAT2 hetero-dimers further interact with IRF9 forming the transcription factor interferon-stimulated gene factor 3 (ISGF3). Both complexes lead to the transcription of ISGs and further enhancement of the antiviral state [118].

Overall, infection of the human intestine with enteric viruses leads to a higher expression of type III IFN and to a lesser extend of type I IFN [119, 120]. It is currently believed that type I IFNs protect from virus dissemination and lamina propria and type III IFNs shields the epithelial surface itself [120, 121]. Moreover, ISG expression kinetics are differently regulated between type I and III IFN [122]. While type I IFN induces a fast and high magnitude in ISG induction, type III IFN is much slower in the expression but more sustained in time. This temporal induction of ISGs results in the creation of a unique antiviral environment [120].

1.5. Acute gastroenteritis

Acute gastroenteritis (AGE) is an inflammation of the mucosal epithelium in the small or large intestine [123]. According to the Global Burden of Diseases, Injuries, and Risk Factors Study from 2016 AGE was the eight leading cause of death among all age groups with estimated 1,655,944 deaths and the fifth cause of death in children under 5 years with more than 446,000 estimated deaths [124]. Despite the significant reduction in mortality in the past 20 years,

AGE still poses a major public health issue [125] especially since virus induced diarrhoea is not declining [126]. While most deaths occur in developing countries, the health systems in developed nations are faced with economic burden due to high rates of hospitalisations [127]. AGE manifests in abrupt symptoms such as vomiting, watery diarrhoea and low-grade fever [128]. Typically, it is self-limited and recovery occurs within 2–5 days with a treatment focus on maintaining patient hydration.

While bacteria and protozoa only account for approximately 10%–20% and less than 10% of AGE cases in children, respectively, viruses are responsible for approximately 70% [129, 130]. The most prominent representatives are rota-, noro-, sapo-, astro-, and adenovirus [131]. Rotavirus belonging to the family *Reoviridae* has caused the majority of deaths in children worldwide and elicits more severe gastroenteritis than most other enteric pathogens [128]. The rotavirus vaccines implemented in 2006 in 95 countries resulted in a 50–90% reduction in hospitalisation. Norovirus belonging to the family *Caliciviridae* is the primary cause for AGE among all age groups, including foodborne outbreaks [128]. Noroviruses are genetically and antigenically highly diverse, which impedes vaccine development.

Despite more than 20 viruses having been identified as aetiological agents for AGE, it is estimated that in up to 40%–50% of incidences the causative viral agent still remains unknown [132-135]. Improved detection methods such as next generation sequencing resulted in the discovery of previously unknown enteric viruses [131]. However, their unequivocal link to cause AGE still has to be established, as for AiV-A1. Additionally, ambiguous epidemiological observations and a lack of suitable cell lines or in vivo models contribute to the uncertainty.

1.5.1. Human intestinal enteroids

The discovery of intestinal stem cells producing high levels of leucine-rich repeat-containing G protein-coupled receptor 5 (Lgr5+) by Hans Clever's group in 2007 advanced the field of stem cell-based tissue culturing [136]. Nowadays, two possibilities to generate "mini-intestines" are available: (i) from human adult stem cells by isolating intestinal crypts or (ii) from human embryonic or inducible pluripotent stem cells (iPSCs) [137] (Figure 7). Adult intestinal crypts are usually obtained from surgical biopsies. While adult stem cells will give rise to enteroids (derived from small intestine) or colonoids (derived from colon), iPSCs will generate organoids. The main difference is that organoids develop a mesenchymal layer essential for maintenance of epithelial tissue identity [138]. After stem cell isolation, they are embedded in Matrigel, which serves as a scaffold, and cultured in growth media enriched with distinct growth factors: Wnt3a, R-spondin, epidermal growth factor (EGF), and Noggin [139]. This will result in the generation of three-dimensional spheroids comprised of a single epithelial layer with an enclosed apical lumen and a basolateral exterior. These spheroids can be transitioned to culture systems on plates or transwells. Due to their close recapitulation of the structural complexity and cellular diversity of the human intestine, organotypic cultures allow for more insight into the pathogenesis of viral infections compared to carcinoma cell lines and animal models [140]. Additionally, cellular tropism, receptor usage and innate immunity can be deeper and more faithfully deciphered compared to previous models [141].

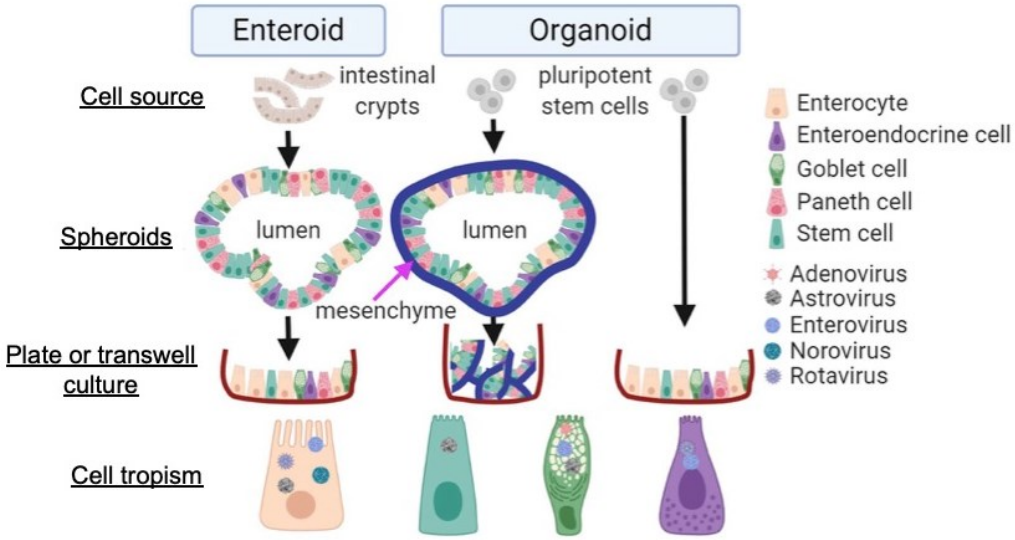

Figure 7. Schematic representation of different intestinal stem cell-derived tissue models. Human intestinal enteroids and organoids are cultured from adult intestinal crypts containing Lgr5+ cells or from iPSCs, respectively. These stem cells are embedded in Matrigel and cultured in growth medium containing Wnt3a, R-spondin, epidermal growth factor (EGF), and Noggin. After their maturation, they closely recapitulate the structural complexity and cellular diversity of the human intestine. Compared to enteroids, organoids possess a mesenchymal layer. Initial enterospheres, with an enclosed apical lumen and a basolateral exterior, can be disaggregated and re-seeded in culture plates or transwells with an accessible apical site. Indicated in the legend (right site) are the common cell types and the so far studied enteric pathogens and their cell tropism. Figure was adapted from Kolawole and Wobus (2020) [142].

This relatedness to a more natural system allowed for the study of previously unculturable enteric pathogens such as human norovirus [143]. Despite the initial successes, not all norovirus genotypes (e.g. GII.3) of the highly diverse group could be propagated. It was found that the pre-treatment of intestinal epithelium with bile acid was necessary for the replication of certain genotypes [144]. Bile acid triggers ceramide production at the cell surface leading to ceramide-rich microdomain formation and thus, receptor clustering promoting norovirus uptake [145]. Recently, the sever pathology and extensive water loss induced by rotavirus infection was found to be due to calcium and nucleotide signalling in human intestinal

enteroids [146, 147]. The viral non-structural protein 4 (NSP4) triggers intercellular calcium waves that facilitate the secretion of adenosine diphosphate (ADP). Bystander cells recognise the ADP via purinergic receptors that again induce intracellular calcium waves. Additionally, the release of inositol trisphosphate (IP3) is triggered via phospholipase C, which allows for the production of cellular factors (e.g. serotonin). All these factors in combination are the main driving forces for acute diarrhoea. The study of different enteroviruses in foetal-derived intestinal enteroids showed that E11 induced a massive epithelial disruption [148, 149]. Adenovirus was found to preferentially infect goblet cells and it was sensitive to type I and type III IFN treatment [150]. More recently, single-cell RNA sequencing (ssRNAseq) of human ileal organoids exhibited the elaborated innate immune evasion in SARS-CoV-2 infected cells [141].

2. MATERIALS AND METHODS

2.1. Cell Lines and Virus Strains

All cell lines were obtained from ATCC, except the A549 cells. Originally from Sigma, (86012804), these were kindly provided by Dr. Walter Berger (Institute of Cancer Research, Medical University of Vienna, Austria) and the RKO cells (originally from ATCC, CRL-2577), which were a generous gift from Dr. Gijs Versteeg (Max Perutz Labs, Vienna, Austria). Cell lines were routinely cultivated in the growth media specified in Table 1 at 37°C in a 5% CO_2 atmosphere. For infection assays, the standard medium was replaced with infection medium prior to viral inoculation (Table 1).

Viruses used in this study were (i) AiV-A1 strain A846/88 (prepared with the plasmid pAV-UCSF (GenBank accession no. JQ281544; kind donation from Joseph L. DeRisi University of California at San Francisco, USA [151]) and (ii) CVB3 strain Nancy (kind donation from Frank Kuppeveld, University of Utrecht, Netherlands). The AiV-A1 A846/88 is also simply referred to as AiV-A1.

Table 1. Immortalized cell lines that were tested for AiV-A1 infection. Cell lines were cultivated in the respective growth medium, as specified by ATCC, and infected in the correspondently adapted infection medium.

Cell line	Tissue	Growth medium	Infection medium
HeLa	Epithelial, human cervix	• DMEM (Gibco, 21063-029) • 10% FBS (Sigma, F7524) • 1% Pen-Strep (Sigma, 15140-122)	• DMEM (Gibco, 21063-029) • 2% FBS (Sigma, F7524) • 1% Pen-Strep (Sigma, 15140-122)
RKO	Epithelial, human colon		
Vero	Epithelial, African green monkey kidney		
A549	Epithelial, human lung	• Ham's F-12K Medium (Gibco, 21127-022) • 10% FBS (Sigma, F 7524) • 1% Pen-Strep (Sigma, 15140-122)	• Ham's F-12K Medium (Gibco, 21127-022) • 2% FBS (Sigma, F7524) • 1% Pen-Strep (Sigma, 15140-122)
T84	Epithelial, human colon		
Caco-2	Epithelial, human colon	• DMEM (Gibco, 21063-029) • 10% FBS (Sigma, F7524) • 0.1 mM NEAA (Lonza, 13-114E) • 1% Pen-Strep (Sigma, 15140-122) • 1 mM Pyruvate (Sigma, S8636)	• DMEM (Gibco, 21063-029) • 2% FBS (Sigma, F7524) • 0.1 mM NEAA (Lonza, 13-114E) • 1% Pen-Strep (Sigma, 15140-122) • 1 mM Pyruvate (Sigma, S8636)
HCEC 1CT	Epithelial, human colon	• DMEM and Medium 199 Earle's, 4+1 (Biochrom, Cat# F0435 and Cat# FG0615) • 4 mM GlutaMAX™-1 (100X), (Gibco, Cat# 35050-038) • 2% Cosmic Calf Serum (Hyclone, Cat# SH30087) • 20 ng/ml EGF (Sigma-Aldrich, Cat# E9644) • 10 μg/ml Insulin (Sigma-Aldrich, Cat# I9278) • 2 μg/ml Apo-Transferrin (Sigma-Aldrich, Cat# T2036) • 5 nM Sodium-Selenite (Sigma-Aldrich, Cat# S5261) • 1 μg/ml Hydrocortisone (Sigma-Aldrich, Cat# H0396) • 1% Pen-Strep (Sigma, 15140-122)	

2.2. Aichivirus A1 strain A846/88 Production

2.2.1. In vitro transcription

AiV-A1 strain A846/88 was generated via transfection of viral RNA obtained by *in vitro* transcription from the plasmid pAV-UCSF into Vero cells; pAV-UCSF carries the full-length cDNA of AiV-A1 strain A846/88. The plasmid was processed similarly as in Corbic Ramljak et al. (2018) [152]. Briefly, pAV-UCSF (20 μg) was linearized with HindIII, the digest was loaded on a 0.5% agarose gel, and run in 0.5x TAE buffer (Table 3) supplemented with 0.5 μg/ml ethidium bromide. The band corresponding to 11.5 kbp was excised and purified with the peqGOLD gel extraction kit (PeqLab, USA). *In vitro* transcription was performed with the T7 Ribomax Large Scale RNA Production System (Promega, USA) for 4 h at 37°C according to the manufacturer's instructions. DNA was removed by RQ1 (provided in the kit) and the RNA was recovered with TRIzol reagent (TRIzol, Invitrogen, USA) (see chapter 2.4).

Size and quality of the *in vitro* transcript was confirmed by agarose gel electrophoresis; two μl of the RNA sample were mixed with 18 μl of the RNA sample buffer and 5 μl of RNA loading buffer, the mix was heated for 10 min at 70°C and applied on a 1% agarose gel in 1xTAE buffer supplemented with 0.5 μg/ml ethidium bromide.

Table 2. Buffers used for gel electrophoresis.

Buffer	Composition
1x TAE buffer	• 40 mM Tris (pH 7.6) • 20 mM acetic acid • 1 mM EDTA
5x MOPS buffer	• 0.2 M MOPS (pH 7.0) • 50 mM sodium acetate • 5 mM EDTA (pH 8.0)
RNA loading buffer	• 50% glycerol • 1 mM EDTA • 0.4% bromophenol blue
RNA sample buffer	• 10 ml deionized formamide • 3.5 ml 37% formaldehyde • 2.0 ml 5x MOPS buffer (final concentration 0.7x)

2.2.2. RNA-lipofectamine transfection

To generate infectious AiV-A1, different cell lines (see Table 1) were transfected with the above *in vitro* transcribed AiV-A1 RNA. The respective cell lines were grown in six-well plates to full confluency in the growth media specified above. 1, 2, and 4 µl of lipofectamine 2000 (Invitrogen, USA) were mixed with 100 µl of Opti-MEM (Gibco, USA). In parallel, three times approximately 1 µg (e.g. 1 µl) of viral RNA was mixed with 100 µl of Opti-MEM. Each of the above three (1, 2, and 4 µl) lipofectamine mixes was then combined with one of the diluted RNA mixes and incubated for 10 min at RT, followed by dropwise addition to the medium of the cells and gentle swirling. One well was used as negative control where the viral RNA in the transfection mixture was replaced by the same volume of ddH_2O. Three days post transfection the cells were examined for the presence of a cytopathic effect (CPE) under the microscope and the contents of the wells were collected using a cell scraper. Progeny virus

was released and crudely purified as described in chapter 2.3., and the viral titre determined as detailed in chapter 2.6..

2.2.1. Large-scale AiV-A1 purification and concentration

Forty-five T-175 cm^2 flasks were infected with a routinely produced, lower titre AiV-A1 seed virus stock (at an MOI = 0.1). Three days post infection (pi) approximately 90% of the cells were lysed and the flasks were transferred to -80°C. On the next day, the flasks were thawed, remaining cells were scraped off with a cell scraper and, together with the medium, collected in fresh tubes on ice. From the obtained, about 950 ml primary cell lysate, seed virus was produced as described in chapter 2.3.. The following steps were adopted with minor changes from a protocol previously established in the lab for large-scale purification of rhinovirus RV-A2 ([153]).

The crude AiV-A1 seed virus suspension was centrifuged at 4,000 rpm for 10 min at RT (Beckman J6-HC centrifuge and Beckman JS-4.2 swinging-bucket rotor) resulting in a pellet and SN. While virus was precipitated from the SN by addition of PEG 6000 to a final concentration of 7% followed by an overnight (o/n) incubation at 4°C, the pellet was resuspended in 20 ml virus buffer B (VB-B) (10 mM Tris/HCl pH 7.4, 10 mM EDTA) and homogenised with 40 strokes in a tight-fitting Dounce homogenizer. The resulting suspension was then centrifuged at 4,000 rpm for 10 min at RT in a table-top centrifuge (Eppendorf 5810R centrifuge and Eppendorf A-4-81 rotor) and the newly formed SN was combined with the first SN-PEG mixture for a second o/n precipitation.

The combined mixture was again centrifuged at 4,000 rpm for 30 min at RT (Beckman J6-HC centrifuge and Beckman JS-4.2 swinging-bucket rotor); the SN was removed and the pellet was covered with 60 ml 20 mM Tris/HCL (pH 7.5), 2 mM $MgCl_2$ (VB-A) and

resuspended by sonication in an ultrasonic bath for 3 min. Any insoluble material was removed by 30 min spinning at 15,000 rpm at 4°C (Beckman Optima Max-XP ultracentrifuge and Beckman TLA-100.3 fixe-angle rotor). Virus was then recovered from the SN by ultracentrifugation at 40,000 rpm for 2 h at 4°C a SW45 Ti fixed-angel rotor (Beckmann Optima L-80 XP ultracentrifuge). The pellet was resuspended in 500 µl VB-A and transferred to an Eppendorf tube. RNase A (Roche, Germany, Ref.: 10109169001) and DNase I (Roche, 10104159001) were added to a final concentration of 5 mg/ml each and the mixtures were incubated for 10 min at RT. Trypsin-EDTA (Sigma, USA, Ref.: 59418C; 250 µl of 0.5% w/v) was then added and incubation continued for 5 min at 37°C. Finally, 75 µl of a saturated (~10%) N-lauroylsarcosin solution in 10 mM Tris/HCl (pH 7.5), 10 mM NaCl was added and the sample was incubated o/n at 4°C. The mixture was then centrifuged for 15 min in a microcentrifuge at 14,000 rpm (Eppendorf 5424 centrifuge). The SN (1 ml) was transferred on top of a 11 ml continuous 7.5–45% (w/w) sucrose density gradient in 20 mM Tris-HCl (pH 7.5), 2 mM $MgCl_2$ and centrifuged for 2 h in a SW40 Ti rotor (Beckmann Optima L-80 XP ultracentrifuge) at 35,000 rpm and 4°C. 2 ml fractions were taken from the top and ultracentrifuged in a SW40 Ti rotor (Beckmann Optima L-80 XP ultracentrifuge) at 35,000 rpm for 16 h. Six fractions yielded visible virus pellets. The SN was discarded and each pellet was resuspended in 100 µl virus buffer C (50 mM Tris/HCl (pH 7.5), 25 mM NaCl) at RT by several times pipetting up and down. An aliquot of 5 µl of each virus sample was analysed by 15% SDS-PAGE (Figure 1). Finally, the virus titre was determined via a $TCID_{50}$ assay (see chapter 2.6)

2.3. AiV-A1 and CVB3 Seed Virus Production

At appropriate times as indicated in the results, cells transfected with AiV-A1 RNA or challenged with infectious AiV-A1 or CVB3 virus were collected in a centrifuge tube together with their medium. They were subjected to three cycles of freezing (in liquid nitrogen) and thawing (at RT) followed by centrifugation at 4,000 rpm for 10 min in a table-top centrifuge (Eppendorf 5810R centrifuge and Eppendorf A-4-81 rotor). Then, freezing and thawing was repeated, and the sample was centrifuged a second time at 4,000 rpm for 10 min. Finally, the supernatant (SN) was transferred to a new tube; it is referred to as seed virus. Seed virus was stored at -80°C until further usage.

2.3.1. AiV-A1 and CVB3 seed virus concentration

AiV-A1 and CVB3 seed virus produced as described above usually had titres of 2–5 x 10^7 and 2 x 10^8 TCID50/m, respectively. Higher titre seed virus was obtained as follows: Four T-175 cm^2 flasks containing confluent Vero cells were infected with a routinely produced, lower titre AiV-A1 or CVB3 seed virus stock (at an MOI = 0.1) for three days, respectively. Seed virus was produced as above yielding a total of approximately 60 ml. Virus particles were pelleted by ultracentrifugation at 40,000 rpm for 2 hours at 4°C in a SW45 Ti fixed-angel rotor (Beckmann Optima L-80 XP ultracentrifuge). After centrifugation, the SN was removed, the pellet was covered with 300 µl of virus buffer C (50 mM Tris/HCl pH 7.5, 25 mM NaCl) and left overnight for resuspension by passive diffusion. On the next day, the suspension and residual pellet were resuspended by multiple pipetting and transferred into a microcentrifuge tube. This concentrated seed virus preparation had a titre of about 2 x 10^8 and 2 x 10^9 $TCID_{50}$/ml respectively and was used for all infection experiments, when not stated otherwise.

2.4. RNA Extraction

RNA was purified by TRIzol reagent (Invitrogen, USA) according to manufacturer's instructions. In short, 1 ml of TRIzol was added to a sample (e.g. cells, tissue, SN etc.) and incubated for 10 min at RT. Chloroform was added, the tube inverted several times and incubated for 3 min at RT. The sample was centrifuged at 11,600 rpm for 15 min at 4°C and the aqueous phase was transferred to a new microcentrifuge tube. Five-hundred µl isopropanol were added, the tube inverted several times and incubated for 10 min at RT, followed by centrifugation at 11,600 rpm for 10 min at 4°C. Pellets were washed three times with 1 ml of 70% ethanol, vortexed shortly and centrifuged at 9,100 rpm for 5 min at 4°C. Remaining ethanol was removed and the pellet was air-dried and suspended in 50 µl of Milli-Q water (Merck, USA). Samples were stored at -80°C until further use.

2.5. Reverse Transcription and Quantitative PCR

A two-step RT-qPCR (reverse transcription-quantitative polymerase chain reaction) was used to measure host and viral gene expression. Total RNA was extracted using the TRIzol reagent and concentrated as described in chapter 2.4.. Nucleic acid concentrations were measured by UV-Vis spectrophotometry (DeNovix, USA). The RNA was reverse transcribed using the M-MLV reverse transcriptase according to the manufacture's instruction (Promega). In short, 1 µg of RNA was incubated with 0.5 µg of random hexamer primers (Promega) in a volume totalling no more than 15 µl. qPCR was then performed using the GoTaq DNA polymerase (Promega) according to the manufacture's instruction with slight modifications (Table 4). Gene expression was calculated by the Pfaffl method [154]. Viral RNA was normalised to the human 18s rRNA examined by RT-qPCR in parallel. Table 5 provides a list of the used primers.

Table 3. RT-qPCR reaction components and parameters.

Component	Concentration
5x GoTaq Colourless Reaction Buffer	1x
dNTPs Mix, 10 mM each	200 μM, each
GoTaq DNA Polymerase (5 u/μl)	0.625 u
Syto 82 (5 mM)	5 μM
Primers (100 μM)	0.5 μM, each
cDNA	1 μg
ddH2O	**X**
Total	**25 μl**

Step	Temperature (°C)	Time	
Initial Denaturation	95	3 min	
Denaturation	95	15 sec	40 cycles
Annealing and Extension	60	1 min	
Hold	4	∞	

Table 4. List of primers used for qPCR analyses.

Primers	Forward 5′-3′	Reverse 5′-3′
AiV-A1 Fw-SQP2	Fw: GCT CAC CCA ACT CCT CAA CT	SQP2: AGA GGA TAA GGG CTC CGG CA
AiV-A1 Rw-SQP1	SQP1: TGT ACA ACA CCC ACT CCA TGT G	Rw: TCC ACA GAG AGG GAG TTC CTG
RV-A54 CVB3 (pan-enterovirus)	GGC CCC TGA ATG TGG CTA A	GAA ACA CGG ACA CCC AAA GTA G
GAPDH	GAA GGT GAA GGT CGG	GAA GAT GGT GAT GGG ATT
18s rRNA	ATC AAC TTT CGA TGG TAG TCG	TCC TTG GAT GTG GTA GCC G
PPIA	AGA CAA GGT CCC AAA GAC AGC AGA	TGT GAA GTC ACC ACC CTG ACA CAT
IFN-α (all 13 subtypes)	TCC ATG AGA TGA TCC AGC AGA	ATT TCT GCT CTG ACA ACC TCC C
IFN-β1	TTG ACA TCC CTG AGG AGA TTA AGC	TTA GCC AGG AGG TTC TCA ACA ATA G

IFN-λ1 (IL-29)	GGA AGA CAG GAG AGC TGC AAC	AAC TGG GAA GGG CTG CCA CAT T
IFN-λ2/3 (IL-28A/B)	GCC AAA GAT GCC TTA GAA GAG	CAG AAC CTT CAG CGT CAG G
Mx1	CACCGTGACGGATATGGTCC	TTCCATCTGGAAGTGGAGGC
Mx2	AACGTGCAGCGAGCTTGTC	TGGCTGTTGCTGGAAGGAAT
IFIT1	ATTTACAGCAACCATGAGTACAAA	TCCCACACTGTATTTGGTGTCT
IFI44L	TGC ACT GAG GCA GAT GCT GCG	TCA TTG CGG CAC ACC AGT ACA G
IRF7	CAC TAA CGA CAG GCG AGG C	TAT AGG AAC GTG CAG CTC GG
USP18	GGCTCCTGAGGCAAATCTGT	CAACCAGGCCATGAGGGTAG

2.6. Viral Titre Quantification

Viral titres were determined as tissue culture infectious dose 50 ($TCID_{50}$). Samples containing AiV-A1 or CVB3 were serially diluted 10-fold in infection medium (Table 2) and 100 µl of each dilution was applied to approximately 80% confluent Vero cells in one well of a 96-well plate. Cells were kept at 37°C, 5% CO_2 and four to five days pi the development of a CPE was observed either by light microscopy (due to the low percentage of CPE at higher virus dilutions) or by crystal violet staining (0.2% crystal violet, 150 mM NaCl, 1% formaldehyde). $TCID_{50}$ were calculated according to Reed and Muench (1938) [155].

2.7. Susceptibility of Different Cell Lines for AiV-A1

Each immortalized cell line (see Table 1) was seeded into three wells (designated mock, T0, T72; hours pi) of a 24-well plate and grown to 100% confluency. Medium was replaced with infection medium and the plate was placed for 30 min at 4°C. Two wells of each cell line received AiV-A1 (at an MOI = 0.1) while one well was mock-infected. The cells were incubated for 1 h at 4°C with gentle shaking, allowing maximal virus attachment. The cells were then washed three times with ice-cold PBS (137 mM NaCl, 2.7 mM KCl, 10 mM Na_2HPO_4, 1.8 mM KH_2PO_4, pH 7.4), infection media was replenished and the "T0 cells" were collected together with the SN using a cell scraper. The plate was subsequently placed in a 37°C, 5% CO_2 incubator for triggering a synchronized virus internalisation. Three days pi, the cells ("T72") were examined for the development of a CPE via light microscopy and individually collected as above. Finally, the samples were processes as described for seed virus production (chapter 2.3.) and the titre was determined as $TCID_{50}$.

2.7.1. Vero cell infection

Vero cells were infected with either AiV-A1 A846/88 or CVB3 Nancy (at an MOI=0.01) for 1 h at 37°C. After incubation, the cells were washed three times with PBS and infection continued for 8 h. Resulting CPE was observed via light microscopy.

2.8. Pharmacological Inhibition of AiV-A1 Entry and Trafficking

Vero cells were cultured in 96-well plates to full confluency and pre-treated for 30 min at 37°C with different pharmacological inhibitors in the infection medium, known to target various endocytic pathways (Table 7 provides a detailed list of inhibitors, their final concentration and their cellular target). After the pre-treatment, AiV-A1 (MOI = 10) was added in the presence

or absence of the respective inhibitors and further incubated for 24 h at 37°C. As soon as a clear cytopathic effect was seen in the solvent control (2% DMSO in infection medium + virus (MOI = 10)) the infection was halted by crystal violet staining of the cells. Images of the stained plates were recorded using a ChemiDoc (Bio-Rad, USA). Using the "Measure Tool" provided in the Fiji plug-in of ImageJ [156], the brightness of the image of each well used in the experiment was quantified. The data were processed in GraphPad Prism (Version 8.4.0. (455) for macOS) (GraphPad Software, USA) using the equation further below and expressed as [%] cell death. The brightness measured for the solvent control plus virus corresponds to 100% cell death ($surv_{min}$; average of four wells), while the brightness of cells treated with the respective drugs but no virus was set to 0% cell death in each instance ($surv_{max}$; average of four wells). Cell death (*value*) was the average brightness of four measurements of cells inoculated with virus in the presence of an inhibitor.

$$\%\ cell\ death = \frac{(surv_{max} - value)}{(surv_{max} - surv_{min})} * 100$$

- *value*… measurements of IM_{+DMSO}+inhibitor +virus
- $surv_{max}$…measurements of IM_{+DMSO} +inhibitor (no virus)
- $surv_{min}$…measurement with IM_{+DMSO}+ virus (no inhibitor)

Table 6. List of pharmacological inhibitors used to target viral intracellular uptake and routing pathways.

Inhibitor	Target	Uptake/Pathway	Stock concentration (in DMSO)	Final concentration
Dynasore	Dynamin	Dynamin-dependent	80 mM	80 μM
Blebbistatin	Myosin II	Macropinocytosis	6.8 mM	50 μM
Filipine	Cholesterol	Lipid raft	2 mg/ml	5 μg/ml
Bafilomycin A1	Vacuolar-type H^+ ATPase	ECV-Lysosomal	5 μM	50 nM
EGA	Late endosome		20 mM	20 μM
NH_4Cl	Endosomal pH		1 M (in PBS)	25 mM
Ciliobrevin A	Dynein	ERC	100 mM	30 μM
Nocodazole	Microtubules		6 mg/ml	10 μg/ml

2.9. Human Intestinal Epithelium Model

2.9.1. Maintenance and infection

The EpiIntestinal SMI-100 system was purchased from MatTek (Ashland, USA). It recapitulates the physiological architecture and the cellular composition of human small intestinal tissue and is based on ileum stem cell-derived adult tissue from a human donor. This human intestinal epithelium model (HIE) was maintained according to the manufacturer's instructions. In short, at the day of arrival, the HIE transwells were washed three times with pre-warmed PBS apically and basolaterally and kept in MatTek maintenance medium (composition disclosed) for 24 h at 37 °C prior to infection in order to allow the tissue to recover from the transportation stress.

For infection, HIE inserts were exposed apically and basolaterally either to the AiV-A1 strain A846/88 or the CVB3 strain Nancy (positive control) with 10^7 PFU in maintenance medium for 1 h at 37°C. The HIE were then washed once in PBS and further cultivated in maintenance medium (5 ml basolaterally and 200 μl apically). One infection assay comprised

five HIE inserts designated T0, T24, T48, T72, T96, according to the time pi until RNA harvest. In 24-hour intervals the basolateral and apical media of all tissues were gently collected and replaced by new maintenance medium by gently pipetting at the wall. At the indicated times, the respective membrane together with the attached HIE was cut out with a scalpel and combined with TRIzol reagent for RNA extraction (see chapter 2.4.). The purified total RNA samples were subject to gene expression profiling using RT-qPCR (chapter 2.5.).

2.9.2. Microscopy analyses

Twenty-four hours pi the media of one HIE insert was removed from both sides and the epithelium immediately fixed in 4% paraformaldehyde in PBS for 20 min at RT. The HIE was then either processed for orthogonal section imaging, which required cryo-sectioning (described further below) or simple top-view imaging of the epithelium.

The following sections describe the processing of the EpiIntestinal tissue model for different staining techniques which was carried out with the help of Irmgard Fischer in the histology facility of the Max Perutz Labs.

Cryo-sectioning

After fixation, the HIE was washed three times with PBS and incubated in 30% sucrose in PBS o/n at 4°C. The HIE was subsequently mounted on cryo-molds using the Tissue-Tek OCT-compound (Sakura, Netherlands) and shock frozen in isopentane cooled by dry ice. The frozen epithelium was then cut into 5 µm thick orthogonal sections with a Cryostat Microm HM 500 OM (Histocom, Switzerland) and stored at -80°C until further usage.

Immunofluorescence

All steps of the immunofluorescence staining were conducted while the HIE was still on the membrane of the transwell insert. After fixation as above, the epithelium was washed three times with cold PBS and the cell membrane was permeabilized with 0.25% Triton X-100 in PBS for 5 min at RT. The HIE was then washed again three times in PBS for 5 min each and transferred into blocking solution (2% BSA, 0.1% Tween 20 in PBS) for 30 min at RT. The HIE was subsequently incubated with the primary antibody diluted in blocking solution for 1 h at RT and washed again three times with PBS for 5 min each (Table 6 provides a detailed list of antibodies, reagents and dilutions). This was followed by incubation with the secondary antibody diluted in blocking solution for 1 h at RT. The HIE was then washed once with PBS for 5 min and counterstained with Hoechst 33258 (final concentration 1 μg/ml blocking solution) for 10 min at RT. Finally, the epithelium was washed three times with PBS for 5 min each, the membrane carrying the HIE was cut out using a scalpel and mounted with Prolong Glass Antifade Mountant (Invitrogen, P36982, USA).

For orthogonal section imaging, a cryosection (described above) was thawed at RT and washed with PBS for 5 min, followed by quenching in 0.1 M glycine in PBS for 10 min at RT. After washing in PBS for 5 min, the section was blocked in 2% BSA in PBS for 30 min at RT. Then the primary antibody diluted in PBS and 0.1% Tween 20 was applied for 1 h at RT. After washing with PBS for 5 min, the secondary antibody (in PBS, 0.1% Tween 20) was applied for 1 h at RT. Working dilutions of antibodies were the same as above (Table 6). After washing or 5 min with PBS, the nuclei were stained with Hoechst 33258 as above. Finally, the section was washed once with PBS for 5 min, then with ddH_2O and air dried followed by mounting with Prolong Diamond Antifade Mountant (Invitrogen, P36961).

Immunohistochemistry

A cryosection (described above) was thawed at RT and washed with ddH_2O for 5 min, followed by incubation in Dako REAL Peroxidase-Blocking Solution (DAKO, S2023, USA) for 7 min at RT and washed again three times with TBS (1.4 M NaCl, 26 mM KCl and 247 mM Tris pH 8.0). The section was blocked with 2% BSA in TBS for 1 h at RT and further incubated with the dsRNA-specific monoclonal antibody J2 (2 μg/ml in TBS and 0.1% Tween 20). After three washes in TBS, the section was incubated with the secondary antibody conjugated to biotin (DAKO, E0413, 1:200 in TBS and 0.1% Tween) for 30 min at RT. The section was washed again 3 times for 5 min each with TBS and then incubated with 120 μl of avidin-biotin-complex (ABC) reagent for 30 min at RT.

For J2 signal detection, the section was first washed 3 times with PBS for 5 min each; a few drops of DAB+ (Dako, K3468) were then added to the section and incubated for 2 min. Signal development was observed continuously under the microscope. When the signal was strong enough, the reaction was stopped with ddH_2O.

For the detection of sulphated and carboxylated proteoglycans (mucus, goblet cells, etc.), the section was washed with ddH_2O for 5 min, followed by incubation in alcian-blue solution (Merck, 1.01647.0500, USA) for 5 min. Then the section was washed again with running tap water for 3 min and rinsed with ddH_2O.

Counterstaining was conducted with nuclear fast red-aluminum sulfate solution 0.1% (Sigma, 1001210500) for 10 min, residual stain was washed off with running tap water for 5 min and the section was rinsed with ddH_2O. For storage, the section was dehydrated through immersion into 50%, 70% and 100% EtOH in ddH_2O, for 1 min each. It was then incubated in n-butyl acetate for 5 min, air-dried and mounted with Eukitt mounting medium.

Table 5. List of primary and secondary antibodies. All antibodies used for immunofluorescence and immunohistochemistry analyses of human intestinal epithelium and patient-derived intestinal tissue are shown with their respective working dilutions.

Primary ABs

Target	Cell type/Name	Company	LOT-Number	Antibody type	Concentration. (Dilution)
dsRNA	J2	English & Scientific Consulting	J2-1301	monoclonal	2 µg/ml (1:500)
AiV-A1 viral capsid protein VP1	Gift from Dr. Tsung-Hsien Chang, Taiwan Chen et al. (2013) [157]			polyclonal, rabbit serum	1:500
Apolipoprotein A1 (ApoA1)	Absorptive enterocyte	Invitrogen	PA5-88109	polyclonal	20 µg/ml (1:50)
Ki-67	Proliferative enterocytes	Abcam	ab15580	polyclonal	1:500

Secondary ABs

DyLight 488 donkey anti-rabbit IgG (H+L)		Thermo Scientific	SA5-10038		1 µg/ml (1:500)
Alexa Fluor 594 donkey anti-mouse IgG (H+L)		Invitrogen	A21203		2 µg/ml (1:1000)
Biotin - Rabbit $F(ab')_2$		DAKO	E0413	polyclonal	1:200

Other staining

Nucleus	Hoechst 33258	Sigma	86140-5		1 µg/ml

2.9.3. Cytotoxicity assay

For measurement of virus-induced cell death in the HIE, a LDH-Glo™ cytotoxicity assay kit (Promega) was used. After infection with AiV-A1 A846/88, the apical SN was collected in 24-hour intervals from infected and non-infected (Mock) epithelium and initially diluted 1:5 in LDH Storage Buffer (200 mM Tris-HCl pH 7.3, 10% Glycerol, 1% BSA) to reduce enzymatic

degradation when stored at –20 °C. As positive control (maximum cell death), epithelia were exposed to Triton X-100 in maintenance media (final concentration 0.25%) for 30 min at RT. A standard curve, using the LDH positive control included in the kit, was established to determine the linear range of the assay. The maximum cell death samples were serially diluted to fit within the linear range and to infer the necessary dilution factor to be used in the measurement of the LDH activity for the viral infected HIE samples. Based on that outcome, the dilution factor was set to 1:2000 for all samples. The measurements were carried out according to manufacturer's instructions in 96-well plates in a Synergy H1 plate reader (BioTek, USA).

2.10. Patient-Derived Intestinal Tissue

A single sample of human intestinal tissue was obtained by Univ. Prof. Dr. Martin Klimpfinger from the KFJ hospital in Vienna. It consisted of a routine biopsy specimen obtained during a Whipple`s operation from an anonymous patient without any possibility of backtracking. Therefore, the approval of an ethics committee of the town of Vienna was not required according to the managing director Reinhard Undeutsch. Immediately after sample collection, the tissue was washed thoroughly with ice-cold Krebs-Henseleit buffer (KHB) prepared according to de Graaf et al. (2010) [158] (118 mM NaCl, 5 mM KCl, 1.1 mM $MgSO_4$, 1.25 mM $CaCl_2$, 1.2 mM KH_2PO_4, 25 mM $NaHCO_3$, 25 mM *D*-glucose, 9.0 mM Hepes, pH 7.4). The layers of serosa, muscularis and submucosa were removed and the tissue was further cut into smaller pieces (approximately 1 x 1 cm). The tissue was then cultured in RPMI 1640 medium (Gibco, 11875093) containing 10% FBS (Sigma, F7524) and 1% Pen-Strep (Sigma, 15140-122) and incubated at 37°C and 5% CO_2. For infection the tissue was incubated with 10^7 PFU of AiV-A1 A846/88 for 1 h at 37°C. After incubation, the tissue was washed with KHB

buffer and the infection continued at 37°C in RPMI 1640. Twenty-four hours later the tissue was fixed in 4% formaldehyde in PBS at 4°C o/n and further processed for cryo-sectioning and immunofluorescence staining as outlined above (chapter 2.9.2.)

2.11. Statistical Analyses

All statistical analyses were performed with GraphPad Prism. Data are shown as mean ± standard deviation (SD). Shapiro-Wilk analysis was used to check for normal distribution of data for parametric testing. Two-tailed student's t-test, one-way and two-way ANOVA with Dunnett's and Sidak's test for multiple comparisons were used to determine statistical significance.

3. RESULTS

3.1. AiV-A1 A846/88 Production and Sequence Confirmation

For studying the early events of the AiV-A1 A846/88 life cycle, infectious virus was produced using the plasmid pAV-UCSF, which contains the full length cDNA of AiV-A1 [151]. AiV-A1 RNA was *in vitro* transcribed from the linearized plasmid (Figure S2), recovered by TRIzol reagent and analysed by agarose gel electrophoresis (Figure 8A). One distinct band was recognisable and according to the DNA ladder, the size of the transcribed RNA fragment was in the expected range of approximately 8,000 bp. Additionally, the positive control, an RNA transcribed from the linearized cDNA included in the kit, exhibited a distinct band at the expected range of approximately 1,800 bp. To confirm the AiV-A1 strain authenticity (e.g. to exclude inadvertent production of an other picornaviruses used in the lab as a result of contamination), the AiV-A1 RNA was reverse transcribed into single-stranded cDNA and used as a template for a qPCR with two different sets of primers amplifying fragments within the coding region of the structural proteins VP0 or VP3. The amplicons were separated on an agarose gel and exhibited the expected size of 887 bp and 461 bp, respectively (Figure 8B). Total yeast RNA (Roche, 10109223001) was processed in the same way and served as negative control. Sanger sequencing further confirmed the identity of these two partial sequences with the GenBank entry for the AiV-A1 A846/88 (accession no. JQ281544) (Figure S1).

Infectious viral particles were obtained by transfecting Vero cells with AiV-A1 RNA. Three days post transfection the contents of the wells were subjected to freeze and thaw cycles for the release of the still mostly cell-associated progeny virus into the medium. The recovered AiV-A1 was further propagated in Vero cells grown in forty-five 175 cm^2 flasks. Progeny

virions were recovered by freeze-thawing as before, resulting in a substantially higher yield of infectious material. This was subject to a multi-step purification procedure, consisting of a series of centrifugations, PEG-precipitation and a sucrose density gradient step. Selected gradient fractions were combined and analysed by SDS-PAGE and stained with Coomassie brilliant blue (Figure 8C). AiV-A1 is one of a few picornaviruses whose mature capsid consists of only three structural proteins (VP0, VP3 and VP1); the other members in this family further cleave VP0 into VP4 and VP2, which then renders them infectious [43]. As expected, the gel image revealed three protein bands corresponding to the calculated molecular weights 39.1 kDa (VP0), 29.9 kDa (VP1), and 24.2 kDa (VP3), respectively. The bands of VP3 and VP1 were recognisable in almost all fractions, while VP0 was barely visible in fractions 1–4 and gave a faint signal in fractions 9–10. This is presumably related to its amino acid composition determining the extent of Coomassie blue binding [159]. Despite the extensive purification consisting of several orthologous methods, residual cellular proteins were still detectable in the AiV-A1 containing fractions, though the top fractions (#1–5) contained more contaminating cellular material than the bottom fractions (#7–12). Taken together, sequencing analysis and SDS-PAGE both confirmed production of AiV-A1 from the infections cDNA clone.

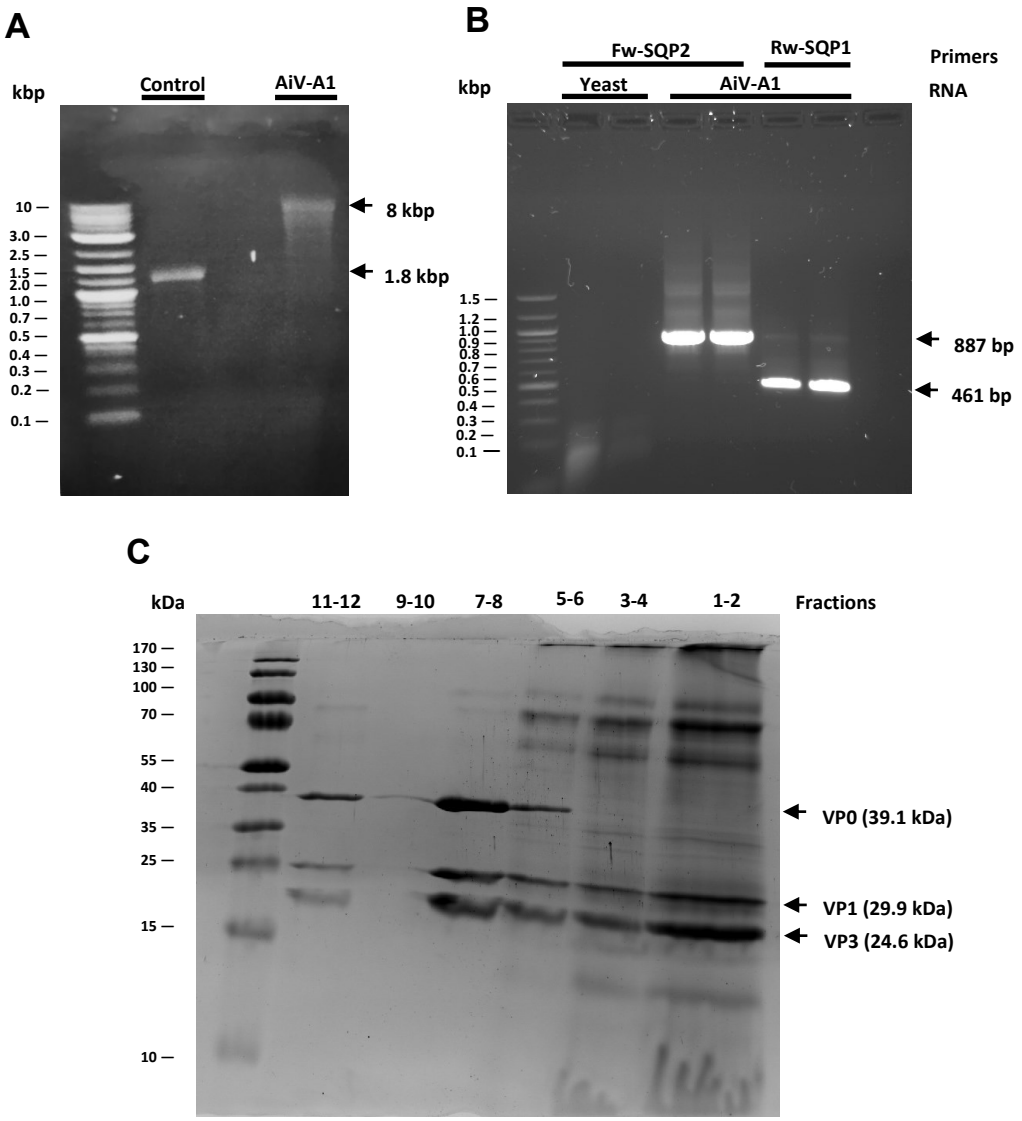

Figure 8. Verification of AiV-A1 production by RT-qPCR and SDS-PAGE. (A) *In vitro* transcribed AiV-A1 RNA (8000 bp) from the linearised pAV-UCSF plasmid. The control is an *in vitro* transcribed RNA (1800 bp) from the linearized plasmid included in the kit. Displayed is a 1% agarose gel. **(B)** AiV-A1 RNA was reversed transcribed and regions encoding parts of the structural proteins VP0 and VP3, respectively, were amplified by qPCR using two different primer sets. The amplicons were visualised by a 1% agarose gel. Total RNA from yeast was used as negative control. The predicted lengths of the amplicons were 887 bp (Fw-SQP2 primers) and 461 bp (Rw-SQP1 primers), respectively, and the corresponding bands are indicated by arrows. **(C)** Following upscaling of AiV-A1 seed virus production, the infectious material was finally purified on a continuous sucrose gradient. Fractions taken from the top (1-12) where combined as indicated and aliquots applied onto a 15% SDS-PAGE gel. The gel was stained with Coomassie brilliant blue.

3.2. AiV-A1 Features a Distinct CPE and Strain-specific Cell Tropism

During the first infection studies of Vero cells with AiV-A1 it was noticed that the appearance of the CPE was different from CVB3 Nancy. Vero cells infected at MOI = 0.01 at 8 h post infection (pi) exhibited granular material surrounding individual damaged cells, resembling vesicles (Figure 9A–B). In contrast, CVB3 infected cells were well-rounded without any material in their vicinity (Figure 9C). It is conceivable that the granular material around AiV-A1 infected Vero cells corresponds to apoptotic bodies due to the large size of the vesicles and the ensuing cell death [160]. Other types of extracellular vesicles such as exosomes and microvesicles are much smaller (range between 40–500 nm) and are linked with cell survival [64]. For CVB3, the cells were not surrounded by granular material following cell death. It has been shown that different enteroviruses (including CVB3) induce the formation of various types of vesicles depending in the cell line they infect [64]. However, the exact nature of the AiV-A1 generated vesicles remains to be examined.

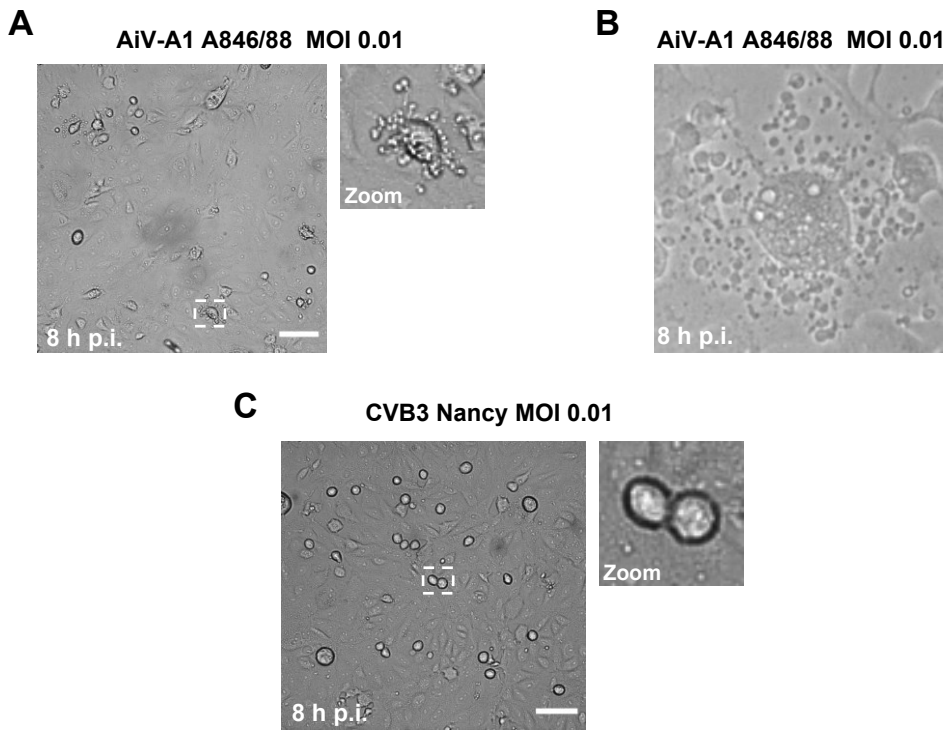

Figure 9. AiV-A1 infected Vero cells are surrounded by granular material. Vero cells were infected with either (A–B) AiV-A1 or (C) CVB3 (MOI = 0.01) and visualised 8 h pi by light microscopy. (B) Close up of one AiV-A1 infected Vero cell; note the granular material surrounding the cell. White boxes indicate zoomed areas. Scale bars, 50 μm.

Chen et al. (2013) [157] reported an AiV-A1 strain isolated from a diarrheal patient in Taiwan (kvgh99012632/2010; GenBank accession no. JX564249), designated here as the Taiwanese strain (AiV-A1 kvgh2010) with the potential to infect various human cancer cell lines inclusively of intestinal and respiratory tissue origin. Since the AiV-A1 strain used in this thesis work (A846/88, GenBank accession no. AB040749.1) differs in a number of amino acids in structural and non-structural proteins, it was of interest to examine its cell tropism. Various immortalised cell lines, including frequently used intestinal, were analysed for permissivity to support AiV-A1 A846/88 infection. The respective cell lines were pre-cooled to 4 °C for 30 min and then exposed to AiV-A1 (MOI = 0.1) for 1 h under shaking allowing for attachment.

After this incubation, loosely bound virus was washed off with cold PBS. A synchronized infection was initiated by warming to 37 °C and allowed to proceed for 3 days. Supernatant (SN) and cells were collected and subjected to freeze-thawing cycles. Following removal of cell debris by low-speed centrifugation, the titre of the progeny virus was measured as $TCID_{50}$. Of all cell lines tested, only Vero cells exhibited an increase in viral titre (Figure 10A). None of the human derivatives, including A549 (lung carcinoma-derived) and T84 (colon carcinoma-derived) were susceptible compared to the reports for AiV-A1 kvgh2010. Additionally, no CPE was recognisable via light microscopy in any of the cell lines.

These results suggested that infection of the examined human cell lines by AiV-A1 A846/88 was blocked at one or more steps of the virus life cycle such as cell entry. To test this hypothesis, each of the cell lines used in the infectivity assay were transfected with 1 μg of AiV-A1 A846/88 RNA and different amounts of lipofectamine. Three days post transfection the contents of the wells (cells and SN) were collected for seed virus production. $TCID_{50}$ measurements clearly indicated that all transfected cell lines produced infectious particles (Figure 10B). Vero cells expectedly showed a 2 log_{10} higher titre compared to the similarly transfected human cells lines. Since these African green monkey kidney cells are fully permissive for AiV A846/88, the progeny virions initially produced by the small number of transfected cells can further infect still untransfected or non-infected cells during the 3-day multi-cycle infection, thereby massively amplifying the viral titre.

Taken together, Vero cells infected with AiV-A1 became surrounded by granular material corresponding to vesicles after the first cycle of infection. Although the exact nature of theses vesicles remains to be investigated, they appear to be apoptotic bodies based on their size and the overall cell shrinkage and cell death. Various standard immortalized cell lines, including prominent colon-derived, failed to support productive infection. The lack of

permissivity for AiV-A846/88 was most likely due to the absence of the receptor and/or other factors required during the initial entry/uncoating steps of viral infection, which were bypassed by viral RNA transfection.

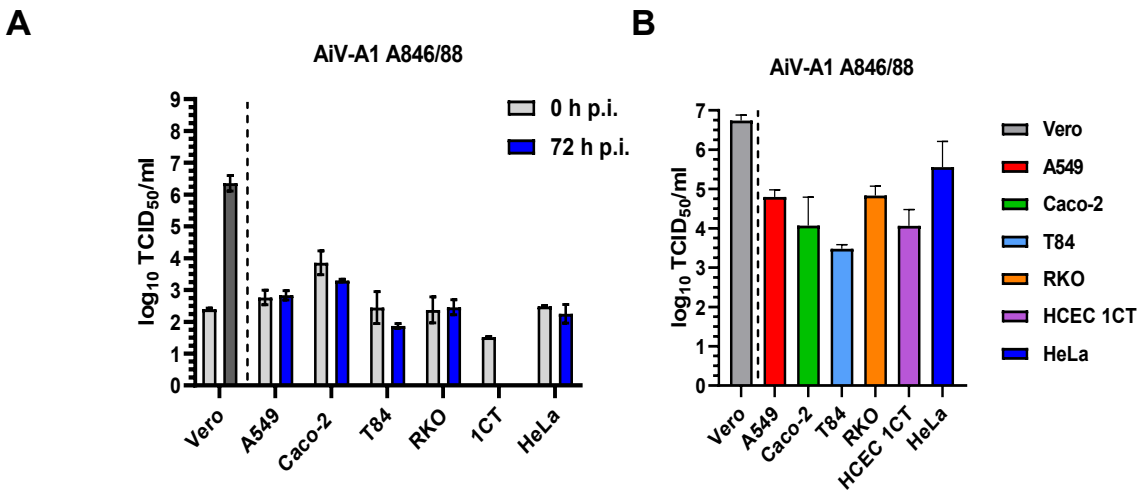

Figure 10. AiV-A1 A846/88 did not infect several prototypic human carcinoma-derived cell lines. **(A)** Virus was pre-absorbed (MOI=0.1) to the indicated cell lines for 1 h at 4°C. After incubation, the cells were washed and the well contents from 0 h pi (T0) and 72 h pi (T72) were collected separately for production of seed virus; virus titre was determined as $TCID_{50}$. Note, no titre was detected for 1CT cells at 72 h pi. N=3. **(B)** Each cell line was transfected with 1 μg of AiV-A1 RNA with different amounts of lipofectamine 2000 (1, 2 and 4 μl) and after three days the well contents were collected for seed virus production; the titre was determined as $TCID_{50}$ as above. Each bar represents the average from the three different lipofectamine amounts (the individual transfection data are shown in Figure S3). Displayed are the mean ± SD.

3.3. AiV-A1 Infection in Vero cells Requires Dynamin and a Low pH

For infection, picornaviruses normally gain access to the target cell via different endocytic pathways suitable for their uncoating [161]. The entry mechanism and intracellular trafficking of AiV-A1 have not been described yet. To fill this gap, we have started to identify the pathway(s) exploited by AiV-A1 A846/88 for productive infection of Vero cells, using a number of well-characterized pharmacological inhibitors.

Vero cells were pre-incubated for 30 min at 37°C with various cell-permeable small molecules that target key players of distinct entry or routing mechanism. The cells were subsequently challenged with AiV-A1 (MOI = 10) in the continuous presence of these drugs. Infection was allowed to proceed at 37°C for 24 h and cell survival was assessed by crystal violet staining and quantified with ImageJ. Although the incubation time of the inhibitors was long, the majority of drugs without the presence of the virus had no cytotoxic effect on the cells at the used concentrations (Figure S4). Only NH_4Cl, dynasore, blebbistatin and nocodazole induced a 10%, 19%, 26% and 37% cell death without virus, respectively.

Dynasore, a well-known inhibitor of the small GTPase isoforms dynamin I and II [162], which is essential for clathrin-, and endophilin-mediated endocytosis [67], completely prevented cell death (Figure 11A). Blebbistatin, which targets non-muscle myosin II required for membrane blebbing and ruffling during macropinocytosis [163] reduced cell death by almost 50% (Figure 11B). Addition of filipin, which aggregates cholesterol in the membrane [164], decreased virus-induced cell death only slightly (Figure 11C), indicating that lipid rafts contributed only little if at all to AiV-A1 internalisation.

Acidification is essential for endosomal maturation along the different trafficking pathways [165, 166] and is brought about by the vacuolar-type H^+-ATPases. Furthermore, rhinoviruses and EV-A71 depend on low endosomal pH for uncoating and genome release

[100, 167]. Using bafilomycin A1, an inhibitor of the proton pump, and NH_4Cl, a lysosomotropic agent that neutralizes the acidic environment, revealed a strong dependence of AiV-A1 on a low vesicular pH for productive infection (Figure 11D). In presence of EGA (4-bromobenzaldehyde N-[2,6-dimethylphenyl] semicarbazone), an inhibitor acting at the stage between early and late endosome [168], cell death diminished by almost 90% (Figure 11D). Finally, we treated the cells with nocodazole and ciliobrevin A to elucidate if AiV-A1 was ferried towards the endocytic recycling compartment (ERC). Depolymerisation of microtubule networks by nocodazole resulted in a minimal decrease of cell death, while the inhibition of the motor protein dynein by ciliobrevin A reduced the virus-mediated cell death by approximately 30% (Figure 11E).

In conclusion, in Vero cells, AiV-A1 strictly depends on dynamin for entry and on low endosomal pH for infection. Additionally, macropinocytosis appears to be exploited to a smaller degree.

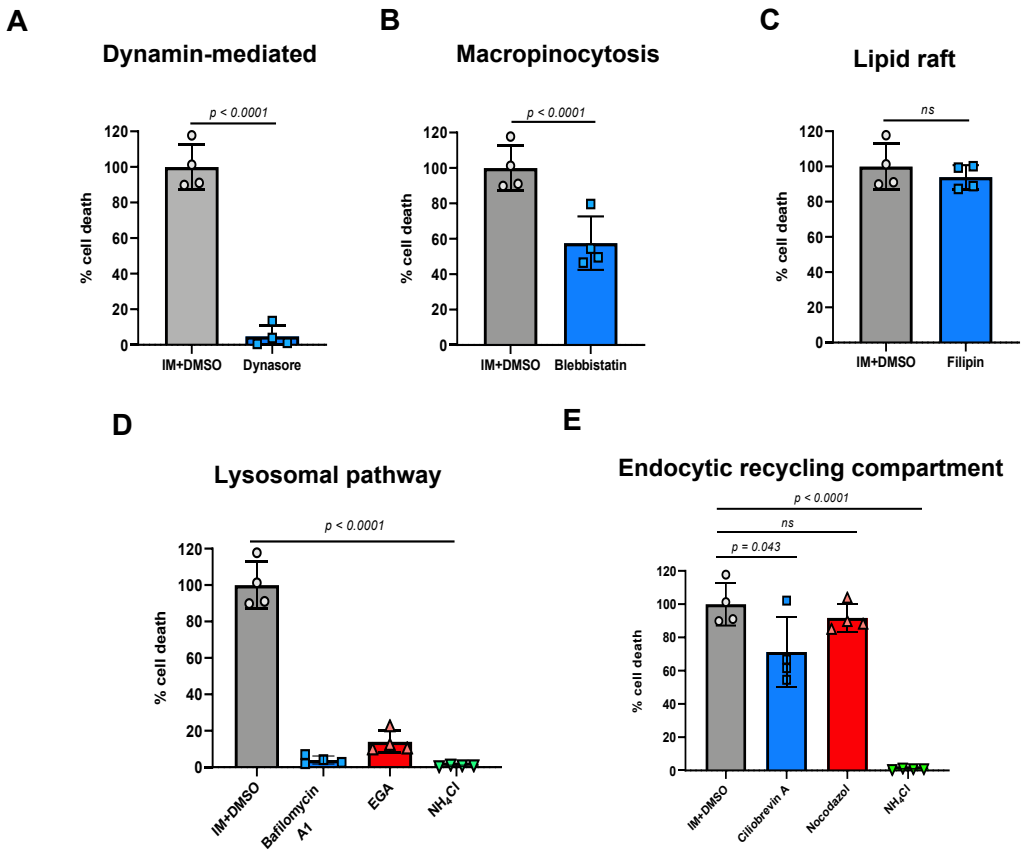

Figure 11. AiV-A1 is likely routed towards the lysosomal pathway and requires a low pH for infection. Vero cells were pre-treated with pharmacological inhibitors as indicated for 30 min at 37°C. Cells were subsequently challenged with AiV-A1 (MOI=10) in the presence (DMSO control) or absence of the inhibitors. The infection was allowed to continue at 37°C and was finally stopped after 24 hours using crystal violet staining. At that time the Vero cells without inhibitor treatment (solvent control) showed a distinct CPE. Using the ImageJ Measurement Tool, the brightness of the stain was quantified and used for calculation of [%] cell death with GraphPad Prism. The solvent control + virus corresponded to 100% cell death, while the cells treated with the respective drugs in absence of AiV-A1 were set to 0% cell death. However, cytotoxicity was detected in non-infected NH_4Cl, dynasore, blebbistatin and nocodazole treated cells, respectively (Figure S4). Displayed is the mean ± SD from one independent experiment with each condition conducted in quadruplicates. Statistical significance was determined by one-way ANOVA with Dunnett's analysis for multiple comparisons (compared to solvent control).

3.4. Replication of AiV-A1 in Human Intestinal Epithelium

The Taiwanese AiV-A1 strain was recently found to replicate in primary mouse intestinal epithelial cells cultivated in 2D and to a lesser extent in the human colon cancer-cell line T84 [169]. As demonstrated further above, none of the human colon cancer cell lines tested by us were permissive for AiV-A1 A846/88. However, these cultured cells do not closely recapitulate the intestinal tissue in architecture and cellular diversity. To overcome this caveat, replication of AiV-A1 A846/88 was investigated here for the first time in a stem-cell derived human small intestinal epithelium model (EpiIntestinal, MatTek). Importantly, this 3D system features an organisation and cellular diversity similar to authentic human small intestinal tract tissue [170] and has already been used for studying the tropism of the distantly related enterovirus A71 (EV-A71) [171]. Drummond et al. (2017) described that human foetal-derived intestinal enteroids could be productively infected with CVB3 from the basolateral side with the strain RD [149]. As shown next, the CVB3 strain Nancy available in the lab was able to robustly replicate in the EpiIntestinal system and hence served as a positive control for all experiments with AiV-A1 A846/88.

Since no information for a possibly preferred apical or basolateral entry was available for AiV-A1, infection was initiated simultaneously from both sides. EpiIntestinal tissue inserts (in the following termed human intestinal epithelia (HIE)) were infected with 10^7 PFU of CVB3 Nancy or AiV-A1 A846/88 for 1 h at 37°C. The tissues were washed once with PBS to remove unbound virus and the infection allowed to proceed at 37°C. The apical and basolateral SN of all the tissues in the wells were collected in 24-hour intervals for titration of *de novo* produced viral particles and replaced with fresh maintenance media. The latter followed MatTek´s recommendation for the EpiIntestinal system of media replenishment after a maximum of 48 h in culture. At the indicated time points, the respective membranes with the attached HIE

were cut out from the inserts for extraction of total cellular and viral RNA. The RNA samples were then used in an RT-qPCR for quantification of newly produced CVB3 and AiV-A1 plus-strand RNA at each collection time point pi, establishing a replication profile for each of the two picornaviruses.

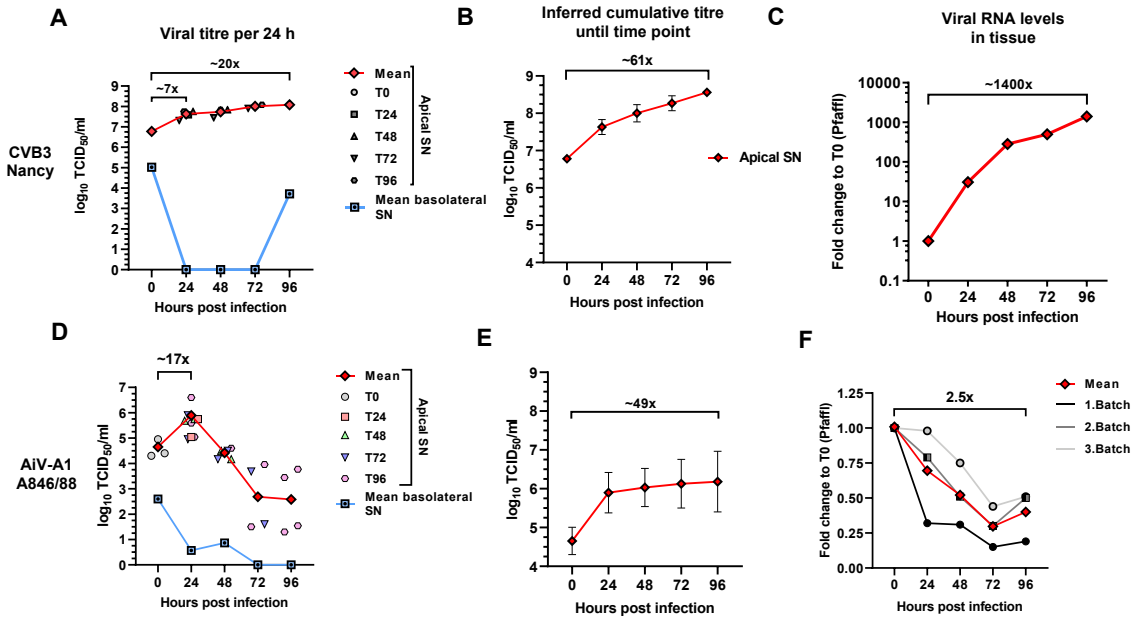

Figure 12. AiV-A1 moderately replicates in HIE. HIE were simultaneously infected from the apical and basolateral side each with 10^7 PFU AiV A846/88 or CVB3 Nancy for 1 h at 37°C. After viral challenge, the epithelia were washed once with PBS before continuing the infection at 37°C. In 24-hour intervals the basolateral and apical media of all HIE (T0–T96) were collected and replaced by new maintenance medium. At the indicated time points, the respective membrane was cut out for total RNA extraction. **(A and D)** Plots of the viral titres in the apical and basolateral SN collected from infected HIE in 24-hour intervals. Note that in (A and D) no progeny virus was detected for some time points in the basolateral SN. Each individual symbol represents the result of an individual HIE insert. **(B and E)** Graphs showing the average cumulative amount of virus produced per HIE insert at each time point pi. It was calculated by summing up the mean virus titres in the apical medium per HIE insert obtained at the previous time points until the indicated times pi. **(C and F)** Replication profile of vRNA in the epithelium over time determined by RT-qPCR. In (C) N=1 and in (F) N= 3 for every time point. Fold change was calculated according to the Pfaffl method. Data in (B) and (E) are shown as the mean ± SD.

The CVB3 Nancy control gave rise to robust apical titres of 10^7 – 10^8 $TCID_{50}$/ml every 24 hours over a period of four days (Figure 12A). The relatively high titre at T0 must stem from attached input virus particles which did not internalize during the first hour of incubation at 37°C and therefore preserved their infectivity. They were evidently recovered on collecting the medium at T0. Their contribution to the much higher titres measured at later times is negligible. At the basolateral side no infectious particles could be detected except at T0 for the same reason stated above and, to a considerably lesser extent, at T96 (related to some progeny virus). The average cumulative amount of apically released CVB3 per HIE insert and time pi was calculated by adding up the average apical titre per HIE insert measured at consecutive 24 h intervals until the indicated time after infection. It exceeded 10^8 $TCID_{50}$/ml at 96 h pi (Figure 12B). A similar steady increase over time was observed for the accumulation of the intracellular viral RNA (vRNA) (Figure 12C). In contrast, the titre of apically released AiV-A1 peaked at 24 h pi, reaching 10^5 $TCID_{50}$/ml, followed by a steady decrease until 72 h pi, eventually levelling off at 96 h pi (Figure 12D). The appreciable T0 titre is again most likely attributable to non-internalized infectious virions at least partially recovered on collection of the supernatant. At the basolateral side, apart from the T0 titre arising for reasons stated above, only low to no amounts of infectious particles were detectable from 24 to 96 h pi. The calculated average titre of the apically accumulating AiV-A1 did not increase progressively from 0 to 96 h pi as found for CVB3, due to the drastically lower amounts of infectious particles released after 24 h of infection (Figure 12E).

Overall, the apical release of virus particles by the infected HIE was the dominant mode for both, AiV-A1 and CVB3. However, AiV-A1 infection resulted in an approximately 2 $logs_{10}$ lower titre. Unexpectedly, the amount of vRNA extracted from the AiV-A1 infected HIE did not increase from T0 onward as observed for CVB3. The vRNA instead exhibited a

steady decline starting at T0 until 72 h pi, followed by a slight, variable increase at 96 h pi. The average drop at T96 was approximately 2.5 times compared to T0 (Figure 12F). As discussed in more detail later, the discrepancy between the titre and vRNA measurements of AiV-A1 compared to CVB3 may be attributable to the background of RNA genomes of non-internalized AiV-A1 remaining attached to the HIE,

To independently confirm AiV-A1 growth in the HIE, an immunofluorescence analysis was carried out with the double-strand RNA specific monoclonal antibody (mAb) J2. It was previously shown that this antibody specifically detects the partially double-stranded replicative intermediate RNA arising during the replication of positive-sense viruses including picornaviruses [172, 173]. Both AiV-A1 and CVB3 exhibited a significant number of infected cells at 24 h pi with the mAb J2 dsRNA signal displaying a typical pattern of distinct foci surrounding the nucleus (Figure 13A) [174]. These results clearly demonstrate that AiV-A1 actively replicated in the HIE at 24 h pi, at the peak of apical virus release. Notably, examination of orthogonal sections of the infected epithelia located the replication factories detecetd by the mAb J2 for both picornaviruses at the apical side.

Chen et al. (2013) [157] generated a polyclonal antibody against the AiV-A1 capsid protein VP1 using the AiV-A1 kvgh2010 strain. By employing this antibody (a gift from Dr. Tsung-Hsien Chang, Taiwan) together with the mAb J2, newly synthesized VP1 was frequently detected in the AiV-A1 infected HIE which stained positive for dsRNA. In a number of instances the VP1 signal was in close proximity to the mAb J2-stained replication centres resulting in a signal overlap, revealed as yellow fluorescence speckles upon merging the fluorescent images of the red (dsRNA) and green (VP1) channel (24 h pi; Figure 13B).

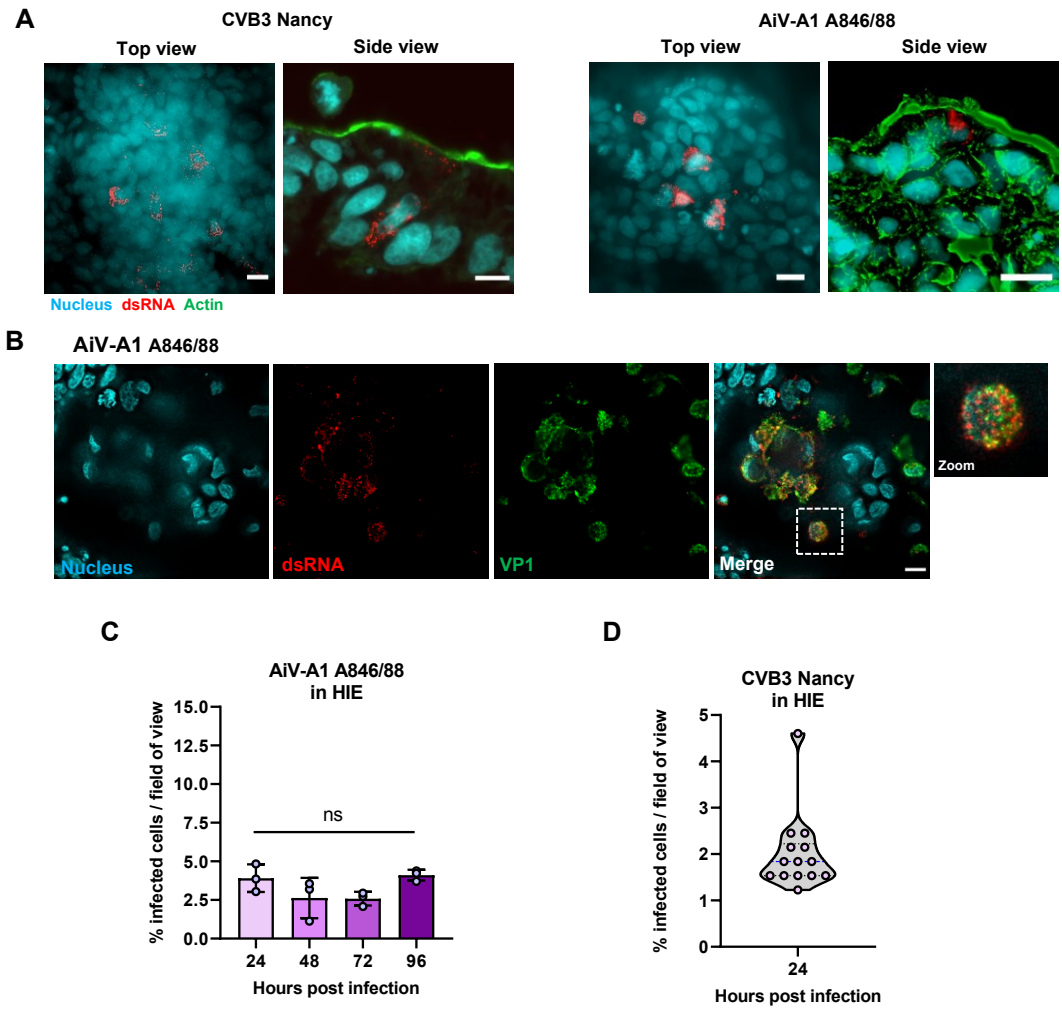

Figure 13. AiV-A1 replicates at the apical side of HIE. (A) Top-view and orthogonal sections of HIE infected with AiV-A1 and CVB3 (each 10^7 PFU) were evaluated 24 h p.i. by immunofluorescence for dsRNA using the mAb J2 antibody (red). Nuclei (cyan) and actin (green) were stained with Hoechst and phalloidin, respectively. Scale bars, 10 µm. **(B)** Immunofluorescence images stained for dsRNA (red) and viral capsid protein VP1 in HIE 24 h after AiV-A1 challenge (10^7 PFU). Scale bar, 10 µm. **(C)** Quantification of AiV-A1 VP1 positive cells in HIE (10^7 PFU) per 10 fields of view for each time point. N=3. One-way ANOVA with Dunnett's test for multiple comparisons was used for statistical analysis (compared to 24 h pi). Shown is the mean ± SD. **(D)** Quantification of CVB3 dsRNA positive cells in HIE per 13 fields of view 24 h pi. N=1.

The number of AiV-A1 infected cells remained relatively stable over the 4 days of observation with an average of approximately 3%, in line with the persistent detection of vRNA by RT-qPCR and the ongoing apical virus release over the same period (Figure 13C).

The inapparent increase of infected cell is likely owing to the low overall virus production as reflected by the modest titres measured in the apical supernatants at sampling times beyond 24 h pi. The infection rate of CVB3 was only determined at 24 h pi and corresponded to approximately 2% infected cells (Figure 13D).

Since only a small fraction of cells within the HIE tissue became infected by AiV-A1, whose number remained practically unchanged until at least 96 h pi, a strong innate immune response may have curtailed virus propagation. This was assessed by quantifying the type I and type III IFN responses at the transcriptional level through RT-qPCR. Type I and Type III interferon production are the main antiviral signalling pathways in mucosal epithelia triggered during viral infection and primarily involved in viral clearance [105, 175]. Additionally, we quantified the downstream activation of selected interferon stimulated genes (ISGs) in response to IFN signalling. These are frequently chosen in similar analysis. Total RNA extracted from AiV-A1 and CVB3-infected HIE at the indicated times pi served as sample.

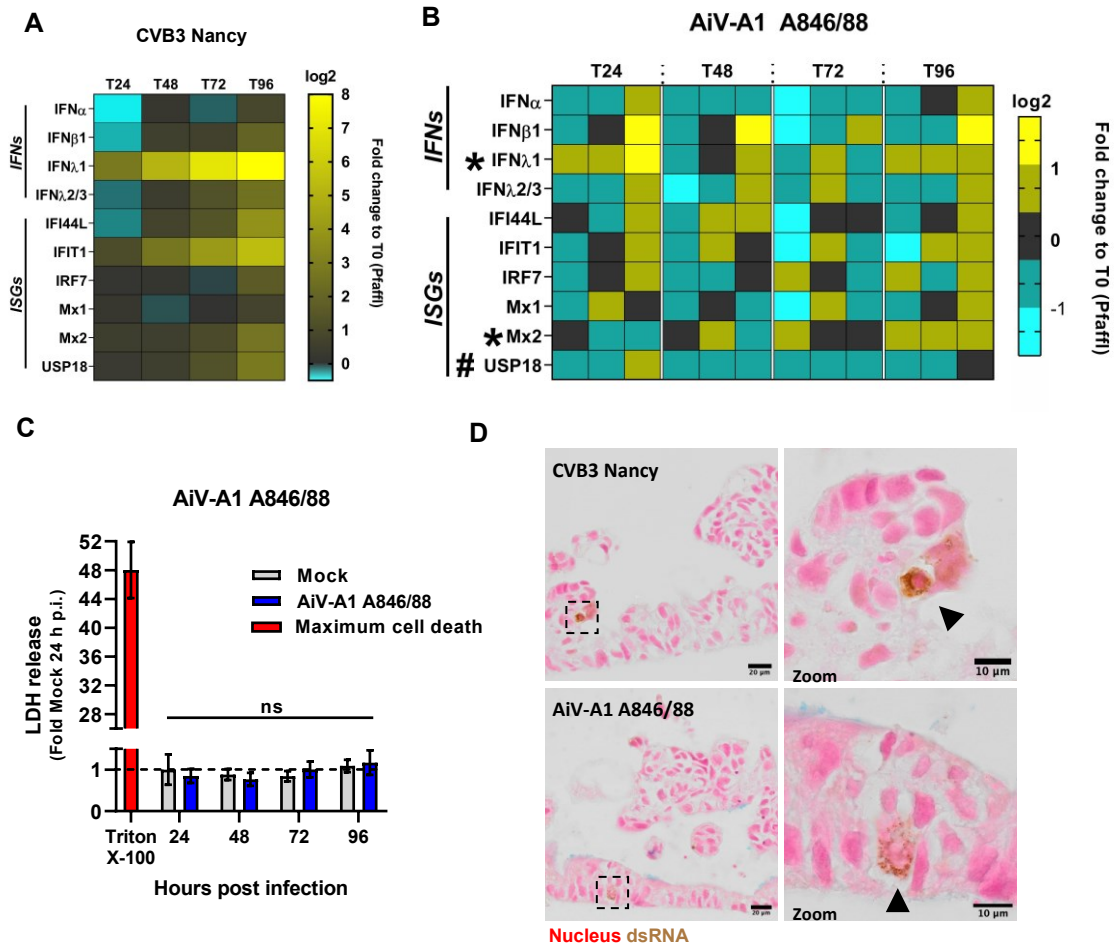

Figure 14. AiV-A1 induces only a weak antiviral response in HIE and does not damage the epithelial barrier. (A-B) Heat map of IFN and ISG gene expression analyses by RT-qPCR in HIE after AiV-A1 and CVB3 (each 10^7 PFU) infection, respectively. Fold change was calculated according to the Pfaffl method. In (A) N=1 and in (B) N=3. Asterisks and rhomb symbol indicate significant transcript upregulation and downregulation, respectively. Significance was determined by Student's t-test compared to T0. Raw data is display in Figure S5. **(C)** Measurement of cell death by apically released LDH at indicated time points after AiV-A1 infection in HIE. N=3. Two-way ANOVA with Sidak's test for multiple comparisons was used for statistical analysis (Mock vs. AiV-A1 at each time point). Displayed are the mean ± SD**. (D)** Immunohistochemical micrographs of HIE orthogonal sections stained with alcian blue (blue) and nuclear fast red-aluminum sulfate solution 0.1% (red) were evaluated for dsRNA (brown, black arrow) via mAb J2 and DAB colourisation 24 h pi. Black boxes represent zoomed areas shown at the right.

Contrary to the observations by Drummond et al. (2017) [149] for CVB3-RD with human foetal-derived enteroids, infection of highly differentiated HIE with CVB3 Nancy

resulted in a strong induction of type I and type III IFNs, including several important ISGs. The strongest increase was detected for the mucosa-associated IFNλ1 and the antiviral effector protein IFIT1 (Figure 14A and S5). AiV-A1 on the other hand, displayed a strong variability between the three independently produced batches with an overall much lower induction of all selected innate immune response genes compared to CVB3 (Figure 14B and S6). The third tissue batch exhibited the strongest upregulated transcripts while with the first batch most transcripts were downregulated. Nevertheless, IFNλ1 and the ISG Mx2 were significantly upregulated at 24, 96 and 96 hours pi. By contrast, USP18 was significantly downregulated at 48 and 72 h pi. Moreover, time points 24 h and 96 h pi exhibited the most upregulated transcripts while at 48 h and 72 h pi the most downregulated transcripts were evident.

Several enteric viruses have been reported to cause cell death in the intestinal epithelium resulting in an overall loss of epithelial integrity (e.g. E11, SARS-CoV-2, rotavirus) [141, 146, 149] By contrast, CVB3-RD (selected for growth in human myosarcoma-derived RD cells ([176]) did not affect the epithelial integrity at 24 h pi.[149]. The impact of AiV-A1 replication on the HIE viability as readout for cell damage and its overall integrity was therefore assessed by using a bioluminescence assay, which quantifies the amount of LDH released by destructed cells into the apical supernatant. Twenty-four hours cultured HIE tissues treated with Triton X-100 served as positive control. No increase of LDH activity in the apical supernatant was detected at any time point after AiV-A1 infection compared to uninfected tissues (Figure 14C), similar to the results reported by others for CVB3-RD as mentioned above. Immunohistochemical micrographs at 24 h pi furthermore confirmed that the epithelial integrity was preserved for both viruses beside dsRNA detection via mAb J2 antibody and DAB colourisation (Figure 14D).

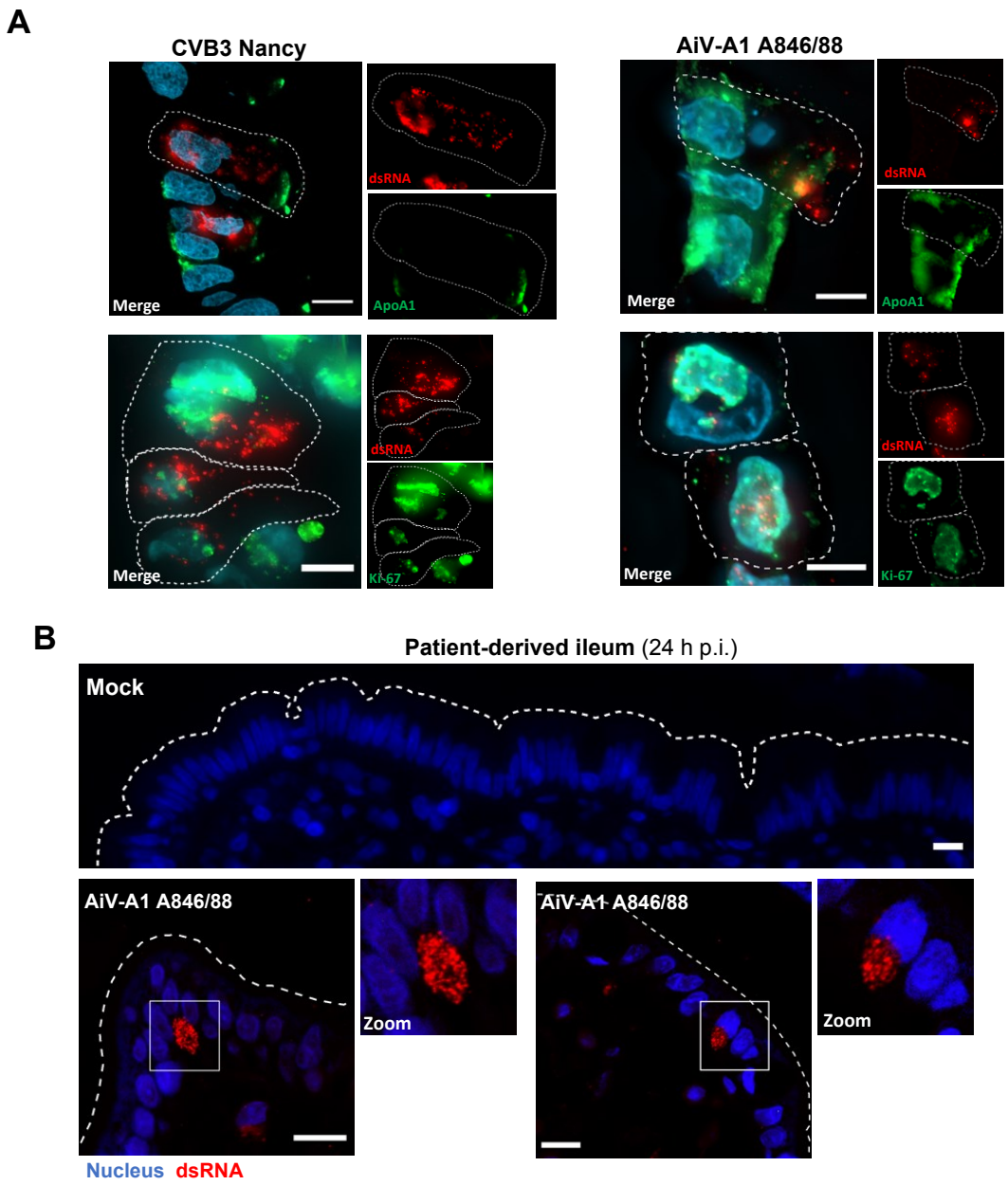

Figure 15. AiV-A1 infects absorptive and proliferative enterocytes and replicates in patient-derived ileum. (A) Immunofluorescence micrographs of HIE after AiV-A1 and CVB3 infection (each 10^7 PFU) co-stained for dsRNA (red) and for the absorptive or proliferative enterocyte marker ApoA1 and Ki-67, respectively (green). Dashed lines indicate cell outlines. Scale bars, 10 μm. **(B)** Patient-derived distal ileal tissue immunostained for dsRNA (red) after AiV-A1 infection (10^7 PFU). Dashed lines indicate luminal interface. White boxes represent zoomed areas shown at the right. Scale bars, 10 μm.

Previous studies on E11 and EV-A71 found that they preferentially infect enterocytes, enteroendocrine cells and goblet cells, respectively. [148, 149]. The intestinal tract tissue tropism of AiV-A1 and CVB3 is still elusive. Enterocytes constitute the main population in the HIE and were therefore examined for their ability to support infection by these two picornaviruses. Enterocytes exhibit different subpopulations, which can be broadly assigned to a mature and inmature lineage [141]. Mature (absorptive) enterocytes predominantly express genes related to carbohydrate or lipid transport found in resting cells while immature (proliferative) enterocyte upregulate genes involved in mitosis [177]. Apolipoprotein A1 (ApoA1), a structural protein component of the high-density lipoprotein (HDL) particle involved in cholesterol transport [178] was thus used as marker for the immunostaining of absorptive enterocytes. Ki-67 served as specific marker for the immunodetection of proliferative enterocytes. It is a nuclear protein expressed in different stages of the cell cycle but not in resting cells and is commonly used to distinguish these type of cells [179]. Immunofluorescence staining of HIE inoculated with AiV-A1 or CVB3 at 24 h pi revealed that all dsRNA positive cells were either positive for ApoA1 or Ki-67. This result showed for the first time that both, absorptive and proliferative enterocytes, are susceptible for AiV-A1 and also CVB3 (Figure 15A).

Finally, human intestinal tissue was acquired at surgery in order to confirm permissivity for infection by AiV-A1 in a model most closely related to a natural infection. A patient-derived ileal slice was challenged from the apical side with 10^7 PFU of AiV-A1 inoculum and kept at 37°C, 5% CO_2. The tissue was not oxygenated, which resulted in localised necrotic changes. Notwithstanding, in the remaining intact areas several dsRNA positive cells could be visualized with the mAb J2 by immunofluorescence microscopy at 24

h pi (Figure 15B). The signal was located in intact villi at the apical side near the luminal interface and displayed distinct foci.

4. DISCUSSION

Virus induced acute gastroenteritis is a continuing public health issue resulting in high mortality worldwide. While many cases can be assigned to a pathogen, in a substantial number of incidences the aetiological agent remains unknown. Aichivirus A1, belonging to genus Kobuvirus within the family *Picornaviridae* was first described in 1989 in Japan during a large outbreak of gastroenteritis [14]. However, it has remained unclear if AiV-A1 is truly an aetiological agent of acute gastroenteritis. Furthermore, while its replication and assembly have been explored in some detail in the past ([44, 50, 63]), practically nothing is known about the early steps of its life cycle leading to productive infection of host cells. In this thesis work, we have identified candidate pathways of AiV-A1 internalization and intracellular trafficking in Vero cells routinely used to amplify this virus. Furthermore, we show for the first time that AiV-A1, while unable to grow in several prototypic human colon cancer-derive cell lines, specifically replicated in enterocytes of a human small intestinal epithelium model. Our results are therefore in support of epidemiological reports placing AiV-A1 in the list of human enteric pathogens.

4.1. Egress and Cell Tropism of AiV-A1

Viruses have a number of ways to achieve the egress of progeny virions which generally can be divided in lytic and non-lytic mechanisms [64]. Which type of mechanism prevails in the end is highly variable and is influenced by the viral strain and the cell type being infected. Enteric picornaviruses (e.g. CVB3, EV-A71, HAV) have been well described in this regard, which engage both lytic (apoptosis and necrosis) and non-lytic (exosomes, microvesicles and secretory autophagosomes) egress mechanisms. Additionally, these mechanisms are being exploited for the dissemination of infectious particles [64].

The observed large granular materials corresponding to vesicles around AiV-A1 infected Vero cells resemble apoptotic bodies due to their large size, cell shrinkage and cell death (Figure 9A–B) [160]. As to why CVB3 infected Vero cells did not exhibit these vesicles is unclear. While in Hela and COS-1 cells, CVB3 triggers apoptosis, polarized Caco-2 cells infected with CVB3 strain RD undergo necrotic cell death [180-182]. The exact nature of the AiV-A1 induced vesicles remains to be investigated and whether they perhaps contain infectious virions. This would then rather point to an exosomal origin as a means of bulk virus dissemination.

Although AiV-A1 is considered a putative agent of acute gastroenteritis, four human colon carcinoma-derived cell lines (Caco-2, T84, RKO and HCEC 1CT) tested by us did not produce a significant viral titre 3 days pi following challenge by the A846/88 strain (Figure 10A). By contrast, transfection with *in vitro* transcribed AiV-A1 A846/88 RNA yielded elevated titres, suggesting that infection was restricted at an early stage of the virus life cycle (Figure 10B). This may be taken to indicate that theses cell lines lack the still elusive entry receptor or that it is expressed at a very low level insufficient for significant progeny virus production. The poor susceptibly of A549 cells for SARS-CoV-2 infection was found to be due to a very

low expression of the ACE2 receptor [183-185]. Of note, AiV-A1 kvgh2010 (Taiwanese strain) productively replicated in isolated mouse intestinal epithelial cells and to a lesser extent in T84 cells [169]. The various amino acid differences in the capsid of the two AiV-A1 strains could be an explanation for the difference in infectivity of T84 cells, perhaps broadening the repertoire of receptors recognized by this strain on its host cells.

4.2. Entry and Cellular Trafficking of AiV-A1

Characterising the entry and intracellular routing of a virus is essential for understanding the underlying pathogenesis and necessary for the development of potential antiviral treatments. Picornaviruses have been described to utilise a variety of different cellular entry and routing pathways [161], depending on the cell type and the respective member of this large family. Group B coxsackieviruses are a very good example of this diversity. While in polarised intestinal epithelial cells CVB entry is dynamin-independent and lipid raft-dependent, combining features of caveolar endocytosis and macropinocytosis, uptake into polarized endothelial cells requires dynamin II and caveolar endocytosis [186].

In the absence of a suitable intestinal cell line supporting AiV-A1 replication, the fully permissive Vero cells were used to gain first insight into the entry pathway(s) of this putative pathogen. We found that AiV-A1 A846/88 uptake into this African green monkey kidney cell line is highly dynamin dependent (Figure 11). This suggests that its endocytosis is mediated by either clathrin or endophilin, since both pathways require the GTPase for membrane fission [67]. Fast endophilin-mediated endocytosis (FEME) has recently been described as a crucial pathway for rapid endocytosis and is clathrin independent but dynamin dependent [73]. It was shown that EV-A71 uptake in polarized Caco-2 is endophilin-A2-mediated [74]. However, dynasore, though nominally an inhibitor of dynamin I/II, reportedly has off-target

effects, potentially impairing actin and thus macropinocytosis and phagocytosis [187]. Indeed, cell death was also reduced by almost 50% when AiV-A1 infected cells were treated with the myosin II inhibitor blebbistatin, indicating the involvement of macropinocytosis. To precisely unravel the dynamin-dependent entry, future experiments designed to achieve clathrin or endophilin A2 depletion by knowdown/out or dominant negative form must be conducted [73, 188, 189]. Additionally, a co-localisation with labelled high molecular dextran would furnish the involvement of macropinocytosis [190].

At the level of intracellular routing for uncoating, AiV-A1 was strongly dependent on endosomal acidification as exemplified in the drastic inhibition of virus production by bafilomycin A1 and ammonium chloride. Zhu et al. (2016) [42], however, showed that exposure of AiV-A1 A846/88 to acidic buffers did not render its genome accessible for RNA binding probes at pH levels found in early to late endosomes. This suggests that, in addition to endosomal acidification, a cellular receptor is likely assisting AiV-A1 uncoating. A precedent is EV-A71, which is also stable at low pH and likewise depends on a receptor combined with an acidic milieu to trigger conformational changes affording genome release [42, 191].

Additionally, the inhibitor EGA strongly decreased cell death of AiV-A1 infected cells. EGA is a aryl semicarbazone, which blocks trafficking between the early and late endosome, and therefore transfer towards lysosomes [168]. Although the cellular target remains unknown, the blockage is not achieved by elevating endosomal pH as for lysosomotropic agents (e.g. bafilomycin A1 and ammonium chloride). When combining the findings with EGA and NH_4Cl with the small reduction of virus-induced cell death upon treatment with nocodazole and ciliobrevin A, it seems likely that AiV-A1 is routed along the lysosomal pathway. This hypothesis is corroborated by studies done with RV-A2 and RV-B14, which

both utilise the lysosomal pathway for infection of HeLa cells [89]. In each instance, treatment with EGA and NH_4Cl reduced viral infection, while ciliobrevin A and nocodazole had no significant effect. Future co-localisation studies with Rab5 or EEA1 (early endosome marker), Rab7 (late endosome marker) and LAMP-1 or 2 [89, 192] in combination with anti-AiV-A1 antibody will be required to confirm the pathway tentatively proposed for intracellular AiV-A1 trafficking and for revealing its precise site of uncoating.

4.3. Infection of Human Intestinal Epithelium

4.3.1. Aichivirus A1 strain A846/88

Previously, it was shown that AiV-A1 kvgh2010, a strain isolated from a Taiwanese gastroenteritis patient, could grow in the human colon-derived T84 cell line [157, 169]. The same strain could also infect isolated primary murine intestinal epithelial cells, resulting in titres of about 10^7 $TCID_{50}$/ml over a period of two days. [169]. Our data importantly extend these findings by unequivocally demonstrating that AiV-A1 A846/88 is able to infect human stem cell-derived small intestinal tissue and short-term cultivated tissue slices prepared from a human intestinal tract biopsy. These findings considerably substantiate epidemiological observations claiming that AiV-A1 is an aetiological agent of acute gastroenteritis in humans. As already noted before, four human colon cancer-derivatives including T84 cells were resistant to infection by AiV-A1 A846/88. This suggests that the receptor(s) required for binding/internalization is/are massively downregulated in these dedifferentiated cell lines. This is strikingly similar to rhinovirus C, which grows only in primary airway tissue explants and highly differentiated human airway epithelial cells cultivated at air-liquid interface [193, 194]

Susceptibility of the EpiIntestinal tissue model to enteric viruses was confirmed by its productive infection with CVB3 Nancy. The level of intracellular viral RNA (vRNA) expectedly increased over time pi, correlating with a steady increase in cumulative virus titre. By comparison, the vRNA and the titre measurements of AiV-A1 produced by this HIE system showed a strikingly different course, where the intracellular vRNA exhibited a peak at 24 h pi and then dropped despite a continuous low titre progeny virus production. This may be explained by background vRNA in the form of non-internalized AiV-A1 remaining attached to the HIE, despite the removal of a substantial amount of virus during collection of the medium at T0 (resulting in the T0 titre) (Figure 12). A likely reason could be the unspecific capture of infectious particles in the mucous layer formed apically, which was probably only incompletely removed by the gentle washing step. This background vRNA conceivably obscured a low-level viral replication examined by RT-qPCR when using total RNA samples (Figure 12F). The background presumably gradually diminished over time pi due to the successive medium collection steps until likely disappearing at about 72 h pi. After this point, the detected small amounts of vRNA remained constant, indicative of a low-level productive infection. Notably, AiV-A1 kvgh2010 vRNA exhibited a comparable drop of approximately 2 times in infected T84 cells and remained stable for three days (later time points were not investigated by these authors) [169]. In contrast, primary murine intestinal epithelial cells allowed a continuously increased replication of AiV-A1 kvgh2010 for two days [169], similar to our results with CVB3 Nancy in HIE. In future experiments, photosensitive compounds (e.g. neutral red, acridine orange) could be incorporated into viral particles during virus production. These particles can be rendered non-infectious when exposed to light at certain wavelengths, which may help to drastically reduce the interfering vRNA background observed in our study [148, 195, 196].

In the past, EV-A71 has been shown to preferentially infect HIE from the apical side whereas human parechovirus (HPeV) infect human airway epithelium (HAE) from the basolateral side [148, 197]. While not yet known for AiV-A1, we did not determine the preferred entry side for infection of the HIE due to the high costs of these tissue equivalents. We instead discovered the preferential release of AiV-A1 progeny from the apical side (Figure 12D). A preferentially apical release of progeny virions from the infected EpiIntestinal tissue was also observed for CVB3-Nancy. Several other enteric picornaviruses similarly favour apical exit of newly produced particles [148, 198, 199]. In contrast, Roodsant et al. (2020) [200], besides apical release, also observed a significant basolateral exit in HIE for EV-A71 strain C1 91-480 (Good et al. (2019) [148] used EV-A71 strain 1095). However, passive leakage caused by a loss in epithelium integrity was found to be responsible, potentially induced by a larger membrane pore size (approximately ten times compared to Good et al. [2019]). Alternatively, the usage of different EV-71 virus strains may underly their variability in polarised cell release. A dominantly apical egress was also observed for various other unrelated enteric viruses such as rotavirus (*Reoviridae)* [201], hepatitis E virus (*Herpeviridae*) [202] and SARS-CoV-2 [203].

The induction of the antiviral state during the AiV-A1 infection in HIE was less pronounced compared to CVB3 (Figure 14A–B). Since the number of infected cells of the EpiIntestinal system at 24 h pi was comparable between the viruses (Figure 13C–D), the distinctly different induction of innate immunity genes might potentially correlate with their different replication rate and thus production of dsRNA recognized by PRRs. Similar conclusions were drawn for differences in the innate immune response towards SARS-CoV-2 in human bronchial epithelial models [183, 204]. Nevertheless, we measured a significant, but rather very weak, upregulation of IFNλ1 and Mx2 in AiV-A1 A846/88 infected HIE. The IFNλ

upregulation is typical for mucosal surfaces. [120, 205]. Previous studies in T84 cells with AiV-A1 kvgh2010 exhibited an inconsistent upregulation of type I IFN and RIG-like receptors (RLRs) [169], similarly as found for the AiV-A1 A846/88 used in our work with HIE. Also, infection of murine intestinal epithelial cells by AiV-A1 kvgh2010 elicited only a moderate type I and III IFN signalling, followed by upregulation of some ISGs [59, 169]. Furthermore, Chang et al. (2019) [169] observed that infections of the murine intestinal epithelial cells with higher MOI of kvgh2010 significantly reduced the antiviral response. The antiviral state established in A549 cells (lung carcinoma-derived) infected with AiV-A1 kvgh2010 was also moderate compared to the exposure with the viral dsRNA analogue polyI:C [59]. The authors further found that in these cells, the AiV-A1 kvgh2010 non-structural protein 3C effectively downregulated the expression of several co-factors along the RLR signalling pathway (e.g. RIG-I, MDA5, MyD88, IKK-ϵ, TBK1, MAVS, IRF3, IRF7), thus damping the antiviral machinery. Previous studies on other enteroviruses 3C proteins (e.g. from CVB3) revealed a similar specific targeting of the RLR signalling pathway [206].

Despite their well-described repertoire of countermeasures to dampen the innate immunity, different stem cell-derived enteroids and organoids infected with enteroviruses E11, EV-A71 and CVB strains exhibited a strong type I, type III IFN and ISG response [148, 149, 206-208]. As already mentioned before, we observed a similar upregulation of innate immune response genes in the EpiIntestinal system infected by the CVB3 Nancy strain. However, human foetal-derived intestinal enteroids exhibited no antiviral response when infected with the strain RD of CVB3 [209]. The reason underlying these strain-specific differences are only incompletely understood and may range from different cleavage efficiencies of the virus-encoded proteases to differences in the recognition of their dsRNA intermediates.

In addition to the weak antiviral state, we observed no loss of the epithelial barrier over four days in AiV-A1 infected HIE (Figure 14C–D). Notably, AiV-A1 kvgh2010 infected primary mouse intestinal epithelial cells also remained intact over a comparable time frame [169]. EV-A71 and human norovirus were similarly reported not to disrupt the integrity of the intestinal mucosa [128, 148], despite the detection of minor cell death for multiple human norovirus GII.4 variants [144]. In contrast, E7, E11, SARS-CoV-2 and rotavirus disrupt the intestinal epithelium [141, 146, 149, 210]. It is still elusive why certain viruses provoke a loss in epithelial barrier and others not.

By immunofluorescence microscopy analysis of AiV-A1 infected HIE, we co-localised the viral dsRNA with distinct markers for absorptive (ApoA1) and proliferative (Ki-67) enterocytes at the apical side (Figure 13A, 14D and 15A). Single-cell transcriptomics analyses on SARS-CoV-2 infected human intestinal organoids delineated immature enterocytes type 2, a subpopulation of enterocytes which is not yet terminally differentiated, as the prime target [203]. It remains to be shown, whether these correspond to the AiV-infected proliferative enterocytes. The spectrum of infected intestinal tract cells substantially varies among different enteric viruses in an unpredictable manner. For example, *in situ* hybridisation studies on small intestinal tissue from immunocompromised patients positive for norovirus found enterocytes, epithelial regions above the GALT and enteroendocrine cells to be infected [144, 211]. Rotavirus infects enterocytes and enterochromaffin cells, a subpopulation of the enteroendocrine cell lineage [212, 213]. Enteroviruses E11 and EV-A71 (strain 1095) primarily replicate in enterocytes, enteroendocrine and goblet cells in human intestinal enteroids, respectively [148, 149], while Zhao et al. (2021) [207] concluded that EV-A71 (strain MY104-9-SAR-97) also infected enterocytes due to co-localisation of VP1 with the general epithelial marker villin (VIL1). Additionally, we located AiV-A1 A846/88 infected cells in thick-cut

patient-derived ileal slices (Figure 15B). However, the quality of the sample was not sufficient for a precise determination of the infected cell type. For a future high quality staining, precision-cut tissue needs to be prepared [214].

In summary, our data show for the first time the infection of a HIE model by AiV-A1, and thus substantiate the epidemiological observations that AiV-A1 is a causative agent for acute gastroenteritis in humans. Nevertheless, several unanswered questions remain. Further studies will be needed to elaborate on the untypical viral growth kinetics regarding viral shedding, RNA replication and tissue spread. Additionally, the precise reason for the weak innate immune response against AiV-A1 in human intestinal cells remains to be investigated. Since the innate immune response may vary between infected and bystander cells, single-cell RNA sequencing would provide an excellent tool to uncover these details in depth as it has been recently done for SARS-CoV-2 and astrovirus [141, 215].

4.3.2. Coxsackievirus B3 strain Nancy

Although CVB3 strain Nancy was primarily utilised as a positive control for the study of AiV-A1, we were able to expand the knowledge on the pathogenesis of CVB3 in the human small intestine in regard to its replication over an extended period of time and the ensuing innate immune response. Drummond et al. (2017) first described the replication of CVB3 with the strain RD in human foetal-derived intestinal enteroids but only until 24 h pi [149].

CVB3 Nancy readily replicated for four days in the HIE shedding high amounts of *de novo* produced infectious particles into the apical compartment every 24 hours (Figure 12A–C). Furthermore, CVB3 preferentially egressed from the apical side as previously reported for EV-A71 and HPeV [148, 197]. The number of infected cells was approximately 2% at 24 h pi (Figure 13D) and the replication centres were located at the apical side (Figure 13A and 14D).

Furthermore, we identified for the first time absorptive and proliferative enterocytes to be infected by CVB3 (Figure 15A). Interestingly, although AiV-A1 and CVB3 replicated in the same intestinal cell types, both viruses behaved completely different in regard to growth kinetics and antiviral induction (Figure 12 and 14). Therefore, the observed differences must be attributed to intrinsic features of each virus rather than to external factors.

Despite the increasing replication of CVB3 over time, IHC micrographs presented no loss in epithelial integrity 24 h pi compared to E11 investigated by others (Figure 14D) [149]. Nevertheless, infectious particles were again present at the basolateral side at 96 h pi, which could indicate a virus-induced cell lysis in the epithelium at a later point resulting in non-directional virus release (Figure 12A).

Furthermore, we measured a high elevation of the type I and type III IFN gene expression, which was contrary to the observations by Drummond et al. (2017) [149] (Figure 14A). IFNλ1 was the most highly induced gene, similar to AiV-A1 but of significantly greater magnitude, which consequently resulted in a substantially increased expression of ISGs. The lack of an antiviral response in Drummond's human foetal-derived enteroids could be explained by a difference in viral strain (CVB3 strain RD) or by organoid culturing. The latter is a known issue due to non-standardised culture conditions for differentiation and maintenance [140]. It is of note that despite the strong innate immune response, the CVB3 infection was not cleared after four days. In contrast, the decreased replication of EV-A71 over four days in HIE was attributed to type III IFN signalling [148].

Our observations with CVB3 may be taken to indicate a perhaps non-lytic persistent infection similar to other enteric viruses (e.g. human adenovirus [216] and SARS-CoV [217]). While not mentioned in the section on AiV-A1, a persistent infection may also underly the continuous low-level production of viral progeny by the infected EpiIntestinal system. Some

support for this hypothesis comes from investigations of other picornaviruses. Though typically exhibiting a lytic life cycle, they can also persistently infect certain cell types and tissues [218-222]. Several chronic diseases (e.g. chronic cardiomyopathies [223, 224], type 1 diabetes [225, 226] and post-polio syndrome [227, 228]) are associated with the persistent infection caused specifically by group B coxsackieviruses [229]. Longer infection times in different HIE model systems would be required to substantiate the proposed persistent infection by CVB3 and perhaps also AiV-A1, since the EpiIntestinal system lasts not longer than two weeks.

APPENDIX

Table S1. Selected AiV-A1 strains used for phylogenetic tree construction.

Strain	GeneBank ID	Genotype	Country	Sequencing	Reference
16317x87	MF947441	B	Vietnam	VP1	[28]
A846/88 1998	AB010145.1	A	Japan	3CD	[17]
A846/88 2001	AB040749.1	A	Japan	3CD	[19]
BAY/1/03/DEU	AY747174.1	A	Germany	3CD	[230]
Chshc7	FJ890523	B	China	3CD	[231]
D/VI2169/2004	GQ927704.2	B	Germany	3CD	[232]
D/VI2244/2004	GQ927712.2	B	Germany	3CD	[232]
D/VI2287/2004	GQ927711.2	A	Germany	3CD	[232]
D/VI2321/2004	GQ927706.2	B	Germany	3CD	[232]
D/VI2359/2004	GQ927705.2	B	Germany	3CD	[232]
FSS693	MG200054.1	B	Australia	3CD	[233]
Goiania/GO/03/01/Brazil	DQ028632.1	B	Brazil	3CD	[230]
kvgh99012632/2010	JX564249.1	A	Taiwan	VP1	[157, 233]
Rn48/2002	EU159259.1	C	France	VP1	[27]

Figure S1. Strain authenticity of *in vitro* transcribed AiV-A1 A846/88 RNA. The i*n vitro* transcribed RNA of AiV-A1 A846/88 from the plasmid pAV-UCSF was reverse transcribed into single-stranded cDNA and used as a template for a qPCR with two different sets of primers (A) RW–SQP1 and (B) Fw–SQP2. The resulting amplicons were sanger sequenced to confirm the identity of the two partial sequences with the GenBank entry for the AiV-A1 A846/88 (accession no. JQ281544). Sequencing alignment was done with Clustal Omega [234].

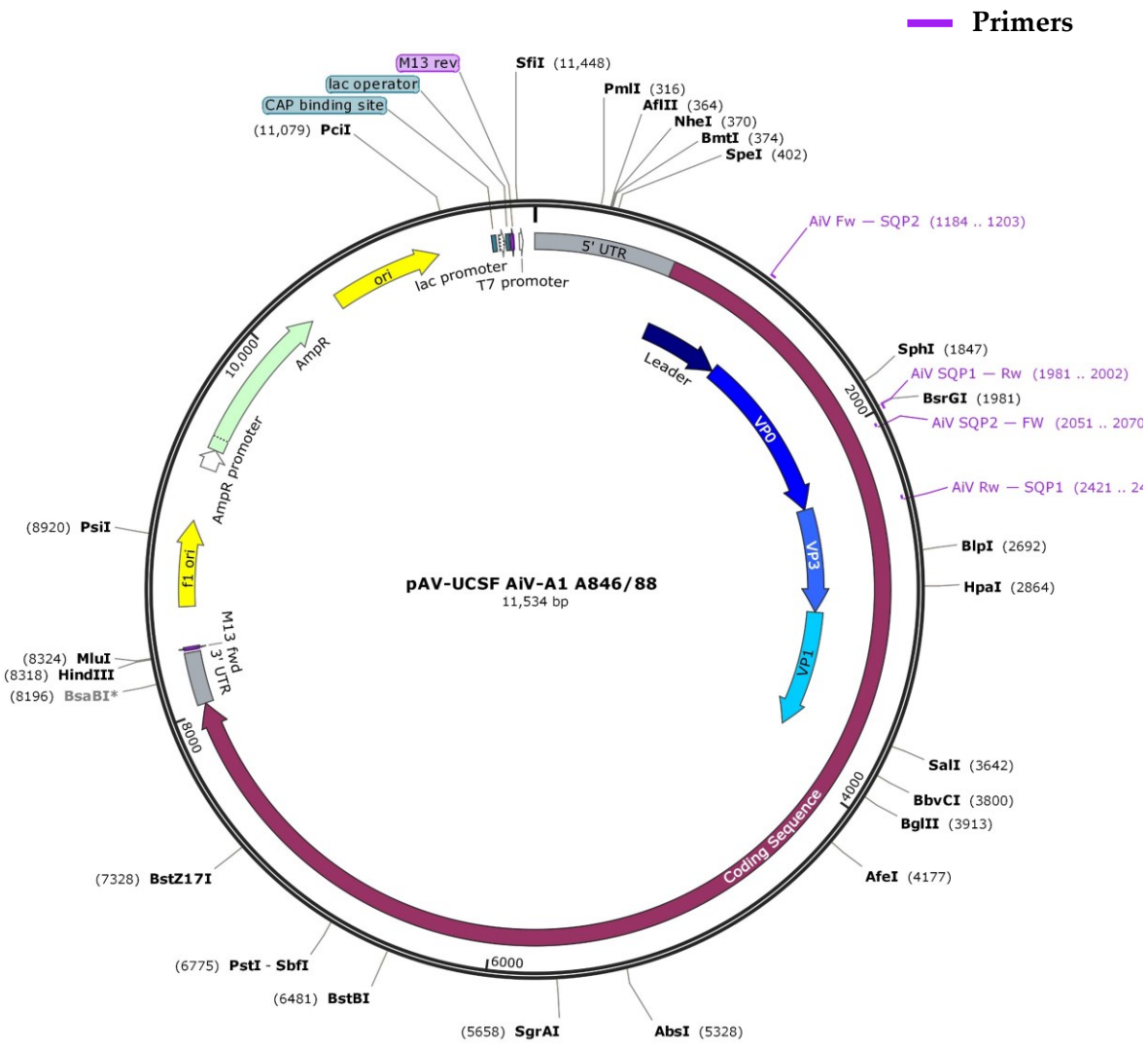

Figure S2. Plasmid map of pAV-UCSF containing the cDNA clone of AiV-A1 strain A846/88. Primers used for strain authentication are displayed in violet.

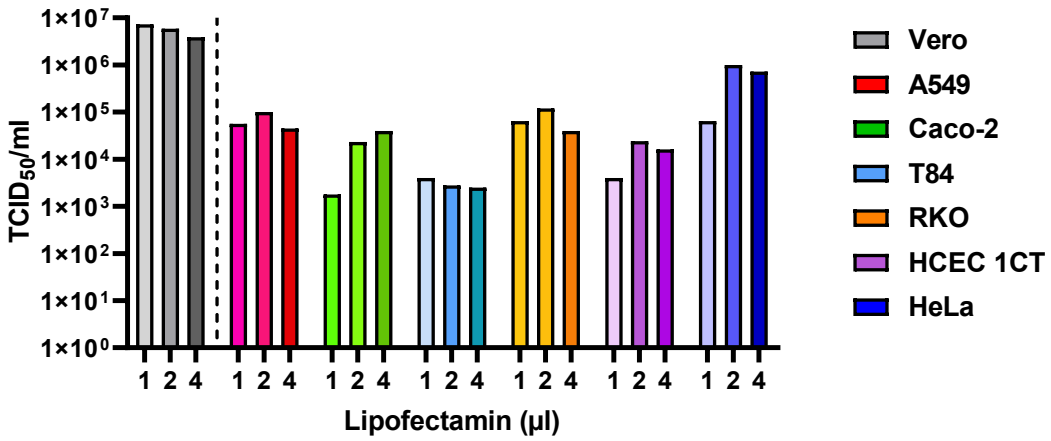

Figure S3. Transfection of AiV-A1 RNA into human cell lines yields higher titres than infection. Each cell line was transfected with 1 μg of AiV-A1 RNA with different amounts of lipofectamine 2000 (1, 2 and 4 μl) and after three days the well contents were collected. Seed virus was produced from well contents and the titre was determined by $TCID_{50}$. Each bar represents the three different lipofectamine amounts.

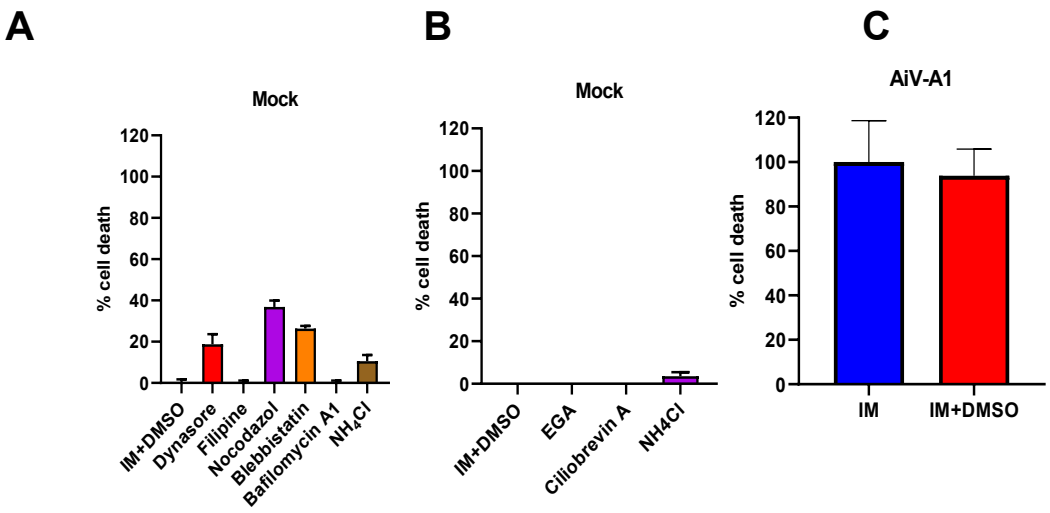

Figure S4. AiV-A1 is likely routed towards the lysosomal pathway. 96-well plates of Vero cells were pre-treated with different pharmacological agents (solved in DMSO) for 1 h at 37°C, before being challenged with AiV-A1 (MOI = 10) for 24 hours at 37°C in the presence of the inhibitors. The infection was stopped using crystal violet staining when the cells without inhibitor treatment (solvent control) showed distinct CPE**. (A–B)** Cytotoxicity analyses of respective drugs in uninfected cells**. (C)** Comparison of infection efficiency between IM and solvent control (IM+DMSO). Using the Measure Tool of the Fiji plug-in of ImageJ, the amount of cell death was measured by the crystal violet stain, normalized in GraphPad Prism and displayed as [%] cell death. Solvent control plus virus was arbitrarily set to 100% cell death and non-infected wells with the respective drugs were set to 0% cell death. Displayed is the mean ± SD from one independent experiment with each condition conducted in quadruplicates.

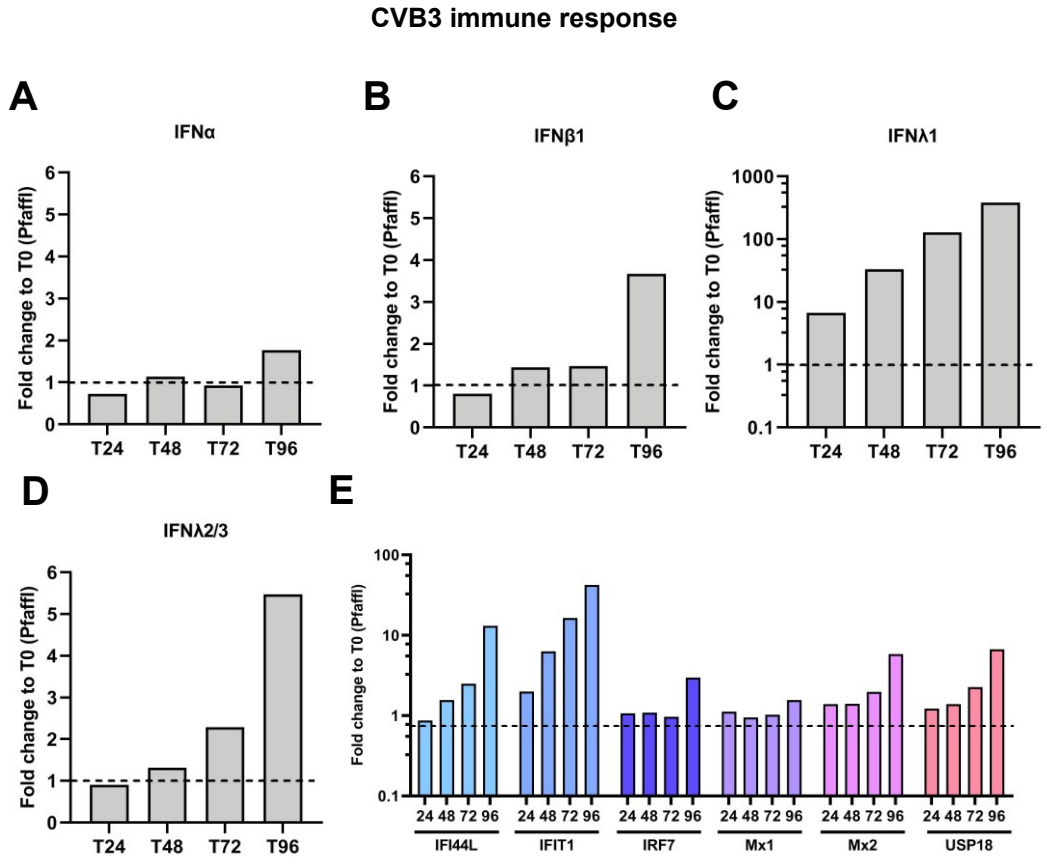

Figure S5. CVB3 Nancy induces a strong antiviral state in HIE. HIE were infected apically and basolaterally with 10^7 PFU of CVB3 Nancy for 1 hour at 37°C, simultaneously. At indicated time points pi, the RNA was extracted from HIE and the induction of the antiviral state was elucidated by RT-qPCR. **(A-D)** Shown is the IFN signalling. **(E)** Displayed is the ISG signalling. Human 18s rRNA was used as housekeeping gene. Fold change was calculated according to the Pfaffl method. Each time point represents an independently prepared HIE.

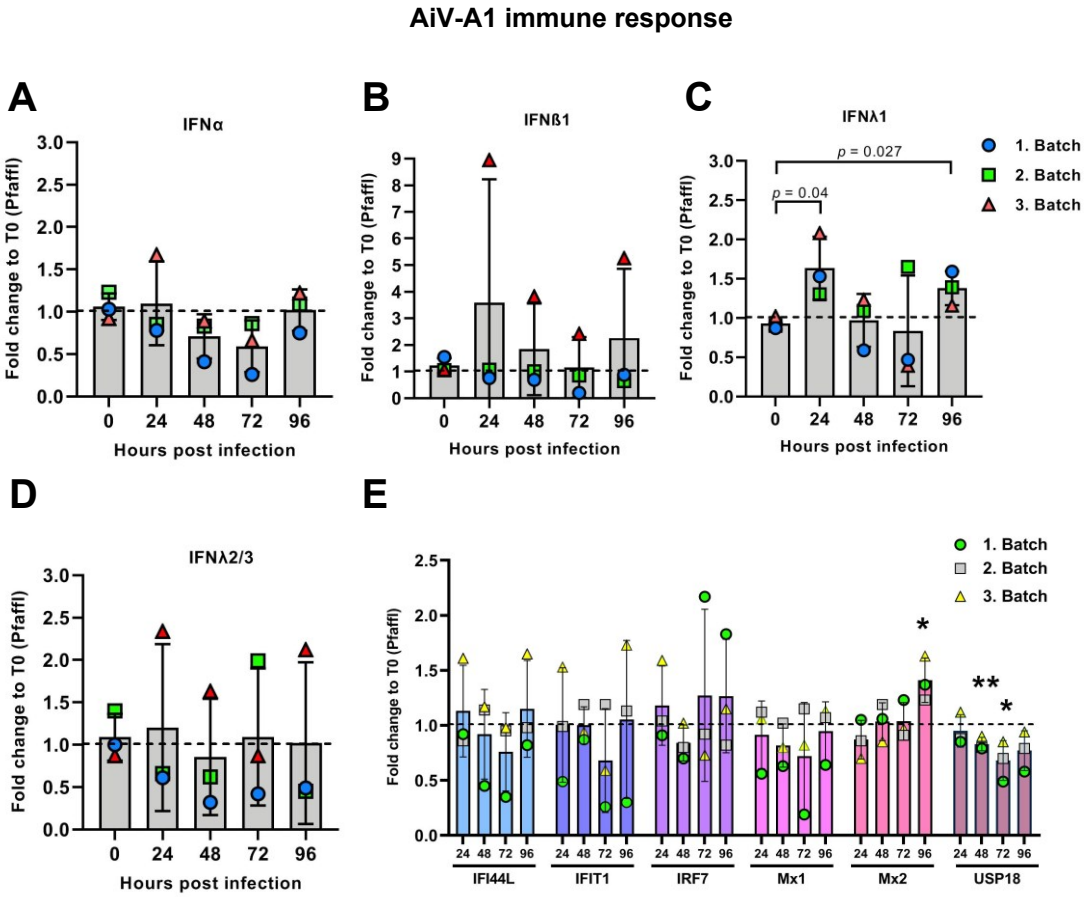

Figure S6. AiV-A1 triggers a weak type III IFN and ISG signalling in HIE. HIE were infected apically and basolaterally with 10^7 PFU of AiV-A1 for 1 hour, simultaneously. At indicated time points post infection, the RNA was extracted from HIE and the induction of the antiviral state was elucidated by RT-qPCR. **(A-D)** Displayed is the IFN signalling. **(E)** Shown is the ISG signalling. Human 18s rRNA was used as housekeeping gene. Fold change was calculated according to the Pfaffl method. Each individual symbol represents an independently produced HIE prepared in three batches. Asterisks (black) indicate statistical significance calculated by Student's t-test ($^*P < 0.05$, $^{**}P < 0.01$).

BIBLIOGRAPHY

1. King, A.M.Q., F. Brown, P. Christian, T. Hovi, T. Hyypiä, N.J. Knowles, S.M. Lemon, P.D. Minor, A.C. Palmenberg, T. Skern, and G. Stanway, *Picornaviridae*, in *Virus Taxonomy. Seventh Report of the International Committee for the Taxonomy of Viruses*, M.H.V. Van Regenmortel, Fauquet C.M., Bishop D.H.L., Calisher C.H., Carsten E.B., Estes M.K., Lemon S.M., Maniloff J., Mayo M.A., McGeoch D.J., Pringle C.R., Wickner R.B., Editor. 1999: Academic Press, New York, San Diego. p. 657–673.

2. Yamashita, T., M. Ito, Y. Kabashima, H. Tsuzuki, A. Fujiura, and K. Sakae, *Isolation and characterization of a new species of kobuvirus associated with cattle.* J Gen Virol, **2003**. 84(Pt 11): p. 3069-3077.

3. Reuter, G., A. Boldizsár, and P. Pankovics, *Complete nucleotide and amino acid sequences and genetic organization of porcine kobuvirus, a member of a new species in the genus Kobuvirus, family Picornaviridae.* Arch Virol, **2009**. 154(1): p. 101-8.

4. Reuter, G., A. Boldizsár, I. Kiss, and P. Pankovics, *Candidate new species of Kobuvirus in porcine hosts.* Emerg Infect Dis, **2008**. 14(12): p. 1968-70.

5. Kapoor, A., P. Simmonds, E.J. Dubovi, N. Qaisar, J.A. Henriquez, J. Medina, S. Shields, and W.I. Lipkin, *Characterization of a canine homolog of human Aichivirus.* Journal of virology, **2011**. 85(21): p. 11520-11525.

6. Wu, Z., X. Ren, L. Yang, Y. Hu, J. Yang, G. He, J. Zhang, J. Dong, L. Sun, J. Du, L. Liu, Y. Xue, J. Wang, F. Yang, S. Zhang, and Q. Jin, *Virome analysis for identification of novel mammalian viruses in bat species from Chinese provinces.* J Virol, **2012**. 86(20): p. 10999-1012.

7. Smits, S.L., V.S. Raj, M.D. Oduber, C.M.E. Schapendonk, R. Bodewes, L. Provacia, K.J. Stittelaar, A.D.M.E. Osterhaus, and B.L. Haagmans, *Metagenomic Analysis of the Ferret Fecal Viral Flora.* PLOS ONE, **2013**. 8(8): p. e71595.

8. Oem, J.K., M.H. Lee, K.K. Lee, and D.J. An, *Novel Kobuvirus species identified from black goat with diarrhea.* Vet Microbiol, **2014**. 172(3-4): p. 563-7.

9. Pankovics, P., Á. Boros, H. Bíró, K.B. Horváth, T.G. Phan, E. Delwart, and G. Reuter, *Novel picornavirus in domestic rabbits (Oryctolagus cuniculus var. domestica).* Infect Genet Evol, **2016**. 37: p. 117-22.

10. Pankovics, P., Á. Boros, T. Kiss, and G. Reuter, *Identification and complete genome analysis of kobuvirus in faecal samples of European roller (Coracias garrulus): for the first time in a bird.* Arch Virol, **2015**. 160(1): p. 345-51.

11. Yamashita, T., M. Sugiyama, H. Tsuzuki, K. Sakae, Y. Suzuki, and Y. Miyazaki, *Application of a reverse transcription-PCR for identification and differentiation of Aichi virus, a new member of the Picornavirus family associated with gastroenteritis in humans.* J Clin Microbiol, **2000**. 38(8): p. 2955-61.

12. Park, S.J., H.K. Kim, H.J. Moon, D.S. Song, S.M. Rho, J.Y. Han, V.G. Nguyen, and B.K. Park, *Molecular detection of porcine kobuviruses in pigs in Korea and their association with diarrhea.* Arch Virol, **2010**. 155(11): p. 1803-11.

13. Khamrin, P., N. Maneekarn, S. Peerakome, S. Okitsu, M. Mizuguchi, and H. Ushijima, *Bovine kobuviruses from cattle with diarrhea.* Emerg Infect Dis, **2008**. 14(6): p. 985-6.

14. Yamashita, T., S. Kobayashi, K. Sakae, S. Nakata, S. Chiba, Y. Ishihara, and S. Isomura, *Isolation of cytopathic small round viruses with BS-C-1 cells from patients with gastroenteritis.* J Infect Dis, **1991**. 164(5): p. 954-7.

15. Otomaru, K., Y. Naoi, K. Haga, T. Omatsu, T. Uto, M. Koizumi, T. Masuda, H. Yamasato, H. Takai, H. Aoki, S. Tsuchiaka, K. Sano, S. Okazaki, Y. Katayama, M. Oba, T. Furuya, J. Shirai, K. Katayama, T. Mizutani, and M. Nagai, *Detection of novel kobu-like viruses in Japanese black cattle in Japan.* J Vet Med Sci, **2016**. 78(2): p. 321-4.

16. Reuter, G., A. Boros, and P. Pankovics, *Kobuviruses - a comprehensive review.* Rev Med Virol, **2011**. 21(1): p. 32-41.

17. Yamashita, T., K. Sakae, H. Tsuzuki, Y. Suzuki, N. Ishikawa, N. Takeda, T. Miyamura, and S. Yamazaki, *Complete nucleotide sequence and genetic organization of Aichi virus, a distinct member of the Picornaviridae associated with acute gastroenteritis in humans.* J Virol, **1998**. 72(10): p. 8408-12.

18. Davis, M., S.M. Sagan, J.P. Pezacki, D.J. Evans, and P. Simmonds, *Bioinformatic and physical characterizations of genome-scale ordered RNA structure in mammalian RNA viruses.* J Virol, **2008**. 82(23): p. 11824-36.

19. Sasaki, J., Y. Kusuhara, Y. Maeno, N. Kobayashi, T. Yamashita, K. Sakae, N. Takeda, and K. Taniguchi, *Construction of an infectious cDNA clone of Aichi virus (a new member of the family Picornaviridae) and mutational analysis of a stem-loop structure at the 5′ end of the genome.* Journal of virology, **2001**. 75(17): p. 8021-8030.

20. Jan, E., I. Mohr, and D. Walsh, *A Cap-to-Tail Guide to mRNA Translation Strategies in Virus-Infected Cells.* Annu Rev Virol, **2016**. 3(1): p. 283-307.

21. Sweeney, T.R., V. Dhote, Y. Yu, and C.U.T. Hellen, *A distinct class of internal ribosomal entry site in members of the Kobuvirus and proposed Salivirus and Paraturdivirus genera of the Picornaviridae.* Journal of virology, **2012**. 86(3): p. 1468-1486.

22. Sasaki, J. and K. Taniguchi, *The 5′-end sequence of the genome of Aichi virus, a picornavirus, contains an element critical for viral RNA encapsidation.* Journal of virology, **2003**. 77(6): p. 3542-3548.

23. Yogo, Y. and E. Wimmer, *Polyadenylic acid at the 3′-terminus of poliovirus RNA.* Proc Natl Acad Sci U S A, **1972**. 69(7): p. 1877-82.

24. Sasaki, J., K. Ishikawa, and K. Taniguchi, *3CD, but not 3C, cleaves the VP1/2A site efficiently during Aichi virus polyprotein processing through interaction with 2A.* Virus Res, **2012**. 163(2): p. 592-8.

25. Rivadulla, E. and J.L. Romalde, *A Comprehensive Review on Human Aichi Virus.* Virologica Sinica, **2020**.

26. Kobayashi, S., T. Morishita, T. Yamashita, K. Sakae, O. Nishio, T. Miyake, Y. Ishihara, and S. Isomura, *A large outbreak of gastroenteritis associated with a small round structured virus among schoolchildren and teachers in Japan.* Epidemiol Infect, **1991**. 107(1): p. 81-6.

27. Ambert-Balay, K., M. Lorrot, F. Bon, H. Giraudon, J. Kaplon, M. Wolfer, P. Lebon, D. Gendrel, and P. Pothier, *Prevalence and Genetic Diversity of Aichi Virus Strains in Stool Samples from Community and Hospitalized Patients*. Vol. 46. 2008. 1252-8.

28. Lu, L., N. Van Dung, A. Ivens, C. Bogaardt, A. O'Toole, J.E. Bryant, J. Carrique-Mas, N. Van Cuong, P.H. Anh, M.A. Rabaa, N.T. Tue, G.E. Thwaites, S. Baker, P. Simmonds, M.E. Woolhouse, and V. Consortium, *Genetic diversity and cross-species transmission of kobuviruses in Vietnam.* Virus evolution, **2018**. 4(1): p. vey002-vey002.

29. Holmes, E.C., S.A. Goldstein, A.L. Rasmussen, D.L. Robertson, A. Crits-Christoph, J.O. Wertheim, S.J. Anthony, W.S. Barclay, M.F. Boni, P.C. Doherty, J. Farrar, J.L. Geoghegan, X. Jiang, J.L. Leibowitz, S.J.D. Neil, T. Skern, S.R. Weiss, M. Worobey, K.G. Andersen, R.F. Garry, and A. Rambaut, *The origins of SARS-CoV-2: A critical review.* Cell, **2021**. 184(19): p. 4848-4856.

30. Kitajima, M. and C.P. Gerba, *Aichi virus 1: environmental occurrence and behavior.* Pathogens, **2015**. 4(2): p. 256-68.

31. Tamura, K., G. Stecher, and S. Kumar, *MEGA11: Molecular Evolutionary Genetics Analysis Version 11.* Molecular Biology and Evolution, **2021**. 38(7): p. 3022-3027.

32. Jonsson, N., K. Wahlström, L. Svensson, L. Serrander, and A.M. Lindberg, *Aichi virus infection in elderly people in Sweden.* Archives of Virology, **2012**. 157(7): p. 1365-1369.

33. Nielsen, A.C., M.L. Gyhrs, L.P. Nielsen, C. Pedersen, and B. Böttiger, *Gastroenteritis and the novel picornaviruses aichi virus, cosavirus, saffold virus, and salivirus in young children.* J Clin Virol, **2013**. 57(3): p. 239-42.

34. Rivadulla, E., M.F. Varela, and J.L. Romalde, *Epidemiology of Aichi virus in fecal samples from outpatients with acute gastroenteritis in Northwestern Spain.* J Clin Virol, **2019**. 118: p. 14-19.

35. Kaikkonen, S., S. Räsänen, M. Rämet, and T. Vesikari, *Aichi virus infection in children with acute gastroenteritis in Finland.* Epidemiol Infect, **2010**. 138(8): p. 1166-71.

36. Yamashita, T., M. Ito, H. Tsuzuki, and K. Sakae, *Identification of Aichi virus infection by measurement of immunoglobulin responses in an enzyme-linked immunosorbent assay.* J Clin Microbiol, **2001**. 39(11): p. 4178-80.

37. Bucciol, G., L. Moens, K. Payne, E. Wollants, D. Mekahli, E. Levtchenko, F. Vermeulen, T. Tousseyn, P. Gray, C.S. Ma, S.G. Tangye, M. Van Ranst, J.R. Brown, J. Breuer, and I. Meyts, *Chronic Aichi Virus Infection in a Patient with X-Linked Agammaglobulinemia.* J Clin Immunol, **2018**. 38(7): p. 748-752.

38. Reuter, G., Á. Boldizsár, G. Papp, and P. Pankovics, *Detection of Aichi virus shedding in a child with enteric and extraintestinal symptoms in Hungary.* Archives of Virology, **2009**. 154(9): p. 1529-1532.

39. Yamashita, T., K. Sakae, Y. Ishihara, S. Isomura, and E. Utagawa, *Prevalence of newly isolated, cytopathic small round virus (Aichi strain) in Japan.* Journal of clinical microbiology, **1993**. 31(11): p. 2938-2943.

40. Ribes, J.M., R. Montava, C.J. Tellez-Castillo, M. Fernandez-Jimenez, and J. Buesa, *Seroprevalence of Aichi virus in a Spanish population from 2007 to 2008.* Clin Vaccine Immunol, **2010**. 17(4): p. 545-9.

41. Le Guyader, F.S., J.C. Le Saux, K. Ambert-Balay, J. Krol, O. Serais, S. Parnaudeau, H. Giraudon, G. Delmas, M. Pommepuy, P. Pothier, and R.L. Atmar, *Aichi virus, norovirus, astrovirus, enterovirus, and rotavirus involved in clinical cases from a French oyster-related gastroenteritis outbreak.* J Clin Microbiol, **2008**. 46(12): p. 4011-7.

42. Zhu, L., X. Wang, J. Ren, A. Kotecha, T.S. Walter, S. Yuan, T. Yamashita, T.J. Tuthill, E.E. Fry, Z. Rao, and D.I. Stuart, *Structure of human Aichi virus and implications for receptor binding.* Nat Microbiol, **2016**. 1(11): p. 16150.

43. Zell, R., *Picornaviridae—the ever-growing virus family.* Archives of Virology, **2018**. 163(2): p. 299-317.

44. Sabin, C., T. Fuzik, K. Skubnik, L. Palkova, A.M. Lindberg, and P. Plevka, *Structure of Aichi virus 1 and its empty particle: clues towards kobuvirus genome release mechanism.* J Virol, **2016**.

45. Tuthill, T.J., E. Groppelli, J.M. Hogle, and D.J. Rowlands, *Picornaviruses.* Curr Top Microbiol Immunol, **2010**. 343: p. 43-89.

46. Berisio, R. and L. Vitagliano, *Polyproline and triple helix motifs in host-pathogen recognition.* Curr Protein Pept Sci, **2012**. 13(8): p. 855-65.

47. Vermeire, J., G. Vanbillemont, W. Witkowski, and B. Verhasselt, *The Nef-infectivity enigma: mechanisms of enhanced lentiviral infection.* Current HIV research, **2011**. 9(7): p. 474-489.

48. Hale, B.G., P.S. Kerry, D. Jackson, B.L. Precious, A. Gray, M.J. Killip, R.E. Randall, and R.J. Russell, *Structural insights into phosphoinositide 3-kinase activation by the influenza A virus NS1 protein.* Proceedings of the National Academy of Sciences, **2010**. 107(5): p. 1954.

49. Baggen, J., H.J. Thibaut, J.R.P.M. Strating, and F.J.M. van Kuppeveld, *The life cycle of non-polio enteroviruses and how to target it.* Nature Reviews Microbiology, **2018**. 16(6): p. 368-381.

50. Sasaki, J. and K. Taniguchi, *Aichi virus 2A protein is involved in viral RNA replication.* J Virol, **2008**. 82(19): p. 9765-9.

51. Hughes, P.J. and G. Stanway, *The 2A proteins of three diverse picornaviruses are related to each other and to the H-rev107 family of proteins involved in the control of cell proliferation.* J Gen Virol, **2000**. 81(Pt 1): p. 201-7.

52. Baggen, J., Y. Liu, H. Lyoo, A.L.W. van Vliet, M. Wahedi, J.W. de Bruin, R.W. Roberts, P. Overduin, A. Meijer, M.G. Rossmann, H.J. Thibaut, and F.J.M. van Kuppeveld, *Bypassing pan-enterovirus host factor PLA2G16.* Nat Commun, **2019**. 10(1): p. 3171.

53. Staring, J., E. von Castelmur, V.A. Blomen, L.G. van den Hengel, M. Brockmann, J. Baggen, H.J. Thibaut, J. Nieuwenhuis, H. Janssen, F.J.M. van Kuppeveld, A. Perrakis, J.E. Carette, and T.R. Brummelkamp, *PLA2G16 represents a switch between entry and clearance of Picornaviridae.* Nature, **2017**. 541: p. 412.

54. Uyama, T., J. Morishita, X.-H. Jin, Y. Okamoto, K. Tsuboi, and N. Ueda, *The tumor suppressor gene H-Rev107 functions as a novel Ca2+-independent cytosolic phospholipase A1/2 of the thiol hydrolase type.* Journal of lipid research, **2009**. 50(4): p. 685-693.

55. Jacobs, S.E., D.M. Lamson, K. St George, and T.J. Walsh, *Human rhinoviruses.* Clinical microbiology reviews, **2013**. 26(1): p. 135-162.

56. Rabouw, H.H., L.J. Visser, T.C. Passchier, M.A. Langereis, F. Liu, P. Giansanti, A.L.W. van Vliet, J.G. Dekker, S.G. van der Grein, J.G. Saucedo, A.A. Anand, M.E. Trellet, A.M.J.J. Bonvin, P. Walter, A.J.R. Heck, R.J. de Groot, and F.J.M. van Kuppeveld, *Inhibition of the integrated stress response by viral proteins that block p-eIF2–eIF2B association.* Nature Microbiology, **2020**.

57. Belov, G.A., *Dynamic lipid landscape of picornavirus replication organelles.* Current Opinion in Virology, **2016**. 19: p. 1-6.

58. Suhy, D.A., T.H. Giddings, Jr., and K. Kirkegaard, *Remodeling the endoplasmic reticulum by poliovirus infection and by individual viral proteins: an autophagy-like origin for virus-induced vesicles.* J Virol, **2000**. 74(19): p. 8953-65.

59. Kung, M.-H., Y.-S. Lin, and T.-H. Chang, *Aichi virus 3C protease modulates LC3- and SQSTM1/p62-involved antiviral response.* Theranostics, **2020**. 10(20): p. 9200-9213.

60. Li, X., M. Wang, A. Cheng, X. Wen, X. Ou, S. Mao, Q. Gao, D. Sun, R. Jia, Q. Yang, Y. Wu, D. Zhu, X. Zhao, S. Chen, M. Liu, S. Zhang, Y. Liu, Y. Yu, L. Zhang, B. Tian, L. Pan, and X. Chen, *Enterovirus Replication Organelles and Inhibitors of Their Formation.* Frontiers in Microbiology, **2020**. 11(1817).

61. Richards, A.L. and W.T. Jackson, *Intracellular vesicle acidification promotes maturation of infectious poliovirus particles.* PLoS pathogens, **2012**. 8(11): p. e1003046-e1003046.

62. Jiang, P., Y. Liu, H.-C. Ma, V. Paul Aniko, and E. Wimmer, *Picornavirus Morphogenesis.* Microbiology and Molecular Biology Reviews, **2014**. 78(3): p. 418-437.

63. Sasaki, J., S. Nagashima, and K. Taniguchi, *Aichi virus leader protein is involved in viral RNA replication and encapsidation.* J Virol, **2003**. 77(20): p. 10799-807.

64. Owusu, I.A., O. Quaye, K.D. Passalacqua, and C.E. Wobus, *Egress of non-enveloped enteric RNA viruses.* Journal of General Virology, **2021**. 102(3).

65. Cossart, P. and A. Helenius, *Endocytosis of viruses and bacteria.* Cold Spring Harb Perspect Biol, **2014**. 6(8).

66. Thottacherry, J.J., M. Sathe, C. Prabhakara, and S. Mayor, *Spoiled for Choice: Diverse Endocytic Pathways Function at the Cell Surface.* Annual review of cell and developmental biology, **2019**. 35: p. 55-84.

67. Rennick, J.J., A.P.R. Johnston, and R.G. Parton, *Key principles and methods for studying the endocytosis of biological and nanoparticle therapeutics.* Nature Nanotechnology, **2021**. 16(3): p. 266-276.

68. Blaas, D., *Viral entry pathways: the example of common cold viruses.* Wiener medizinische Wochenschrift (1946), **2016**. 166(7-8): p. 211-226.

69. Kaksonen, M. and A. Roux, *Mechanisms of clathrin-mediated endocytosis.* Nat Rev Mol Cell Biol, **2018**. 19(5): p. 313-326.

70. Elkin, S.R., A.M. Lakoduk, and S.L. Schmid, *Endocytic pathways and endosomal trafficking: a primer.* Wiener medizinische Wochenschrift (1946), **2016**. 166(7-8): p. 196-204.

71. Snyers, L., H. Zwickl, and D. Blaas, *Human Rhinovirus Type 2 Is Internalized by Clathrin-Mediated Endocytosis.* Journal of Virology, **2003**. 77(9): p. 5360-5369.

72. Ganjian, H., C. Zietz, D. Mechtcheriakova, D. Blaas, and R. Fuchs, *ICAM-1 Binding Rhinoviruses Enter HeLa Cells via Multiple Pathways and Travel to Distinct Intracellular Compartments for Uncoating.* Viruses, **2017**. 9(4).

73. Boucrot, E., A.P. Ferreira, L. Almeida-Souza, S. Debard, Y. Vallis, G. Howard, L. Bertot, N. Sauvonnet, and H.T. McMahon, *Endophilin marks and controls a clathrin-independent endocytic pathway.* Nature, **2015**. 517(7535): p. 460-5.

74. Chen, S.-L., Y.-G. Liu, Y.-T. Zhou, P. Zhao, H. Ren, M. Xiao, Y.-Z. Zhu, and Z.-T. Qi, *Endophilin-A2-mediated endocytic pathway is critical for enterovirus 71 entry into caco-2 cells.* Emerging microbes & infections, **2019**. 8(1): p. 773-786.

75. Howes, M.T., M. Kirkham, J. Riches, K. Cortese, P.J. Walser, F. Simpson, M.M. Hill, A. Jones, R. Lundmark, M.R. Lindsay, D.J. Hernandez-Deviez, G. Hadzic, A. McCluskey, R. Bashir, L. Liu, P. Pilch, H. McMahon, P.J. Robinson, J.F. Hancock, S. Mayor, and R.G. Parton, *Clathrin-independent carriers form a high capacity endocytic sorting system at the leading edge of migrating cells.* J Cell Biol, **2010**. 190(4): p. 675-91.

76. Sathe, M., G. Muthukrishnan, J. Rae, A. Disanza, M. Thattai, G. Scita, R.G. Parton, and S. Mayor, *Small GTPases and BAR domain proteins regulate branched actin polymerisation for clathrin and dynamin-independent endocytosis.* Nature Communications, **2018**. 9(1): p. 1835.

77. Lakshminarayan, R., C. Wunder, U. Becken, M.T. Howes, C. Benzing, S. Arumugam, S. Sales, N. Ariotti, V. Chambon, C. Lamaze, D. Loew, A. Shevchenko, K. Gaus, R.G. Parton, and L. Johannes, *Galectin-3 drives glycosphingolipid-dependent biogenesis of clathrin-independent carriers.* Nature Cell Biology, **2014**. 16(6): p. 592-603.

78. Condon, N.D., J.M. Heddleston, T.-L. Chew, L. Luo, P.S. McPherson, M.S. Ioannou, L. Hodgson, J.L. Stow, and A.A. Wall, *Macropinosome formation by tent pole ruffling in macrophages.* Journal of Cell Biology, **2018**. 217(11): p. 3873-3885.

79. Lin, X.P., J.D. Mintern, and P.A. Gleeson, *Macropinocytosis in Different Cell Types: Similarities and Differences.* Membranes (Basel), **2020**. 10(8).

80. Mercer, J. and A. Helenius, *Virus entry by macropinocytosis.* Nat Cell Biol, **2009**. 11(5): p. 510-20.

81. Vandesande, H., M. Laajala, T. Kantoluoto, V. Ruokolainen, A.M. Lindberg, and V. Marjomäki, *Early entry events in Echovirus 30 infection.* Journal of Virology, **2020**: p. JVI.00592-20.

82. Parton, R.G., M.A. Del Pozo, S. Vassilopoulos, I.R. Nabi, S. Le Lay, R. Lundmark, A.K. Kenworthy, A. Camus, C.M. Blouin, W.C. Sessa, and C. Lamaze, *Caveolae: The FAQs.* Traffic, **2020**. 21(1): p. 181-185.

83. Parton, R.G., *Caveolae: Structure, Function, and Relationship to Disease.* Annu Rev Cell Dev Biol, **2018**. 34: p. 111-136.

84. Pietiäinen, V.M., V. Marjomäki, J. Heino, and T. Hyypiä, *Viral entry, lipid rafts and caveosomes.* Ann Med, **2005**. 37(6): p. 394-403.

85. Nunes-Correia, I., A. Eulálio, S. Nir, and M.C. Pedroso de Lima, *Caveolae as an additional route for influenza virus endocytosis in MDCK cells.* Cell Mol Biol Lett, **2004**. 9(1): p. 47-60.

86. Nomura, R., A. Kiyota, E. Suzaki, K. Kataoka, Y. Ohe, K. Miyamoto, T. Senda, and T. Fujimoto, *Human Coronavirus 229E Binds to CD13 in Rafts and Enters the Cell through Caveolae.* Journal of Virology, **2004**. 78(16): p. 8701-8708.

87. Salzman, N.H. and F.R. Maxfield, *Intracellular fusion of sequentially formed endocytic compartments.* J Cell Biol, **1988**. 106(4): p. 1083-91.

88. Jovic, M., M. Sharma, J. Rahajeng, and S. Caplan, *The early endosome: a busy sorting station for proteins at the crossroads.* Histology and histopathology, **2010**. 25(1): p. 99-112.

89. Conzemius, R., H. Ganjian, D. Blaas, and R. Fuchs, *ICAM-1 Binding Rhinoviruses A89 and B14 Uncoat in Different Endosomal Compartments.* J Virol, **2016**. 90(17): p. 7934-42.

90. Carpentier, J.L., P. Gorden, R.G. Anderson, J.L. Goldstein, M.S. Brown, S. Cohen, and L. Orci, *Co-localization of 125I-epidermal growth factor and ferritin-low density lipoprotein in coated pits: a quantitative electron microscopic study in normal and mutant human fibroblasts.* J Cell Biol, **1982**. 95(1): p. 73-7.

91. Neutra, M.R., A. Ciechanover, L.S. Owen, and H.F. Lodish, *Intracellular transport of transferrin- and asialoorosomucoid-colloidal gold conjugates to lysosomes after receptor-mediated endocytosis.* J Histochem Cytochem, **1985**. 33(11): p. 1134-44.

92. Mellman, I., R. Fuchs, and A. Helenius, *Acidification of the endocytic and exocytic pathways.* Annu Rev Biochem, **1986**. 55: p. 663-700.

93. Fuchs, R. and D. Blaas, *Uncoating of human rhinoviruses.* Rev Med Virol, **2010**. 20(5): p. 281-97.

94. Cullen, P.J. and F. Steinberg, *To degrade or not to degrade: mechanisms and significance of endocytic recycling.* Nat Rev Mol Cell Biol, **2018**. 19(11): p. 679-696.

95. Huotari, J. and A. Helenius, *Endosome maturation.* The EMBO journal, **2011**. 30(17): p. 3481-3500.

96. Kornilova, E.S., *Receptor-mediated endocytosis and cytoskeleton.* Biochemistry (Moscow), **2014**. 79(9): p. 865-878.

97. Aniento, F., N. Emans, G. Griffiths, and J. Gruenberg, *Cytoplasmic dynein-dependent vesicular transport from early to late endosomes.* Journal of Cell Biology, **1993**. 123(6): p. 1373-1387.

98. Baravalle, G., D. Schober, M. Huber, N. Bayer, R.F. Murphy, and R. Fuchs, *Transferrin recycling and dextran transport to lysosomes is differentially affected by bafilomycin, nocodazole, and low temperature.* Cell and Tissue Research, **2005**. 320(1): p. 99-113.

99. Horgan, C.P., S.R. Hanscom, R.S. Jolly, C.E. Futter, and M.W. McCaffrey, *Rab11-FIP3 links the Rab11 GTPase and cytoplasmic dynein to mediate transport to the endosomal-recycling compartment.* Journal of Cell Science, **2010**. 123(2): p. 181-191.

100. Blaas, D. and R. Fuchs, *Mechanism of human rhinovirus infections.* Molecular and cellular pediatrics, **2016**. 3(1): p. 21-21.

101. Prchla, E., E. Kuechler, D. Blaas, and R. Fuchs, *Uncoating of human rhinovirus serotype 2 from late endosomes.* Journal of virology, **1994**. 68(6): p. 3713-3723.

102. Bayer, N., D. Schober, E. Prchla, R.F. Murphy, D. Blaas, and R. Fuchs, *Effect of bafilomycin A1 and nocodazole on endocytic transport in HeLa cells: implications for viral uncoating and infection.* J Virol, **1998**. 72(12): p. 9645-55.

103. Schober, D., P. Kronenberger, E. Prchla, D. Blaas, and R. Fuchs, *Major and minor receptor group human rhinoviruses penetrate from endosomes by different mechanisms.* Journal of virology, **1998**. 72(2): p. 1354-1364.

104. Abbas, A.K., A.H. Lichtman, S. Pillai, and A.K. Abbas, *Cellular and molecular immunology / Abul K. Abbas, Andrew H. H. Lichtman, Shiv Pillai ; illustrations by David L. Baker, Alexandra Baker*. Ninth edition. ed. 2018, Philadelphia, PA: Elsevier.

105. Mesev, E., R. Ledesma, and A. Ploss, *Decoding type I and III interferon signalling during viral infection.* Nature Microbiology, **2019**. 4: p. 924.

106. Stanifer, M.L., K. Pervolaraki, and S. Boulant, *Differential Regulation of Type I and Type III Interferon Signaling.* Int J Mol Sci, **2019**. 20(6).

107. Hoffmann, H.H., W.M. Schneider, and C.M. Rice, *Interferons and viruses: an evolutionary arms race of molecular interactions.* Trends Immunol, **2015**. 36(3): p. 124-38.

108. Kyogoku, C., B. Smiljanovic, J.R. Grün, R. Biesen, U. Schulte-Wrede, T. Häupl, F. Hiepe, T. Alexander, A. Radbruch, and A. Grützkau, *Cell-Specific Type I IFN Signatures in Autoimmunity and Viral Infection: What Makes the Difference?* PLOS ONE, **2014**. 8(12): p. e83776.

109. Novick, D., B. Cohen, and M. Rubinstein, *The human interferon alpha/beta receptor: characterization and molecular cloning.* Cell, **1994**. 77(3): p. 391-400.

110. de Weerd, N.A. and T. Nguyen, *The interferons and their receptors--distribution and regulation.* Immunol Cell Biol, **2012**. 90(5): p. 483-91.

111. Kotenko, S.V., G. Gallagher, V.V. Baurin, A. Lewis-Antes, M. Shen, N.K. Shah, J.A. Langer, F. Sheikh, H. Dickensheets, and R.P. Donnelly, *IFN-lambdas mediate antiviral protection through a distinct class II cytokine receptor complex.* Nat Immunol, **2003**. 4(1): p. 69-77.

112. Onabajo, O.O., B. Muchmore, and L. Prokunina-Olsson, *The IFN-λ4 Conundrum: When a Good Interferon Goes Bad.* J Interferon Cytokine Res, **2019**. 39(10): p. 636-641.

113. Sommereyns, C., S. Paul, P. Staeheli, and T. Michiels, *IFN-Lambda (IFN-λ) Is Expressed in a Tissue-Dependent Fashion and Primarily Acts on Epithelial Cells In Vivo.* PLOS Pathogens, **2008**. 4(3): p. e1000017.

114. Mordstein, M., E. Neugebauer, V. Ditt, B. Jessen, T. Rieger, V. Falcone, F. Sorgeloos, S. Ehl, D. Mayer, G. Kochs, M. Schwemmle, S. Günther, C. Drosten, T. Michiels, and P. Staeheli, *Lambda interferon renders epithelial cells of the respiratory and gastrointestinal tracts resistant to viral infections.* J Virol, **2010**. 84(11): p. 5670-7.

115. Rehwinkel, J. and M.U. Gack, *RIG-I-like receptors: their regulation and roles in RNA sensing.* Nature Reviews Immunology, **2020**. 20(9): p. 537-551.

116. Chow, K.T., M. Gale, Jr., and Y.M. Loo, *RIG-I and Other RNA Sensors in Antiviral Immunity.* Annu Rev Immunol, **2018**. 36: p. 667-694.

117. Dolasia, K., M.K. Bisht, G. Pradhan, A. Udgata, and S. Mukhopadhyay, *TLRs/NLRs: Shaping the landscape of host immunity.* International Reviews of Immunology, **2018**. 37(1): p. 3-19.

118. Ye, L., D. Schnepf, and P. Staeheli, *Interferon-λ orchestrates innate and adaptive mucosal immune responses.* Nat Rev Immunol, **2019**. 19(10): p. 614-625.

119. Hosmillo, M., Y. Chaudhry, K. Nayak, F. Sorgeloos, B.K. Koo, A. Merenda, R. Lillestol, L. Drumright, M. Zilbauer, and I. Goodfellow, *Norovirus Replication in Human Intestinal Epithelial Cells Is Restricted by the Interferon-Induced JAK/STAT Signaling Pathway and RNA Polymerase II-Mediated Transcriptional Responses.* mBio, **2020**. 11(2).

120. Stanifer, M.L., C. Guo, P. Doldan, and S. Boulant, *Importance of Type I and III Interferons at Respiratory and Intestinal Barrier Surfaces.* Front Immunol, **2020**. 11: p. 608645.

121. Baldridge, M.T., S. Lee, J.J. Brown, N. McAllister, K. Urbanek, T.S. Dermody, T.J. Nice, and H.W. Virgin, *Expression of Ifnlr1 on Intestinal Epithelial Cells Is Critical to the Antiviral Effects of Interferon Lambda against Norovirus and Reovirus.* J Virol, **2017**. 91(7).

122. Pervolaraki, K., S. Rastgou Talemi, D. Albrecht, F. Bormann, C. Bamford, J.L. Mendoza, K.C. Garcia, J. McLauchlan, T. Höfer, M.L. Stanifer, and S. Boulant, *Differential induction of interferon stimulated genes between type I and type III interferons is independent of interferon receptor abundance.* PLoS Pathog, **2018**. 14(11): p. e1007420.

123. Chow, C.M., A.K. Leung, and K.L. Hon, *Acute gastroenteritis: from guidelines to real life.* Clinical and experimental gastroenterology, **2010**. 3: p. 97-112.

124. Troeger, C., B.F. Blacker, I.A. Khalil, P.C. Rao, S. Cao, S.R.M. Zimsen, S.B. Albertson, J.D. Stanaway, A. Deshpande, Z. Abebe, N. Alvis-Guzman, A.T. Amare, S.W. Asgedom, Z.A. Anteneh, C.A.T. Antonio, O. Aremu, E.T. Asfaw, T.M. Atey, S. Atique, E.F.G.A. Avokpaho, A. Awasthi, H.T. Ayele, A. Barac, M.L. Barreto, Q. Bassat, S.A. Belay, I.M. Bensenor, Z.A. Bhutta, A. Bijani, H. Bizuneh, C.A. Castañeda-Orjuela, A.F. Dadi, L. Dandona, R. Dandona, H.P. Do, M. Dubey, E. Dubljanin, D. Edessa, A.Y. Endries, B. Eshrati, T. Farag, G.T. Feyissa, K.J. Foreman, M.H. Forouzanfar, N. Fullman, P.W. Gething, M.D. Gishu, W.W. Godwin, H.C. Gugnani, R. Gupta, G.B. Hailu, H.Y. Hassen, D.T. Hibstu, O.S. Ilesanmi, J.B. Jonas, A. Kahsay, G. Kang, A. Kasaeian, Y.S. Khader, I.A. Khalil, E.A. Khan, M.A. Khan, Y.-H. Khang, N. Kissoon, S. Kochhar, K.L. Kotloff, A. Koyanagi, G.A. Kumar, H. Magdy Abd El Razek, R. Malekzadeh, D.C. Malta, S. Mehata, W. Mendoza, D.T. Mengistu, B.G. Menota, H.B. Mezgebe, F.W. Mlashu, S. Murthy, G.A. Naik, C.T. Nguyen, T.H. Nguyen, D.N.A. Ningrum, F.A. Ogbo, A.T. Olagunju, D. Paudel, J.A. Platts-Mills, M. Qorbani, A. Rafay, R.K. Rai, S.M. Rana, C.L. Ranabhat, D. Rasella, S.E. Ray, C. Reis, A.M.N. Renzaho, M.S. Rezai, G.M. Ruhago, S. Safiri, J.A. Salomon, J.R. Sanabria, B. Sartorius, M. Sawhney, S.G. Sepanlou, M. Shigematsu, M. Sisay, R. Somayaji, C.T. Sreeramareddy, B.L. Sykes, G.R. Taffere, R. Topor-Madry, B.X. Tran, K.B. Tuem, K.N. Ukwaja, S.E. Vollset, J.L. Walson, M.R. Weaver, K.G. Weldegwergs, A. Werdecker, A. Workicho, M. Yenesew, B.D. Yirsaw, N. Yonemoto, M. El Sayed Zaki, T. Vos, S.S. Lim, M. Naghavi, C.J.L. Murray, A.H. Mokdad, S.I. Hay and R.C. Reiner, Jr., *Estimates of the global, regional, and national morbidity, mortality, and aetiologies of diarrhoea in 195 countries: a systematic analysis for the Global Burden of Disease Study 2016.* The Lancet Infectious Diseases, **2018**. 18(11): p. 1211-1228.

125. Kosek, M., C. Bern, and R.L. Guerrant, *The global burden of diarrhoeal disease, as estimated from studies published between 1992 and 2000.* Bull World Health Organ, **2003**. 81(3): p. 197-204.

126. Dennehy, P.H., *Viral Gastroenteritis in Children.* The Pediatric Infectious Disease Journal, **2011**. 30(1).

127. Bartsch, S.M., B.A. Lopman, S. Ozawa, A.J. Hall, and B.Y. Lee, *Global Economic Burden of Norovirus Gastroenteritis.* PloS one, **2016**. 11(4): p. e0151219-e0151219.

128. Bányai, K., M.K. Estes, V. Martella, and U.D. Parashar, *Viral gastroenteritis.* The Lancet, **2018**. 392(10142): p. 175-186.

129. Webb, A. and M. Starr, *Acute gastroenteritis in children.* Aust Fam Physician, **2005**. 34(4): p. 227-31.

130. Elliott, E.J., *Acute gastroenteritis in children.* BMJ (Clinical research ed.), **2007**. 334(7583): p. 35-40.

131. Oude Munnink, B.B. and L. van der Hoek, *Viruses Causing Gastroenteritis: The Known, The New and Those Beyond.* Viruses, **2016**. 8(2).

132. Wilhelmi, I., E. Roman, and A. Sánchez-Fauquier, *Viruses causing gastroenteritis.* Clin Microbiol Infect, **2003**. 9(4): p. 247-62.

133. Holtz, L.R., S.R. Finkbeiner, G. Zhao, C.D. Kirkwood, R. Girones, J.M. Pipas, and D. Wang, *Klassevirus 1, a previously undescribed member of the family Picornaviridae, is globally widespread.* Virology Journal, **2009**. 6(1): p. 86.

134. Simpson, R., S. Aliyu, M. Iturriza-Gómara, U. Desselberger, and J. Gray, *Infantile viral gastroenteritis: on the way to closing the diagnostic gap.* J Med Virol, **2003**. 70(2): p. 258-62.

135. Vocale, C., S.G. Rimoldi, C. Pagani, R. Grande, F. Pedna, M. Arghittu, G. Lunghi, A. Maraschini, M.R. Gismondo, M.P. Landini, E. Torresani, F. Topin, and V. Sambri, *Comparative evaluation of the new xTAG GPP multiplex assay in the laboratory diagnosis of acute gastroenteritis. Clinical assessment and potential application from a multicentre Italian study.* Int J Infect Dis, **2015**. 34: p. 33-7.

136. Barker, N., J.H. van Es, J. Kuipers, P. Kujala, M. van den Born, M. Cozijnsen, A. Haegebarth, J. Korving, H. Begthel, P.J. Peters, and H. Clevers, *Identification of stem cells in small intestine and colon by marker gene Lgr5.* Nature, **2007**. 449(7165): p. 1003-7.

137. Zachos, N.C., O. Kovbasnjuk, J. Foulke-Abel, J. In, S.E. Blutt, H.R. de Jonge, M.K. Estes, and M. Donowitz, *Human Enteroids/Colonoids and Intestinal Organoids Functionally Recapitulate Normal Intestinal Physiology and Pathophysiology.* J Biol Chem, **2016**. 291(8): p. 3759-66.

138. Lanik, W.E., M.A. Mara, B. Mihi, C.B. Coyne, and M. Good, *Stem Cell-Derived Models of Viral Infections in the Gastrointestinal Tract.* Viruses, **2018**. 10(3): p. 124.

139. Sato, T., R.G. Vries, H.J. Snippert, M. van de Wetering, N. Barker, D.E. Stange, J.H. van Es, A. Abo, P. Kujala, P.J. Peters, and H. Clevers, *Single Lgr5 stem cells build crypt-villus structures in vitro without a mesenchymal niche.* Nature, **2009**. 459(7244): p. 262-5.

140. Sridhar, A., S. Simmini, C.M.S. Ribeiro, C. Tapparel, M.M. Evers, D. Pajkrt, and K. Wolthers, *A Perspective on Organoids for Virology Research.* Viruses, **2020**. 12(11): p. 1341.

141. Triana, S., C. Metz-Zumaran, C. Ramirez, C. Kee, P. Doldan, M. Shahraz, D. Schraivogel, A.R. Gschwind, A.K. Sharma, L.M. Steinmetz, C. Herrmann, T. Alexandrov, S. Boulant, and M.L. Stanifer, *Single-cell analyses reveal SARS-CoV-2 interference with intrinsic immune response in the human gut.* Mol Syst Biol, **2021**. 17(4): p. e10232.

142. Kolawole, A.O. and C.E. Wobus, *Gastrointestinal organoid technology advances studies of enteric virus biology.* PLoS Pathog, **2020**. 16(1): p. e1008212.

143. Costantini, V., E. Morantz, H. Browne, K. Ettayebi, X.-L. Zeng, R. Atmar, M. Estes, and J. Vinjé, *Human Norovirus Replication in Human Intestinal Enteroids as Model to Evaluate Virus Inactivation.* Emerging Infectious Disease journal, **2018**. 24(8): p. 1453.

144. Ettayebi, K., S.E. Crawford, K. Murakami, J.R. Broughman, U. Karandikar, V.R. Tenge, F.H. Neill, S.E. Blutt, X.L. Zeng, L. Qu, B. Kou, A.R. Opekun, D. Burrin, D.Y. Graham, S. Ramani, R.L. Atmar, and M.K. Estes, *Replication of human noroviruses in stem cell-derived human enteroids.* Science, **2016**. 353(6306): p. 1387-1393.

145. Murakami, K., V.R. Tenge, U.C. Karandikar, S.-C. Lin, S. Ramani, K. Ettayebi, S.E. Crawford, X.-L. Zeng, F.H. Neill, B.V. Ayyar, K. Katayama, D.Y. Graham, E. Bieberich, R.L. Atmar, and M.K. Estes, *Bile acids and ceramide overcome the entry restriction for GII.3 human norovirus replication in human intestinal enteroids.* Proceedings of the National Academy of Sciences, **2020**. 117(3): p. 1700.

146. Stanifer, M. and S. Boulant, *The origin of diarrhea in rotavirus infection.* Science, **2020**. 370(6519): p. 909-910.

147. Chang-Graham, A.L., J.L. Perry, M.A. Engevik, K.A. Engevik, F.J. Scribano, J.T. Gebert, H.A. Danhof, J.C. Nelson, J.S. Kellen, A.C. Strtak, N.P. Sastri, M.K. Estes, R.A. Britton, J. Versalovic, and J.M. Hyser, *Rotavirus induces intercellular calcium waves through ADP signaling.* Science, **2020**. 370(6519).

148. Good, C., A.I. Wells, and C.B. Coyne, *Type III interferon signaling restricts enterovirus 71 infection of goblet cells.* Sci Adv, **2019**. 5(3): p. eaau4255.

149. Drummond, C.G., A.M. Bolock, C. Ma, C.J. Luke, M. Good, and C.B. Coyne, *Enteroviruses infect human enteroids and induce antiviral signaling in a cell lineage-specific manner.* Proc Natl Acad Sci U S A, **2017**. 114(7): p. 1672-1677.

150. Holly, M.K. and J.G. Smith, *Adenovirus Infection of Human Enteroids Reveals Interferon Sensitivity and Preferential Infection of Goblet Cells.* Journal of virology, **2018**. 92(9): p. e00250-18.

151. Greninger, A.L., G.M. Knudsen, M. Betegon, A.L. Burlingame, and J.L. Derisi, *The 3A protein from multiple picornaviruses utilizes the golgi adaptor protein ACBD3 to recruit PI4KIIIbeta.* J Virol, **2012**. 86(7): p. 3605-16.

152. Corbic Ramljak, I., J. Stanger, A. Real-Hohn, D. Dreier, L. Wimmer, M. Redlberger-Fritz, W. Fischl, K. Klingel, M.D. Mihovilovic, D. Blaas, and H. Kowalski, *Cellular N-myristoyltransferases play a crucial picornavirus genus-specific role in viral assembly, virion maturation, and infectivity.* PLoS pathogens, **2018**. 14(8): p. e1007203-e1007203.

153. Allmaier, G., D. Blaas, C. Bliem, T. Dechat, S. Fedosyuk, I. Gösler, H. Kowalski, and V.U. Weiss, *Monolithic anion-exchange chromatography yields rhinovirus of high purity.* J Virol Methods, **2018**. 251: p. 15-21.

154. Pfaffl, M.W., *A new mathematical model for relative quantification in real-time RT-PCR.* Nucleic acids research, **2001**. 29(9): p. e45-e45.

155. Reed, L.J. and H. Muench, *A SIMPLE METHOD OF ESTIMATING FIFTY PER CENT ENDPOINTS12.* American Journal of Epidemiology, **1938**. 27(3): p. 493-497.

156. Schindelin, J., I. Arganda-Carreras, E. Frise, V. Kaynig, M. Longair, T. Pietzsch, S. Preibisch, C. Rueden, S. Saalfeld, B. Schmid, J.-Y. Tinevez, D.J. White, V. Hartenstein, K. Eliceiri, P. Tomancak, and A. Cardona, *Fiji: an open-source platform for biological-image analysis.* Nature Methods, **2012**. 9(7): p. 676-682.

157. Chen, Y.S., B.C. Chen, Y.S. Lin, J.T. Chang, T.S. Huang, J.J. Chen, and T.H. Chang, *Detection of Aichi virus with antibody targeting of conserved viral protein 1 epitope.* Appl Microbiol Biotechnol, **2013**. 97(19): p. 8529-36.

158. de Graaf, I.A.M., P. Olinga, M.H. de Jager, M.T. Merema, R. de Kanter, E.G. van de Kerkhof, and G.M.M. Groothuis, *Preparation and incubation of precision-cut liver and intestinal slices for application in drug metabolism and toxicity studies.* Nature Protocols, **2010**. 5(9): p. 1540-1551.

159. Smejkal, G., *The Coomassie chronicles: Past, present and future perspectives in polyacrylamide gel staining.* Expert review of proteomics, **2005**. 1: p. 381-7.

160. Battistelli, M. and E. Falcieri, *Apoptotic Bodies: Particular Extracellular Vesicles Involved in Intercellular Communication.* Biology, **2020**. 9(1): p. 21.

161. Bergelson, J.M. and C.B. Coyne, *Picornavirus entry.* Adv Exp Med Biol, **2013**. 790: p. 24-41.

162. Macia, E., M. Ehrlich, R. Massol, E. Boucrot, C. Brunner, and T. Kirchhausen, *Dynasore, a Cell-Permeable Inhibitor of Dynamin.* Developmental Cell, **2006**. 10(6): p. 839-850.

163. Mercer, J. and A. Helenius, *Gulping rather than sipping: macropinocytosis as a way of virus entry.* Current Opinion in Microbiology, **2012**. 15(4): p. 490-499.

164. Ivanov, A.I., *Pharmacological inhibition of endocytic pathways: is it specific enough to be useful?* Methods Mol Biol, **2008**. 440: p. 15-33.

165. Aniento, F., F. Gu, R.G. Parton, and J. Gruenberg, *An endosomal beta COP is involved in the pH-dependent formation of transport vesicles destined for late endosomes.* Journal of Cell Biology, **1996**. 133(1): p. 29-41.

166. Mellman, I., R. Fuchs, and A. Helenius, *ACIDIFICATION OF THE ENDOCYTIC AND EXOCYTIC PATHWAYS.* Annual Review of Biochemistry, **1986**. 55(1): p. 663-700.

167. Kobayashi, K. and S. Koike, *Cellular receptors for enterovirus A71.* Journal of Biomedical Science, **2020**. 27(1): p. 23.

168. Gillespie, E.J., C.-L.C. Ho, K. Balaji, D.L. Clemens, G. Deng, Y.E. Wang, H.J. Elsaesser, B. Tamilselvam, A. Gargi, S.D. Dixon, B. France, B.T. Chamberlain, S.R. Blanke, G. Cheng, J.C. de la Torre, D.G. Brooks, M.E. Jung, J. Colicelli, R. Damoiseaux, and K.A. Bradley, *Selective inhibitor of endosomal trafficking pathways exploited by multiple toxins and viruses.* Proceedings of the National Academy of Sciences, **2013**. 110(50): p. E4904.

169. Chang, Y.T., M.H. Kung, T.H. Hsu, W.T. Hung, Y.S. Chen, L.C. Yen, and T.H. Chang, *Aichi Virus Induces Antiviral Host Defense in Primary Murine Intestinal Epithelial Cells.* Viruses, **2019**. 11(8).

170. Dutton, J.S., S.S. Hinman, R. Kim, Y. Wang, and N.L. Allbritton, *Primary Cell-Derived Intestinal Models: Recapitulating Physiology.* Trends Biotechnol, **2019**. 37(7): p. 744-760.

171. Tseligka, E.D., K. Sobo, L. Stoppini, V. Cagno, F. Abdul, I. Piuz, P. Meylan, S. Huang, S. Constant, and C. Tapparel, *A VP1 mutation acquired during an enterovirus 71 disseminated infection confers heparan sulfate binding ability and modulates ex vivo tropism.* PLOS Pathogens, **2018**. 14(8): p. e1007190.

172. Schönborn, J., J. Oberstrass, E. Breyel, J. Tittgen, J. Schumacher, and N. Lukacs, *Monoclonal antibodies to double-stranded RNA as probes of RNA structure in crude nucleic acid extracts.* Nucleic acids research, **1991**. 19(11): p. 2993-3000.

173. Weber, F., V. Wagner, S.B. Rasmussen, R. Hartmann, and S.R. Paludan, *Double-stranded RNA is produced by positive-strand RNA viruses and DNA viruses but not in detectable amounts by negative-strand RNA viruses.* J Virol, **2006**. 80(10): p. 5059-64.

174. Stanifer, M.L., C. Kee, M. Cortese, C.M. Zumaran, S. Triana, M. Mukenhirn, H.-G. Kraeusslich, T. Alexandrov, R. Bartenschlager, and S. Boulant, *Critical Role of Type III Interferon in Controlling SARS-CoV-2 Infection in Human Intestinal Epithelial Cells.* Cell Reports, **2020**. 32(1): p. 107863.

175. Lazear, H.M., J.W. Schoggins, and M.S. Diamond, *Shared and Distinct Functions of Type I and Type III Interferons.* Immunity, **2019**. 50(4): p. 907-923.

176. Reagan, K.J., B. Goldberg, and R.L. Crowell, *Altered receptor specificity of coxsackievirus B3 after growth in rhabdomyosarcoma cells.* J Virol, **1984**. 49(3): p. 635-40.

177. Gassler, N., D. Newrzella, C. Böhm, S. Lyer, L. Li, O. Sorgenfrei, L. van Laer, B. Sido, J. Mollenhauer, A. Poustka, P. Schirmacher, and N. Gretz, *Molecular characterisation of non-absorptive and absorptive enterocytes in human small intestine.* Gut, **2006**. 55(8): p. 1084-1089.

178. Mangaraj, M., R. Nanda, and S. Panda, *Apolipoprotein A-I: A Molecule of Diverse Function.* Indian journal of clinical biochemistry : IJCB, **2016**. 31(3): p. 253-259.

179. Sun, X. and P.D. Kaufman, *Ki-67: more than a proliferation marker.* Chromosoma, **2018**. 127(2): p. 175-186.

180. van Kuppeveld, F.J., J.G. Hoenderop, R.L. Smeets, P.H. Willems, H.B. Dijkman, J.M. Galama, and W.J. Melchers, *Coxsackievirus protein 2B modifies endoplasmic reticulum membrane and plasma membrane permeability and facilitates virus release.* The EMBO journal, **1997**. 16(12): p. 3519-3532.

181. Xin, L., Z. Xiao, X. Ma, F. He, H. Yao, and Z. Liu, *Coxsackievirus B3 induces crosstalk between autophagy and apoptosis to benefit its release after replicating in autophagosomes through a mechanism involving caspase cleavage of autophagy-related proteins.* Infection, Genetics and Evolution, **2014**. 26: p. 95-102.

182. Bozym, R.A., K. Patel, C. White, K.-H. Cheung, J.M. Bergelson, S.A. Morosky, and C.B. Coyne, *Calcium signals and calpain-dependent necrosis are essential for release of coxsackievirus B from polarized intestinal epithelial cells.* Molecular biology of the cell, **2011**. 22(17): p. 3010-3021.

183. Blanco-Melo, D., B.E. Nilsson-Payant, W.-C. Liu, S. Uhl, D. Hoagland, R. Møller, T.X. Jordan, K. Oishi, M. Panis, D. Sachs, T.T. Wang, R.E. Schwartz, J.K. Lim, R.A. Albrecht, and B.R. tenOever, *Imbalanced Host Response to SARS-CoV-2 Drives Development of COVID-19.* Cell, **2020**. 181(5): p. 1036-1045.e9.

184. Harcourt, J., A. Tamin, X. Lu, S. Kamili, S.K. Sakthivel, J. Murray, K. Queen, Y. Tao, C.R. Paden, J. Zhang, Y. Li, A. Uehara, H. Wang, C. Goldsmith, H.A. Bullock, L. Wang, B. Whitaker, B. Lynch, R. Gautam, C. Schindewolf, K.G. Lokugamage, D. Scharton, J.A. Plante, D. Mirchandani, S.G. Widen, K. Narayanan, S. Makino, T.G. Ksiazek, K.S. Plante, S.C. Weaver, S. Lindstrom, S. Tong, V.D. Menachery, and N.J. Thornburg, *Severe Acute Respiratory Syndrome Coronavirus 2 from Patient with Coronavirus Disease, United States.* Emerging infectious diseases, **2020**. 26(6): p. 1266-1273.

185. Jia, H.P., D.C. Look, L. Shi, M. Hickey, L. Pewe, J. Netland, M. Farzan, C. Wohlford-Lenane, S. Perlman, and P.B. McCray, Jr., *ACE2 receptor expression and severe acute respiratory syndrome coronavirus infection depend on differentiation of human airway epithelia.* Journal of virology, **2005**. 79(23): p. 14614-14621.

186. Delorme-Axford, E., Y. Sadovsky, and C.B. Coyne, *Lipid raft- and SRC family kinase-dependent entry of coxsackievirus B into human placental trophoblasts.* Journal of virology, **2013**. 87(15): p. 8569-8581.

187. Park, R.J., H. Shen, L. Liu, X. Liu, S.M. Ferguson, and P. De Camilli, *Dynamin triple knockout cells reveal off target effects of commonly used dynamin inhibitors.* J Cell Sci, **2013**. 126(Pt 22): p. 5305-12.

188. Gilleron, J., W. Querbes, A. Zeigerer, A. Borodovsky, G. Marsico, U. Schubert, K. Manygoats, S. Seifert, C. Andree, M. Stöter, H. Epstein-Barash, L. Zhang, V. Koteliansky, K. Fitzgerald, E. Fava, M. Bickle, Y. Kalaidzidis, A. Akinc, M. Maier, and M. Zerial, *Image-based analysis of lipid nanoparticle–mediated siRNA delivery, intracellular trafficking and endosomal escape.* Nature Biotechnology, **2013**. 31(7): p. 638-646.

189. Liu, S.H., M.S. Marks, and F.M. Brodsky, *A dominant-negative clathrin mutant differentially affects trafficking of molecules with distinct sorting motifs in the class II major histocompatibility complex (MHC) pathway.* J Cell Biol, **1998**. 140(5): p. 1023-37.

190. Commisso, C., R.J. Flinn, and D. Bar-Sagi, *Determining the macropinocytic index of cells through a quantitative image-based assay.* Nat Protoc, **2014**. 9(1): p. 182-92.

191. Yamayoshi, S., S. Ohka, K. Fujii, and S. Koike, *Functional comparison of SCARB2 and PSGL1 as receptors for enterovirus 71.* J Virol, **2013**. 87(6): p. 3335-47.

192. Kim, C. and J.M. Bergelson, *Echovirus 7 entry into polarized intestinal epithelial cells requires clathrin and Rab7.* mBio, **2012**. 3(2): p. e00304-11.

193. Bochkov, Y.A., A.C. Palmenberg, W.-M. Lee, J.A. Rathe, S.P. Amineva, X. Sun, T.R. Pasic, N.N. Jarjour, S.B. Liggett, and J.E. Gern, *Molecular modeling, organ culture and reverse genetics for a newly identified human rhinovirus C.* Nature Medicine, **2011**. 17(5): p. 627-632.

194. Ashraf, S., R. Brockman-Schneider, and J.E. Gern, *Propagation of rhinovirus-C strains in human airway epithelial cells differentiated at air-liquid interface.* Methods in molecular biology (Clifton, N.J.), **2015**. 1221: p. 63-70.

195. Brandenburg, B., L.Y. Lee, M. Lakadamyali, M.J. Rust, X. Zhuang, and J.M. Hogle, *Imaging poliovirus entry in live cells.* PLoS biology, **2007**. 5(7): p. e183-e183.

196. Crowther, D. and J.L. Melnick, *The incorporation of neutral red and acridine orange into developing poliovirus particles making them photosensitive.* Virology, **1961**. 14: p. 11-21.

197. Karelehto, E., C. Cristella, X. Yu, A. Sridhar, R. Hulsdouw, K. de Haan, H. van Eijk, S. Koekkoek, D. Pajkrt, M.D. de Jong, and K.C. Wolthers, *Polarized Entry of Human Parechoviruses in the Airway Epithelium.* Front Cell Infect Microbiol, **2018**. 8: p. 294.

198. Tucker, S.P., C.L. Thornton, E. Wimmer, and R.W. Compans, *Vectorial release of poliovirus from polarized human intestinal epithelial cells.* Journal of virology, **1993**. 67(7): p. 4274-4282.

199. Freeman, M.C., A.I. Wells, J. Ciomperlik-Patton, M.M. Myerburg, L. Yang, J. Konopka-Anstadt, and C. Coyne, *Respiratory and intestinal epithelial cells exhibit differential susceptibility and innate immune responses to EV-D68.* Elife, **2021**. 10.

200. Roodsant, T., M. Navis, I. Aknouch, I.B. Renes, R.M. van Elburg, D. Pajkrt, K.C. Wolthers, C. Schultsz, K.C.H. van der Ark, A. Sridhar, and V. Muncan, *A Human 2D Primary Organoid-Derived Epithelial Monolayer Model to Study Host-Pathogen Interaction in the Small Intestine.* Front Cell Infect Microbiol, **2020**. 10: p. 272.

201. Cevallos Porta, D., S. López, C.F. Arias, and P. Isa, *Polarized rotavirus entry and release from differentiated small intestinal cells.* Virology, **2016**. 499: p. 65-71.

202. Emerson, S.U., H.T. Nguyen, U. Torian, D. Burke, R. Engle, and R.H. Purcell, *Release of genotype 1 hepatitis E virus from cultured hepatoma and polarized intestinal cells depends on open reading frame 3 protein and requires an intact PXXP motif.* Journal of virology, **2010**. 84(18): p. 9059-9069.

203. Lamers, M.M., J. Beumer, J. van der Vaart, K. Knoops, J. Puschhof, T.I. Breugem, R.B.G. Ravelli, J. Paul van Schayck, A.Z. Mykytyn, H.Q. Duimel, E. van Donselaar, S. Riesebosch, H.J.H. Kuijpers, D. Schippers, W.J. van de Wetering, M. de Graaf, M. Koopmans, E. Cuppen, P.J. Peters, B.L. Haagmans, and H. Clevers, *SARS-CoV-2 productively infects human gut enterocytes.* Science, **2020**: p. eabc1669.

204. Rebendenne, A., A.L. Chaves Valadão, M. Tauziet, G. Maarifi, B. Bonaventure, J. McKellar, R. Planès, S. Nisole, M. Arnaud-Arnould, O. Moncorgé, and C. Goujon, *SARS-CoV-2 Triggers an MDA-5-Dependent Interferon Response Which Is Unable To Control Replication in Lung Epithelial Cells.* Journal of Virology, **2021**. 95(8): p. e02415-20.

205. Ingle, H., S.T. Peterson, and M.T. Baldridge, *Distinct Effects of Type I and III Interferons on Enteric Viruses.* Viruses, **2018**. 10(1).

206. Zhang, X., M. Paget, C. Wang, Z. Zhu, and H. Zheng, *Innate immune evasion by picornaviruses.* Eur J Immunol, **2020**.

207. Zhao, X., C. Li, X. Liu, M.C. Chiu, D. Wang, Y. Wei, H. Chu, J.-P. Cai, I. Hau-Yee Chan, K. Kak-Yuen Wong, J. Fuk-Woo Chan, K. Kai-Wang To, K.Y. Yuen, and J. Zhou, *Human Intestinal Organoids Recapitulate Enteric Infections of Enterovirus and Coronavirus.* Stem Cell Reports, **2021**. 16(3): p. 493-504.

208. Su, R., M.A. Shereen, X. Zeng, Y. Liang, W. Li, Z. Ruan, Y. Li, W. Liu, Y. Liu, K. Wu, Z. Luo, and J. Wu, *The TLR3/IRF1/Type III IFN Axis Facilitates Antiviral Responses against Enterovirus Infections in the Intestine.* mBio, **2020**. 11(6): p. e02540-20.

209. Drummond, C.G., *The Development of Physiologically Relevant Cell Culture Models for Intestinal Enterovirus Infection*. 2017, ProQuest Dissertations Publishing.

210. Lulla, V., A.M. Dinan, M. Hosmillo, Y. Chaudhry, L. Sherry, N. Irigoyen, K.M. Nayak, N.J. Stonehouse, M. Zilbauer, I. Goodfellow, and A.E. Firth, *An upstream protein-coding region in enteroviruses modulates virus infection in gut epithelial cells.* Nature Microbiology, **2019**. 4(2): p. 280-292.

211. Green, K.Y., S.S. Kaufman, B.M. Nagata, N. Chaimongkol, D.Y. Kim, E.A. Levenson, C.M. Tin, A.B. Yardley, J.A. Johnson, A.B.F. Barletta, K.M. Khan, N.A. Yazigi, S. Subramanian, S.R. Moturi, T.M. Fishbein, I.N. Moore, and S.V. Sosnovtsev, *Human norovirus targets enteroendocrine epithelial cells in the small intestine.* Nature Communications, **2020**. 11(1): p. 2759.

212. Hagbom, M., C. Istrate, D. Engblom, T. Karlsson, J. Rodriguez-Diaz, J. Buesa, J.A. Taylor, V.M. Loitto, K.E. Magnusson, H. Ahlman, O. Lundgren, and L. Svensson, *Rotavirus stimulates release of serotonin (5-HT) from human enterochromaffin cells and activates brain structures involved in nausea and vomiting.* PLoS Pathog, **2011**. 7(7): p. e1002115.

213. Bellono, N.W., J.R. Bayrer, D.B. Leitch, J. Castro, C. Zhang, T.A. O'Donnell, S.M. Brierley, H.A. Ingraham, and D. Julius, *Enterochromaffin Cells Are Gut Chemosensors that Couple to Sensory Neural Pathways.* Cell, **2017**. 170(1): p. 185-198.e16.

214. Krimmling, T., A. Beineke, and C. Schwegmann-Weßels, *Infection of porcine precision cut intestinal slices by transmissible gastroenteritis coronavirus demonstrates the importance of the spike protein for enterotropism of different virus strains.* Veterinary microbiology, **2017**. 205: p. 1-5.

215. Triana, S., M.L. Stanifer, M. Shahraz, M. Mukenhirn, C. Kee, D. Ordoñez-Rueda, M. Paulsen, V. Benes, S. Boulant, and T. Alexandrov, *Single-cell transcriptomics reveals immune response of intestinal cell types to viral infection.* bioRxiv, **2020**: p. 2020.08.19.255893.

216. Kosulin, K., *Intestinal HAdV Infection: Tissue Specificity, Persistence, and Implications for Antiviral Therapy.* Viruses, **2019**. 11(9).

217. Mossel, E.C., C. Huang, K. Narayanan, S. Makino, R.B. Tesh, and C.J. Peters, *Exogenous ACE2 expression allows refractory cell lines to support severe acute respiratory syndrome coronavirus replication.* Journal of virology, **2005**. 79(6): p. 3846-3850.

218. Riabi, S., I. Gaaloul, R. Harrath, and M. Aouni, *Persistent infection of human intestinal Caco-2 cell line by Coxsackieviruses B.* Pathologie Biologie, **2012**. 60(6): p. 347-351.

219. Sane, F., D. Caloone, V. Gmyr, I. Engelmann, S. Belaich, J. Kerr-Conte, F. Pattou, R. Desailloud, and D. Hober, *Coxsackievirus B4 can infect human pancreas ductal cells and persist in ductal-like cell cultures which results in inhibition of Pdx1 expression and disturbed formation of islet-like cell aggregates.* Cellular and Molecular Life Sciences, **2013**. 70(21): p. 4169-4180.

220. Frisk, G., *Mechanisms of chronic enteroviral persistence in tissue.* Current Opinion in Infectious Diseases, **2001**. 14(3).

221. Lietzen, N., K. Hirvonen, A. Honkimaa, T. Buchacher, J.E. Laiho, S. Oikarinen, M.A. Mazur, M. Flodstrom-Tullberg, E. Dufour, A.B. Sioofy-Khojine, H. Hyoty, and R. Lahesmaa, *Coxsackievirus B Persistence Modifies the Proteome and the Secretome of Pancreatic Ductal Cells.* iScience, **2019**. 19: p. 340-357.

222. Kim, K.S., N.M. Chapman, and S. Tracy, *Replication of Coxsackievirus B3 in Primary Cell Cultures Generates Novel Viral Genome Deletions.* Journal of Virology, **2008**. 82(4): p. 2033.

223. Massilamany, C., A. Gangaplara, and J. Reddy, *Intricacies of cardiac damage in coxsackievirus B3 infection: Implications for therapy.* International Journal of Cardiology, **2014**. 177(2): p. 330-339.

224. N'Guyen, Y., F. Lesaffre, D. Metz, S. Tassan, Y. Saade, C. Boulagnon, P. Fornes, F. Renois, and L. Andreoletti, *Enterovirus but not Parvovirus B19 is associated with idiopathic dilated cardiomyopathy and endomyocardial CD3, CD68, or HLA-DR expression.* Journal of Medical Virology, **2017**. 89(1): p. 55-63.

225. Hyöty, H., *Viruses in type 1 diabetes.* Pediatric Diabetes, **2016**. 17(S22): p. 56-64.

226. Richardson, S.J. and N.G. Morgan, *Enteroviral infections in the pathogenesis of type 1 diabetes: new insights for therapeutic intervention.* Current opinion in pharmacology, **2018**. 43: p. 11-19.

227. Baj, A., M. Colombo, J.L. Headley, J.R. McFarlane, M.-a. Liethof, and A. Toniolo, *Post-poliomyelitis syndrome as a possible viral disease.* International Journal of Infectious Diseases, **2015**. 35: p. 107-116.

228. Chen, B.-S., H.-C. Lee, K.-M. Lee, Y.-N. Gong, and S.-R. Shih, *Enterovirus and Encephalitis.* Frontiers in Microbiology, **2020**. 11(261).

229. Sin, J., V. Mangale, W. Thienphrapa, R.A. Gottlieb, and R. Feuer, *Recent progress in understanding coxsackievirus replication, dissemination, and pathogenesis.* Virology, **2015**. 484: p. 288-304.

230. Oh, D.Y., P.A. Silva, B. Hauroeder, S. Diedrich, D.D. Cardoso, and E. Schreier, *Molecular characterization of the first Aichi viruses isolated in Europe and in South America.* Arch Virol, **2006**. 151(6): p. 1199-206.

231. Yang, S., W. Zhang, Q. Shen, Z. Yang, J. Zhu, L. Cui, and X. Hua, *Aichi virus strains in children with gastroenteritis, China.* Emerging infectious diseases, **2009**. 15(10): p. 1703-1705.

232. Drexler, J.F., S. Baumgarte, L.K. de Souza Luna, M. Eschbach-Bludau, A.N. Lukashev, and C. Drosten, *Aichi virus shedding in high concentrations in patients with acute diarrhea.* Emerg Infect Dis, **2011**. 17(8): p. 1544-8.

233. Northill, J.A., R.J. Simmons, D. Genge, and F.A. Moore, *Molecular characterization of the first reported Aichivirus A in Australia.* Access Microbiol, **2020**. 2(4): p. acmi000099.

234. Sievers, F., A. Wilm, D. Dineen, T.J. Gibson, K. Karplus, W. Li, R. Lopez, H. McWilliam, M. Remmert, J. Söding, J.D. Thompson, and D.G. Higgins, *Fast, scalable generation of high-quality protein multiple sequence alignments using Clustal Omega.* Molecular Systems Biology, **2011**. 7(1): p. 539.